

Spring 2023

The Anatomy and Phylogeny of a New Large Plioplatecarpine Mosasaur From the Campanian Bearpaw Shale of Montana (USA)

Richard A. Carr
Fort Hays State University, rcarrmontanastate@gmail.com

Follow this and additional works at: <https://scholars.fhsu.edu/theses>

 Part of the [Evolution Commons](#), [Geology Commons](#), [Paleobiology Commons](#), [Paleontology Commons](#), and the [Zoology Commons](#)

Recommended Citation

Carr, Richard A., "The Anatomy and Phylogeny of a New Large Plioplatecarpine Mosasaur From the Campanian Bearpaw Shale of Montana (USA)" (2023). *Master's Theses*. 3216.
DOI: 10.58809/VAKW6568
Available at: <https://scholars.fhsu.edu/theses/3216>

This Thesis is brought to you for free and open access by FHSU Scholars Repository. It has been accepted for inclusion in Master's Theses by an authorized administrator of FHSU Scholars Repository. For more information, please contact ScholarsRepository@fhsu.edu.

THE ANATOMY AND PHYLOGENY OF A NEW LARGE
PLIOPLATECARPINE MOSASAUR FROM THE
CAMPANIAN BEARPAW SHALE
OF MONTANA (USA).

A Thesis Presented to the Graduate Faculty
of Fort Hays State University in
Partial Fulfillment of the Requirements for
the Degree of Master of Science

by

Richard Carr

Bachelor of Arts, University of Florida

Date 24 April 2023

Approved 
Major Professor

Approved 
Graduate Dean

GRADUATE COMMITTEE APPROVAL

The graduate committee of Richard A. Carr approves this thesis as meeting partial fulfillment of the requirements for the Degree of Master of Science

Approved *Laura E. Wil*

Approved *[Signature]*

Approved *Reese E. Smith*

Date 24 April 2023

ABSTRACT:

In 2018, a large and associated plioplatecarpine mosasaur skull, pectoral girdle, and rib cage, whose total body length may have exceeded five meters, was uncovered in the Late Campanian Bearpaw Shale of Northeast Montana (USA). Phylogenetic analysis of this specimen, MOR 10855, recovers this individual as a basal member of the genus *Plioplatecarpus*. This specimen, which may exceed five meters in length, is unique in that it is estimated to be nearly twice the size of any of the other species of *Plioplatecarpus* found in the Western Interior Seaway during this part of the Cretaceous. While the included phylogenetic study suggests MOR 10855 represents a new species within the genus *Plioplatecarpus*, as supported by the presence of diagnostic features in the frontal, quadrate, and scapula, a poor understanding of individual variation and ontogeny in the related species prevents the confident assignment of a new taxon at this time. In addition to the exceptionally well-preserved skull and anterior skeleton, this specimen also preserves two bite marks on the skull possibly inflicted by a similarly sized mosasaur. These bites exhibit evidence of healing, suggesting one of the first documented cases of non-lethal face biting in a Plioplatecarpine mosasaur. The size disparity between this *Plioplatecarpus* specimen and other species of *Plioplatecarpus* known from the Bearpaw Shale (*P. peckensis* and *P. primaevus*) is reminiscent of size variance observed in some extant cetacean clades, including physeteroids and delphinids. The discovery of MOR 10855 suggests that this portion of the Western Interior Seaway was exceptionally productive during this part of the Cretaceous, and that ecological niche partitioning among the resident mosasaurs was probable.

ACKNOWLEDGMENTS

I would like to acknowledge my advisor, Dr. Laura Wilson, and committee members, Drs. Amanda Adams and Reese Barrick for their mentorship and academic input throughout my thesis. I would also like to acknowledge the staff at the Museum of the Rockies for collecting, preparing, and granting access to this specimen; in particular I would like to thank Dr. John Scannella, Scott Williams, Carrie Ancell, Eric Metz, Amy Atwater, and the late Bob Harmon. This study would not have been possible without the CT technicians and machinery at Deaconess Hospital in Bozeman, Montana. Special thanks to the Montana Department of Natural Resources and Conservation and the Bureau of Land Management for access to the locality while excavating and extracting the specimen. I would like to thank the many collaborators on this project who have been involved in much of this project including, Drs. Johan Lindgren, Mike Polcyn, Mary Schweitzer, and Holly Woodward. Lastly, I want to thank the numerous colleagues and friends I have discussed this project with over the years for acting as a sounding board for many of my ideas.

TABLE OF CONTENTS

Introduction.....	8
Systematic Paleontology.....	10
Referred Material.....	8
Diagnosis.....	10
Locality and Horizon.....	11
Taphonomy.....	13
Descriptions and Comparisons.....	15
Phylogenetic Analysis.....	50
Methods.....	50
Results.....	51
Discussion.....	53
Cranial Kinesis.....	54

Plioplatecarpine Size and Ecology.....	56
Non-Lethal Face Biting.....	59
Conclusions.....	62
References Cited.....	63
APPENDIX.....	71

LIST OF FIGURES

1. Map of the extent of the Bearpaw Shale across Montana, Alberta, and Saskatchewan...12	12
2. <i>Plioplatecarpus</i> sp. (MOR 10855) skull in lateral view.....15	15
3. <i>Plioplatecarpus</i> sp. (MOR 10855) reconstructed skull diagram in lateral view.....16	16
4. <i>Plioplatecarpus</i> sp. (MOR 10855) skull in ventral view.....17	17
5. <i>Plioplatecarpus</i> sp. (MOR 10855) reconstructed skull diagram in dorsal view.....18	18
6. <i>Plioplatecarpus</i> sp. (MOR 10855) left maxilla and premaxilla in lateral view.....21	21
7. <i>Plioplatecarpus</i> sp. (MOR 10855) frontal in dorsal view.....24	24
8. <i>Plioplatecarpus</i> sp. (MOR 10855) frontal in ventral view.....25	25
9. <i>Plioplatecarpus</i> sp. (MOR 10855) left postorbitofrontal in ventral (left) and dorsal (right) views.....27	27
10. <i>Plioplatecarpus</i> sp. (MOR 10855) CT scan of palatal elements in ventral view.....29	29
11. <i>Plioplatecarpus</i> sp. (MOR 10855) left and right squamosals.....31	31
12. <i>Plioplatecarpus</i> sp. (MOR 10855) left quadrate in lateral (left) and medial (right) views.....33	33
13. <i>Plioplatecarpus</i> sp. (MOR 10855) left Jugal in lateral view.....36	36
14. <i>Plioplatecarpus</i> sp. (MOR 10855) CT scan of braincase in right lateral view.....37	37

15. <i>Plioplatecarpus sp.</i> (MOR 10855) CT scan of braincase in poster view.....	38
16. <i>Plioplatecarpus sp.</i> (MOR 10855) left sclerotic ring in lateral view.....	41
17. <i>Plioplatecarpus sp.</i> (MOR 10855) right mandible in medial (top) and lateral (bottom) views.....	42
18. <i>Plioplatecarpus sp.</i> (MOR 10855) right scapula (left) and coracoid (right) in lateral view.....	49
19. Strict consensus tree of Plioplatecarpinae including biostratigraphic ranges of each species	52
20. Right lateral view of the reconstructed skull of MOR 10855 with red circles indicating location of bite marks on the specimen.....	60
21. Photos of the right jugal and right dentary of MOR 10855 highlighting the two preserved bite marks.....	61
22. Hypothetical arrangement of <i>Plioplatecarpus sp.</i> skulls based on position of bite marks on MOR 10855.....	62

LIST OF APPENDICES

1. Matrix Addendums.....	71
2. Character Matrix.....	71
3. Recovered Trees.....	73
4. Unique Combination of Features.....	83

INTRODUCTION:

Plioplatecarpines are the second most diverse clade of mosasaurs after the mosasaurines (Polcyn et al., 2014) and are among the best sampled (Driscoll et al., 2019). The past decade has seen a significant increase in new plioplatecarpine taxa, as new specimens are recovered and older specimens are redescribed. Despite gaps in the collective understanding of ontogenetic and other intraspecific variation among plioplatecarpines, this clade provides significant insight into many broader aspects of mosasaur biology. In particular, much of what is known about mosasaur soft tissue anatomy comes from the plioplatecarpine fossil record, including scale impressions, pigment, caudal fin anatomy, and even putative internal organ preservation (Lindgren et al., 2010, 2011).

Both Konishi and Caldwell (2011) and Cuthbertson and Holmes (2015) provide an overview of the current state of plioplatecarpine systematics and biogeography. Specifically, the results of the phylogenetic analysis provided in Konishi and Caldwell (2011) statistically supported the phylogenetic placement of the most basal and derived members of the plioplatecarpines and placed them in a stratigraphically bound and biogeographically informed context. Meanwhile Cuthbertson and Holmes (2015) produced the most recent phylogenetic analysis regarding the placement of plioplatecarpines from the Western Interior Seaway via a modification of the dataset from Konishi and Caldwell (2011). Konishi and Caldwell (2011) established the origination and diversification of plioplatecarpines within the Western Interior Seaway with more derived species diverging within Europe.

This study describes mosasaur remains from the Bearpaw Shale of Montana (see Cuthbertson and Holmes, 2015, Ikejiri and Lucas, 2015). The Bearpaw Shale represents one of the last transgressive pulses of the Western Interior Seaway and is suggested by some to be

equivalent to and indistinguishable from the Pierre Shale (Feldman et al., 2012, Serratos et al., 2017, Tourtelot, 1962). The Bearpaw Shale typically outcrops as a thick and uniform bentonitic shale with occasional siderite nodules. Dinoflagellate fossils from the Bearpaw shale are thought to indicate a productive, low salinity environment (Bergstresser and Krebs, 1983, Palamarczuk and Landman, 2011). While shark teeth and osteichthyan microvertebrate remains have been recovered from the Bearpaw Shale, the majority of the published vertebrate fossils from this formation are marine reptiles, including both elasmosaur and polycotyloid plesiosaurs, sea turtles, and mosasaurs (Brinkman et al., 2006, Cook et al., 2017, Cuthbertson and Holmes, 2015, Holmes, 1996, Ikejiri and Lucas, 2015, Jiménez-Huidobro et al., 2018, Konishi et al., 2011, 2014, Kubo et al., 2012, Sato, 2003, 2005, Serratos et al., 2017, Street et al., 2019). The Bearpaw Shale is known to preserve a wide array of mosasaur taxa in exquisite condition from Alberta and Saskatchewan (Konishi & Brinkman et al., 2011, Konishi et al., 2014, Jiménez-Huidobro et al., 2019) but sampling of the Bearpaw in Montana is still in its infancy. This new specimen described here is remarkable for its large size, which represents one of the largest known specimens of *Plioplatecarpus* to date. The size disparity between this new specimen and the coeval species of *Plioplatecarpus* known from the Bearpaw (*Plioplatecarpus peckensis* and *Plioplatecarpus primaevus*), as well as other similarly sized contemporaneous mosasaurs, provides significant insights into the trophic structure of the Western Interior Seaway in the Late Campanian.

Institutional abbreviations: MOR, Museum of the Rockies, Bozeman, Montana, U.S.A.

SYSTEMATIC PALEONTOLOGY:

SQUAMATA Opper, 1811

MOSASAURIDAE Gervais, 1853

RUSSELOSAURINA Polcyn and Bell, 2005

PLIOPATECARPINAE (Dollo, 1882) Williston, 1897

PLIOPATECARPUS Dollo, 1882

REFERRED MATERIAL:

MOR 10855 is a nearly complete and mostly articulated cranium, complete and articulated left mandible, partial right mandible, and complete pectoral girdles with numerous ribs (Figures 2, 4, 17, and 18). The cranium, frontal, left quadrate, left sclerotic ring, left jugal, and right mandible were scanned via computed tomography (CT scan) conducted by Advanced Medical Imaging at Bozeman Deaconess Hospital in Bozeman, Montana, USA using a Toshiba Aquilion 64 CT Scanner. Scan DICOM data was uploaded into the segmentation software, SlicerMorph.

DIAGNOSIS:

[Following Cuthbertson et al. (2007)] Anterior rim of large parietal foramen approaching or traversing the frontoparietal suture. Frontal plate widens anterior to orbits, forming rectangular or quasi-rectangular shield between orbits and external nares. Frontal plate forms acute process anteriorly slotting into posterior margin of internarial bar of the premaxilla. Otophenoidal crest of prootic absent. Postorbital process of postorbitofrontal extremely short, forming a “peg-and-socket” joint with jugal. Quadrate large. Tympanic ala greatly expanded to form conch. Reduced infrastapedial process. Scapula with posteriorly expanded blade. A transversely oriented ectopterygoid process of the pterygoid.

LOCALITY AND HORIZON:

MOR 10855 was discovered as surficial float that led to the discovery of an in situ bone layer excavated from the *Placenticeras meeki/Baculites compressus* zone of the Bearpaw Shale (Late Cretaceous: Campanian). This zone is approximately 73 Ma (Cobban et al., 2006). The

locality is in Valley County near Hinsdale, Montana, USA (Figure 1). More detailed locality data can be found on file at the MOR by request.



Figure 1. Map of the extent of the Bearpaw Shale across Montana, Alberta, and Saskatchewan. Discovery site (star) of MOR 10855 near Hinsdale, Montana.

This section of the Bearpaw Shale consists of a massive and uniform bentonitic shale that is at least 18m deep at its thickest exposures. Locally, the shale occasionally produces siderite nodules, which often form around concentrations of inoceramid or ammonite shells. No depositional structures were observed to indicate flow direction or energy of the system, suggesting this mosasaur's skeleton was deposited in quiet waters below the wave base. The lack of any terrigenous clasts in the surrounding shale suggests this horizon represents an offshore deposit.

TAPHONOMY:

MOR 10855 consists of a nearly complete skull (Figures 2 and 3) and pectoral girdle with numerous ribs also preserved. The mandibles, cranium, and pectoral girdles, while slightly dissociated from one another, are articulated as individual units. Both scapulae are articulated with their respective coracoids and both mandibles are still associated at the symphysis. The only element missing from the cranium is the parietal and the only elements not articulated with the rest of the cranium are the frontal, postorbitofrontals, squamosals, and quadrates. The cranium is slightly dorsoventrally crushed, resulting in a minor degree of lateral shear and torsion in some of the elements which is most notable in the premaxilla, braincase, and palatal elements of MOR 10855. Disarticulated elements such as the frontal, quadrate, jugals, and pectoral girdles do not show any signs of distortion. The mandibles, which were both preserved with the tooth rows facing dorsally, do not show any obvious signs of postmortem distortion aside from the left splenial which is crushed medially towards the dentary.

The right jugal and right dentary each bear a single circular tooth mark. The bite mark on the jugal goes straight through the suborbital ramus of the element but the bite mark on the medial surface of the dentary does not completely puncture the element. The margins of the

injury in the dentary are rounded and imply this was a nonlethal wound that was beginning to heal before this individual died.

The lack of preserved vertebral and pelvic elements in MOR 10855 is unusual but may be explained by the classic bloat and float model of taphonomy proposed by Sternberg (1933). In this scenario, the heavier anterior portion of the skeleton of MOR 10855 including the skull and pectoral girdle, decayed enough to disarticulate from the more buoyant abdomen. The presence of the interclavicle and sternal cartilage at the site suggests that the pectoral girdles detached from the rest of the skeleton during decomposition. Multiple ribs were recovered in close association at the site, which suggests that a significant portion of the rib cage may have still been articulated via cartilage and was pulled to the sea floor with the rest of the anterior skeleton. The site did not produce any shark teeth, nor did any of the elements bear any post-mortem tooth marks or other scars from scavengers or encrusting organisms. As such, the carcass does not appear to be significantly altered or transported by scavenging activity. The apparent lack of scavenging and the shale-dominated lithology of the site suggests that this carcass was deposited in poorly oxygenated bottom water conditions. While the mandibles were displaced from the cranium, their proximity and the relative placement of the pectoral girdle behind the cranium suggests there were little to no currents influencing the placement of elements at the site. Additionally, there were no obvious signs (e.g. bedforms) from the local sedimentology suggesting directional flow from currents or debris flows. Ligamentous attachments to the parietal may have served as a disarticulating factor that kept this element associated with the missing cervical series. However, this does not explain the missing elements from the fore-paddles and their absence cannot be firmly explained at this time.

DESCRIPTION AND COMPARISONS

Dermal Skull:

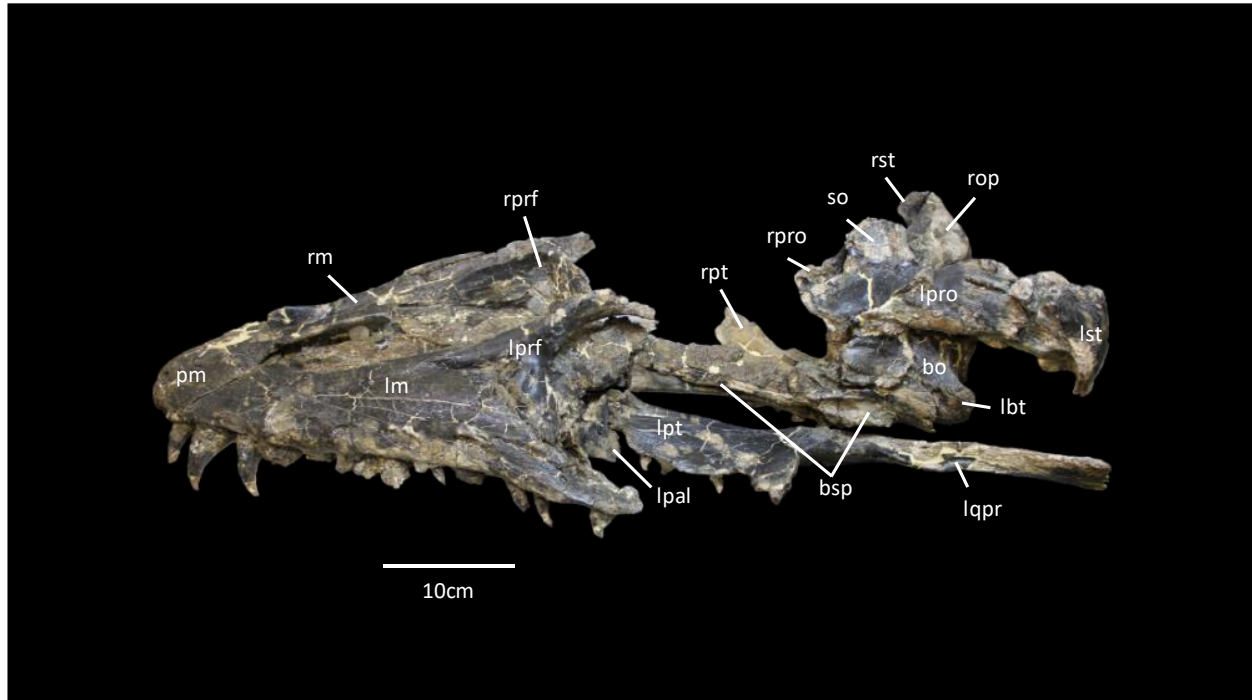


Figure 2. *Plioplatecarpus* sp. (MOR 10855) skull in lateral view. Abbreviations: bo, basioccipital; bsp, basisphenoid; lbt, left basal tubercle of basioccipital; lm, left maxilla; lpal, left palatine; lprf, left prefrontal; lpro, left prootic; lpt, left pterygoid; lqpr, left quadrate process of the pterygoid; lst, left supratemporal; pm, premaxilla; rm, right maxilla; rop, right opisthotic; rprf, right prefrontal; rpro, right prootic; rpt, right pterygoid; rst, right supratemporal, so, supraoccipital. Scale bar is 10 cm.

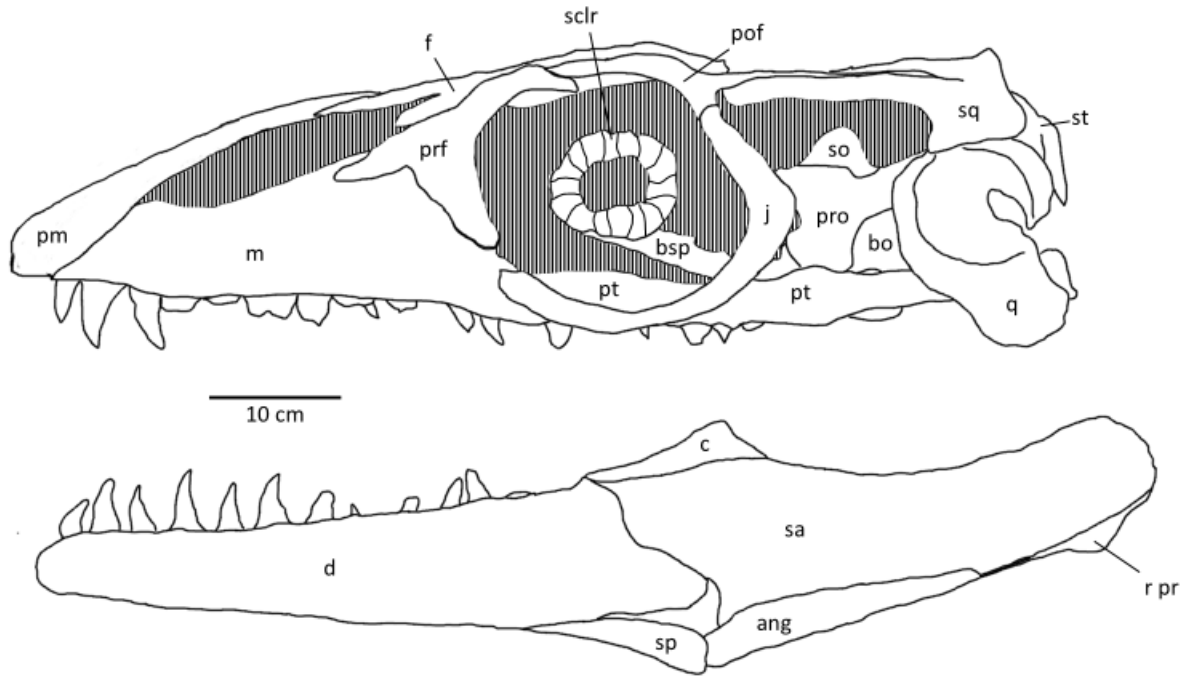


Figure 3. *Plioplatecarpus* sp. (MOR 10855) reconstructed skull diagram in lateral view. Frontal, sclerotic ring, postorbitofrontal, squamosal, and quadrate are preserved as isolated elements in MOR 10855 but rearticulated for this reconstruction. Abbreviations: ang, angular; bo, basioccipital; bsp, basisphenoid; c, coronoid; d, dentary; f, frontal; j, jugal; pm, premaxilla; pof, postorbitofrontal; prf, prefrontal; pro, prootic; pt, pterygoid; q, quadrate; r pr, retroarticular process; sa, surangular; sclr, sclerotic ring; so, supraoccipital; sp, splenial; sq, squamosal; st supratemporal. Scale is 10 cm.

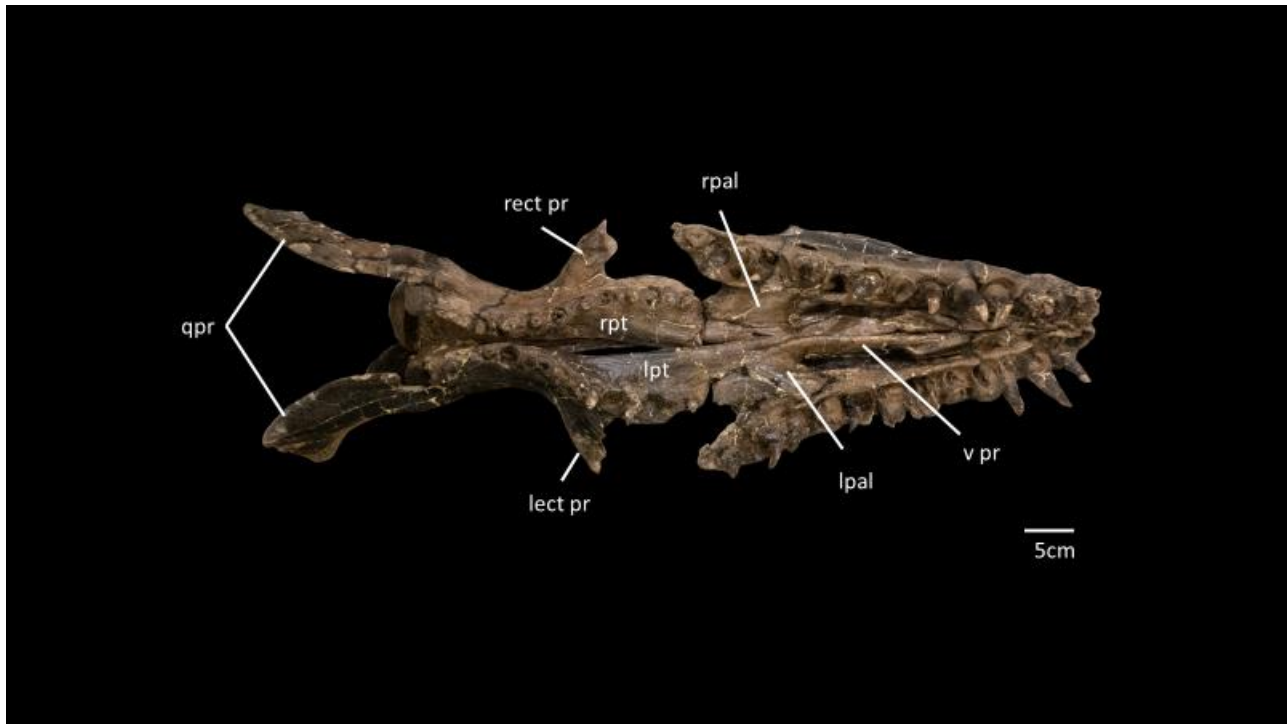


Figure 4. *Plioplatecarpus* sp. (MOR 10855) skull in ventral view. Abbreviations: *lect pr*, ectopterygoid process of the left pterygoid; *lpal*, left palatine; *lpt*, left pterygoid; *qpr*, quadrate processes of the pterygoids; *rect pr*, ectopterygoid process of the right pterygoid; *rpal*, right palatine; *rpt*, right pterygoid; *v pr* vomeric process of the palatine. Scale bar is 5 cm.

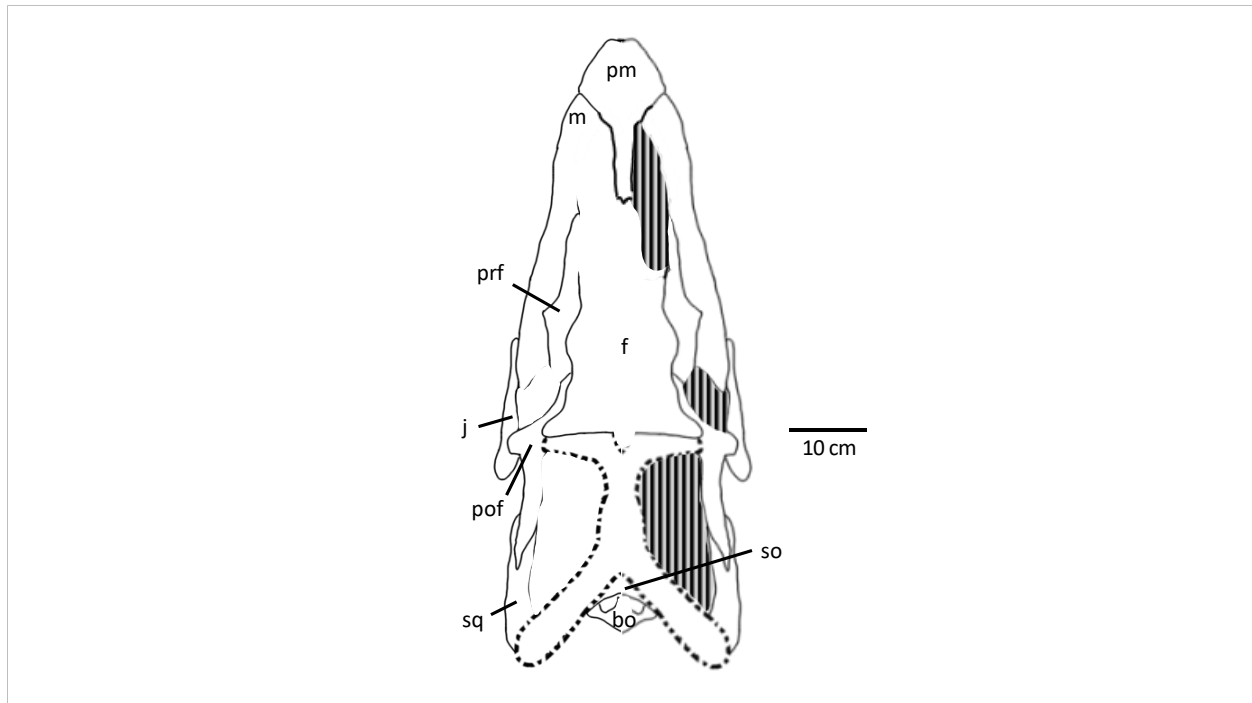


Figure 5. *Plioplatecarpus* sp. (MOR 10855) reconstructed skull diagram in dorsal view. The parietal is the only missing cranial element and its morphology is approximated here with a dashed line. Abbreviations: bo, basioccipital; f, frontal; j, jugal; m, maxilla; pm, premaxilla; pof, postorbitofrontal; prf, prefrontal; so, supraoccipital; sq, squamosal. Scale bar is 10 cm.

Premaxilla:

The prenarial portion of the premaxilla and the anterior part of the internarial bar is preserved in MOR 10855 (Figures 2, 3, and 5). The dentigerous prenarial portion of the premaxilla has a roughly hexagonal outline in dorsal view and is not medially constricted. This part of the element also lacks a dorsal ridge or crest. The anterior edge of the premaxilla lacks a predental rostrum and instead, this border is scalloped and closely follows the contours of the first two premaxillary teeth. This anteriorly abbreviated premaxilla is consistent with the short, to non-existent, premaxillary rostra noted in all other members of *Plioplatecarpinae*. The premaxillo-maxillary suture posteriorly terminates above the space between the first and second maxillary teeth as in *P. primaevus* (Holmes, 1996). In cross section, the anterior portion of the

internarial bar appears as an inverted triangle as in *Plesioplatecarpus planifrons*, *Latoplatecarpus willistoni*, *Plioplatecarpus nichollsae*, and *P. peckensis* (Cuthbertson and Holmes, 2015, Konishi and Caldwell, 2007, 2009, 2011). At the midsection of the bar, the ventral surface becomes fluted by two parallel depressions that likely accommodate the bifurcated anteromedian process of the frontal. The anterior portion of the internarial bar is narrow, but around the midpoint, which bears ventral emarginations and is just anterior to the fractured portion in this specimen, the element appears to expand laterally. The preserved portion of the internarial bar is mildly compressed but appears straight in lateral view, lacking the characteristic arch of *L. willistoni* (Konishi and Caldwell, 2011). There are a total of four premaxillary tooth positions with only the second premaxillary teeth on either side preserved (Figure 4). The preserved premaxillary teeth appear mildly procumbent but this may also be caused by taphonomic distortion of the premaxilla. While the two anterior-most premaxillary teeth are not preserved, the elliptical shape of their alveoli suggests that these first two teeth were procumbent. Laterally, these teeth appear longitudinally fluted. There are five large foramina on the dorsal surface of the dentigerous portion of the premaxilla. The anterior-most foramina are the largest. Posterior to these, there are two smaller foramina on the left dorsal side and one foramen on the right.

Maxilla:

Both maxillae are completely preserved in articulation with the rest of the muzzle unit (Figures 2, 3, and 4). In MOR 10855 the anteriorly deepest portion of the maxilla is located immediately behind the posterior termination of the premaxillo-maxillary suture. This is true for most other plioplatecarpines, except *P. peckensis* (Cuthbertson and Holmes, 2015). Similar to *L. willistoni*, the external nares appear laterally expanded above the area between the second and

sixth maxillary teeth (Konishi and Caldwell, 2011). As in *L. willistoni* and *Platecarpus tympaniticus*, a thin and flat posterodorsal process of the maxilla overlaps the anterior edge of the prefrontal along its dorsal sulcus (Konishi and Caldwell, 2011, Konishi et al. 2012). The medial border of this process reaches the posterolateral border of the external nares. Both maxillae bear 12 teeth (Figures 2, 4, and 6), as seen in *L. willistoni*, *P. planifrons*, *P. tympaniticus*, *P. nichollsae*, and *P. peckensis* (Konishi and Caldwell, 2007, 2009, 2011, Konishi et al., 2012). Like *L. willistoni* and *P. nichollsae*, the last two maxillary teeth are located suborbitally (Konishi and Caldwell, 2009, 2011). Approximately one quarter of the total length of the tooth roots are exposed in lateral view. The maxillary teeth get progressively shorter posteriorly.

On both maxillae, there are six foramina for the exits of the maxillary branch of the fifth cranial nerve starting above the space between the second and third maxillary teeth and extending to the eighth maxillary tooth positions on each side. The first four foramina do not exceed 9mm in length; the last foramina range from 30 to 40 mm in length. The first two foramina open anteriorly, while the last four open posteriorly. The posterior portion of the maxilla of MOR 10855 appears downwardly curved giving the ventral margin of the maxilla an arched profile, which is also noted in *Plioplatecarpus houzeaui*, *P. peckensis*, and *L. willistoni*, and is not consistent with the taphonomic distortion other parts of this specimen were subjected to (Cuthbertson and Holmes, 2015, Konishi and Caldwell, 2011, Lingham-Soliar, 1994). The posterior dorsolateral surface of the left maxilla of MOR 10855 bears a longitudinal groove, which starts below the prefrontal lamina and either terminates or opens above the start of the eleventh maxillary tooth. Similar to *P. peckensis*, this groove may have accommodated the anterior portion of the jugal, neither of which are preserved in place, and the ventral portion of the lacrimal, which is not preserved on either side, (Cuthbertson and Holmes, 2015).

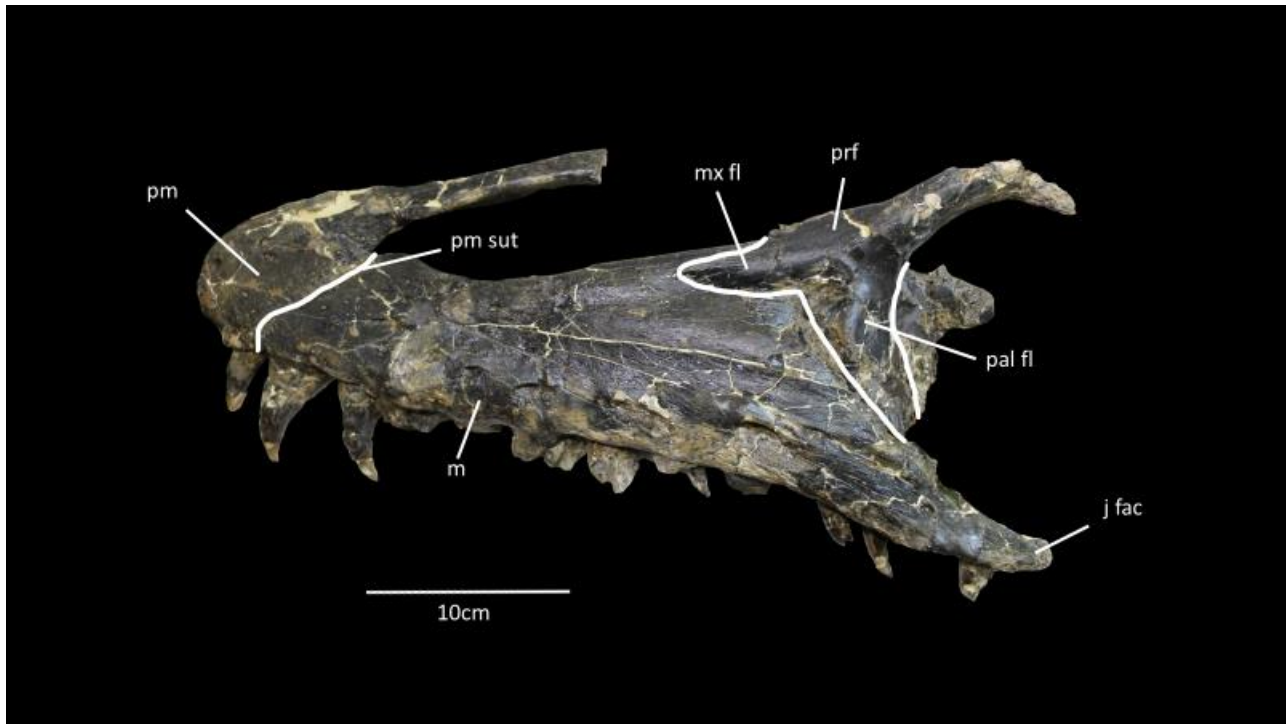


Figure 6. *Plioplatecarpus* sp. (MOR 10855) left maxilla and premaxilla in lateral view. Abbreviations: j fac, jugal facet of the maxilla; m, maxilla; mx fl, maxillary flange of prefrontal; pal fl, palatine flange of prefrontal; pm, premaxilla; pm sut, premaxillo-maxillary suture; prf, prefrontal. Scale bar is 10 cm.

Prefrontal:

Both prefrontals are articulated with their respective maxillae (Figures 2 and 6). The triradiate prefrontals of MOR 10855 more closely resemble the prefrontals of *P. peckensis*, *P. nichollsae*, and *P. primaevus* than the blockier prefrontals reported in *P. tympaniticus*, *L. willistoni*, and *P. planifrons*, (Cuthbertson and Holmes, 2015, Holmes, 1996, Konishi and Caldwell 2007, 2009, 2011, Konishi et al., 2012). Despite the similarity in shape to the prefrontals of other *Plioplatecarpus* specimens, MOR 10855 lacks the simple suture of a prefrontal lamina found in this genus. Instead, MOR 10855 has a complex prefrontal suture that closely resembles the more basal plioplatecarpines. The anterior process of the prefrontal is located medially to the maxilla and extends to the posterior edge of the enlarged emargination of the external nares, roughly above the sixth maxillary tooth. The suborbital ramus of the right prefrontal is strongly deflected medially, as in *P. peckensis*, forming the anterior wall of the orbit

(Cuthbertson and Holmes, 2015); it also articulates with the dorsal surface of the palatine. Medial and posterior to the contact with the posterodorsal process of the maxilla, the prefrontals each bear a groove for articulation with the frontal. The prefrontal contacts the frontal laterally along the anterior half of the total length of the frontal. Despite the length of this contact, a small region of the anteromedial portion of the prefrontal does appear to form part of the posterolateral margin of the external nares. Similar to the condition noted in *L. willistoni* and *P. nichollsae*, the ventral surface of the supraorbital ramus of the left prefrontal bears a small concavity for articulation with the anterior portion of the postorbitofrontal (Konishi and Caldwell, 2009, 2011). This arrangement prevents the frontal from forming any part of the supraorbital border, as in *L. willistoni*, *P. tympaniticus*, and *Plioplatecarpus* (Konishi and Caldwell, 2009, 2011, Konishi et al., 2012). Like *P. nichollsae*, *L. willistoni*, *P. planifrons*, and *P. tympaniticus*, the left prefrontal of MOR 10855 bears at least one, but no more than two, incipient supraorbital tuberosities (Konishi and Caldwell, 2007, 2009, 2011, Konishi et al., 2012).

Frontal:

The frontal of MOR 10855 is subrectangular and more closely resembles the general morphology of *Plioplatecarpus* than *Platecarpus*, *Latoplatecarpus*, or *Plesioplatecarpus* (Figure 7). The posterolateral alae of MOR 10855 are rounded, most closely resembling the shape of *P. nichollsae* (Konishi and Caldwell, 2009). The posterior margin of the frontal is straight and appears mildly excavated as in *L. willistoni* (Konishi and Caldwell, 2011). Also similar to *L. willistoni*, the supraorbital border of the frontal in MOR 10855 is thickened (Konishi and Caldwell, 2011). The lateral margins of the frontal of MOR 10855 are subparallel and exhibit a sinusoidal profile leading from the frontal ala to the anterolateral processes that make the posterior borders of the external nares. A tall and thin median dorsal keel is present on the frontal

and it is laterally bounded by deep emarginations, similar to *L. willistoni* and *Plioplatecarpus* (Konishi and Caldwell, 2011). This keel begins anterior to the supraorbital emarginations of the frontal on its dorsal surface and extends anteriorly along the entire length of the frontal. Starting about 3 cm behind the posterior border of the external nares, this keel bifurcates dorsally and contributes to the premaxillary process of the frontal.

While the posterior portion of the internarial bar of MOR 10855 is not preserved, the bifurcation of the premaxillary process is likely for accepting the ventral median keel of the premaxilla's internarial bar rather than a result of delayed ossification, as suggested by Cuthbertson and Holmes, (2015) in their description of a similar bifurcation in the frontal of *P. peckensis*. The frontal does not bear posterodorsal median embayments, but the posterior portion of the frontal appears slightly ventrally deflected in roughly the same region of these embayments in *L. willistoni*. The dorsal surface of the frontal that surrounds the slightly raised anterior half of the pineal foramen is slightly depressed, though this may also be from taphonomic distortion. Based on the depth of the ventrolateral sulci on either side of the frontal's ventral surface, it is likely that the postorbitofrontals significantly underlapped the frontal medially, as in *Selmasaurus johnsoni* (Polcyn and Everhart, 2008). Posterior to the anterolateral processes of the frontal, but anterior to the contact between the prefrontals and the postorbitofrontals, the edge of the frontal dramatically billows dorsally before flattening and becoming posteriorly planar in lateral profile. In oblique dorsal view, this lateral flare is exaggerated medially by the depth of the depressions that flank the median dorsal keel.

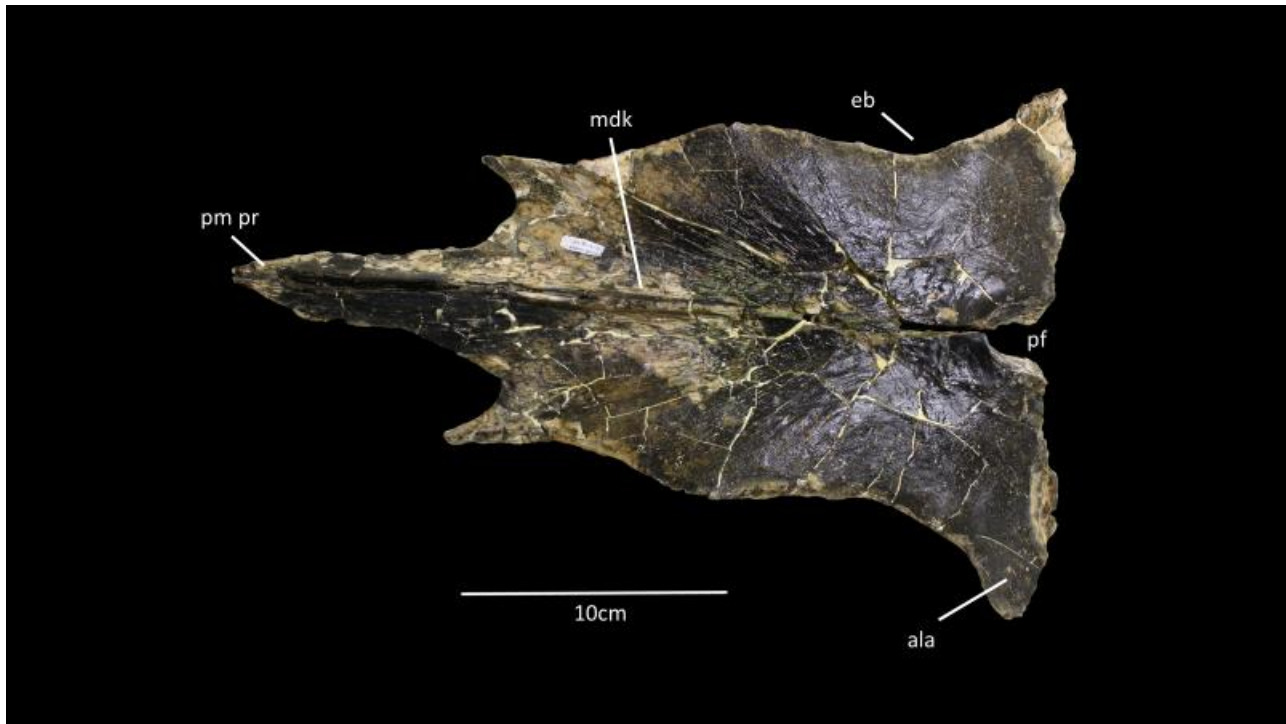


Figure 7. *Plioplatecarpus* sp. (MOR 10855) frontal in dorsal view. Abbreviations: *ala*, frontal ala; *24e*, supraorbital embayment; *mdk*, median dorsal keel; *pf*, pineal foramen; *pm pr*, premaxillary process. Scale bar is 10 cm.

Similar to *P. planifrons* (Konishi and Caldwell, 2007), the dorsal surface of the frontal of MOR 10855 bears numerous small foramina that appear more concentrated on the posterior surface of the element; likewise, there are numerous large, thin, and straight grooves that radiate anteriorly on either side of the posterior origin of the median dorsal keel. On the dorsal surface of the posterior margin of MOR 10855's frontal, there are two very subtle medial planar emarginations on either side of the pineal foramen that resemble the broad and squared emarginations reported in *P. nichollsae* (Konishi and Caldwell, 2009). Similarly, the ventral margin of these emarginations retreat anteriorly on either side of the anterior half of the large, oval shaped pineal foramen, which presumably allowed the parietal to make up the posteroventral three quarters of the pineal foramen as in *P. nichollsae* (Konishi and Caldwell, 2009).

The fronto-parietal suture becomes increasingly complex medially. Around the midpoint of each frontal ala, a posteriorly projecting shelf of bone emerges on the ventral surface of the suture. Within 2-3 cm on either side of the pineal foramen, three short radiating grooves are present on the dorsal surface of this suture. While the parietal is not preserved, the ventral shelf of the posterior margin on the frontal suggests that the postorbital process of the parietal would have overlapped this element at the fronto-parietal suture. As in *P. nichollsae*, curved excavations for the cartilaginous *solia suprasedale* (which Russell, 1967 and subsequent authors erroneously identified as the cerebral hemispheres), flank either side of the olfactory tract; likewise, the olfactory tract is visible and extends anteriorly as a narrow parallel-sided channel for the majority of its length before broadening anteriorly (Konishi and Caldwell, 2009, Oelrich, 1956).

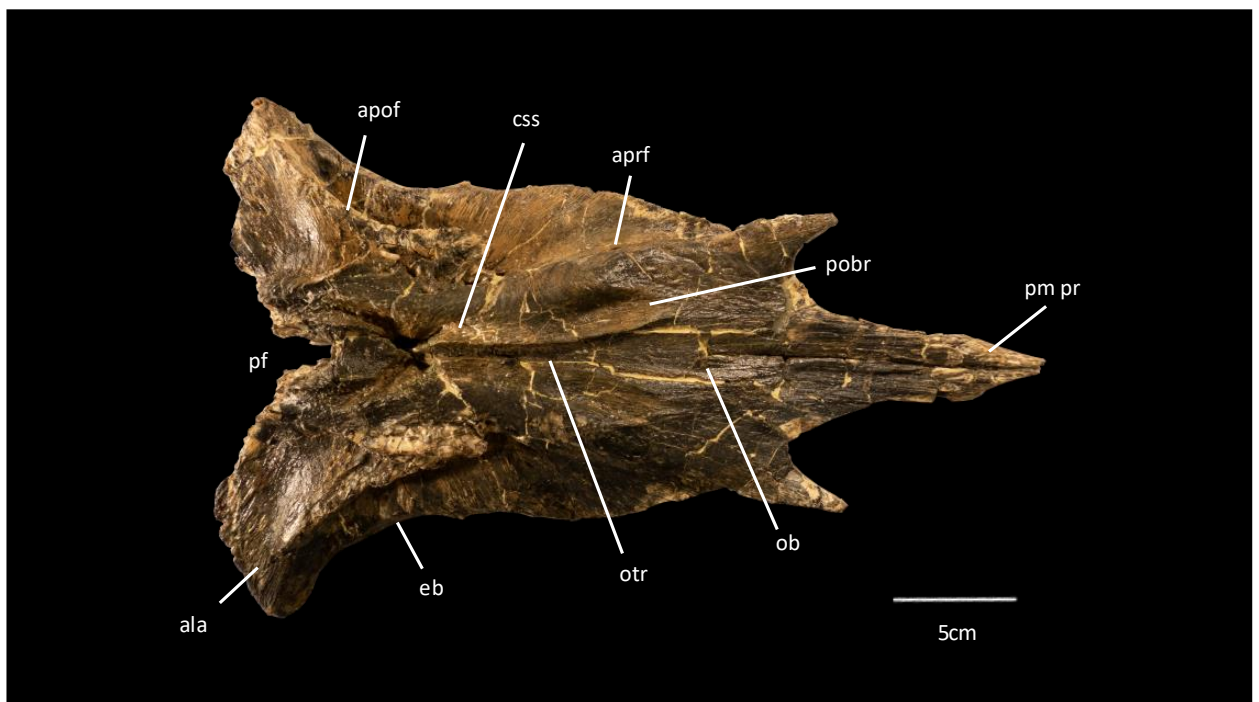


Figure 8. *Plioplatecarpus* sp (MOR 10855) frontal in ventral view. Abbreviations: *ala*, frontal ala; *apof*, articulation for postorbitofrontal; *aprf*, articulation for prefrontal; *css*, excavations for the cartilaginous *solia suprasedale*; *25e*, supraorbital embayment; *ob*, olfactory bulbs; *otr*, olfactory tract; *pf*, pineal foramen; *pm pr*, premaxillary process; *pobr*, parolfactory-bulb recess. Scale bar is 5 cm.

The paraolfactory-bulb recesses are pronounced in MOR 10855. Posteriorly, they contact the excavations for the *solia suprasedale* and extend anteriorly as two roughly parallel grooves for most of their length. Around where the olfactory tract broadens to accommodate the olfactory bulbs, (approximately 20 cm behind the anterior tip of the premaxillary process of the frontal, the paraolfactory-bulb recesses also widen and diverge (Figure 8). MOR 10855 bears a pair of thick anteriorly diverging *descensus processus frontales*, which Konishi and Caldwell (2011) suggests unites *L. willistoni* with all species of *Plioplatecarpus* and North American specimens of “*P. somenensis*”. Excluding the premaxillary process, the narrowest part of the frontal in dorsal view is the antorbital region posterior to the anterolateral processes but anterior to the supraorbital margin. However, this constriction is only marginally narrower than the supraorbital region of the frontal.

Postorbitofrontal:

Both postorbitofrontals are preserved, though disarticulated. The left postorbitofrontal is nearly complete while the right postorbitofrontal lacks its squamosal process (Figure 9). The preservation of the anterior portion of the skull roof is consistent with the trend Konishi and Caldwell (2011) noted among more basal plioplatecarpines: the frontal, postorbitofrontals, and parietal are disarticulated and preserved as separate elements as opposed to one single unit like many specimens of *Plioplatecarpus*. Both elements bear facets for the frontal ala, reflecting the lateroventral morphology of the frontal which the postorbitofrontals would articulate with in life. Posterior to this articulation facet for the frontal ala is another articulation facet for the postorbital process of the parietal. Anterior to the dorsal facet for the frontal ala, each postorbitofrontal has another facet intermediate in length to the frontal ala and parietal postorbital process facets. This third facet appears to articulate with a ventral projection on the

anterior portion of the frontal ala. On the ventral surface of the postorbitofrontals, medial to the jugal process, there are three prominent grooves. The jugal process projects posterolaterally at a shallow angle in both postorbitofrontals. The posterior margin of the jugal process of the right postorbitofrontal is complete and preserves an elongate subtriangular flange of bone on the lateral margin of the process. The anterior margin of this process does not seem to extend as far as the posterior margin. The squamosal process bears a ventral groove for articulating with the squamosal, as in *P. planifrons* (Konishi and Caldwell, 2007).

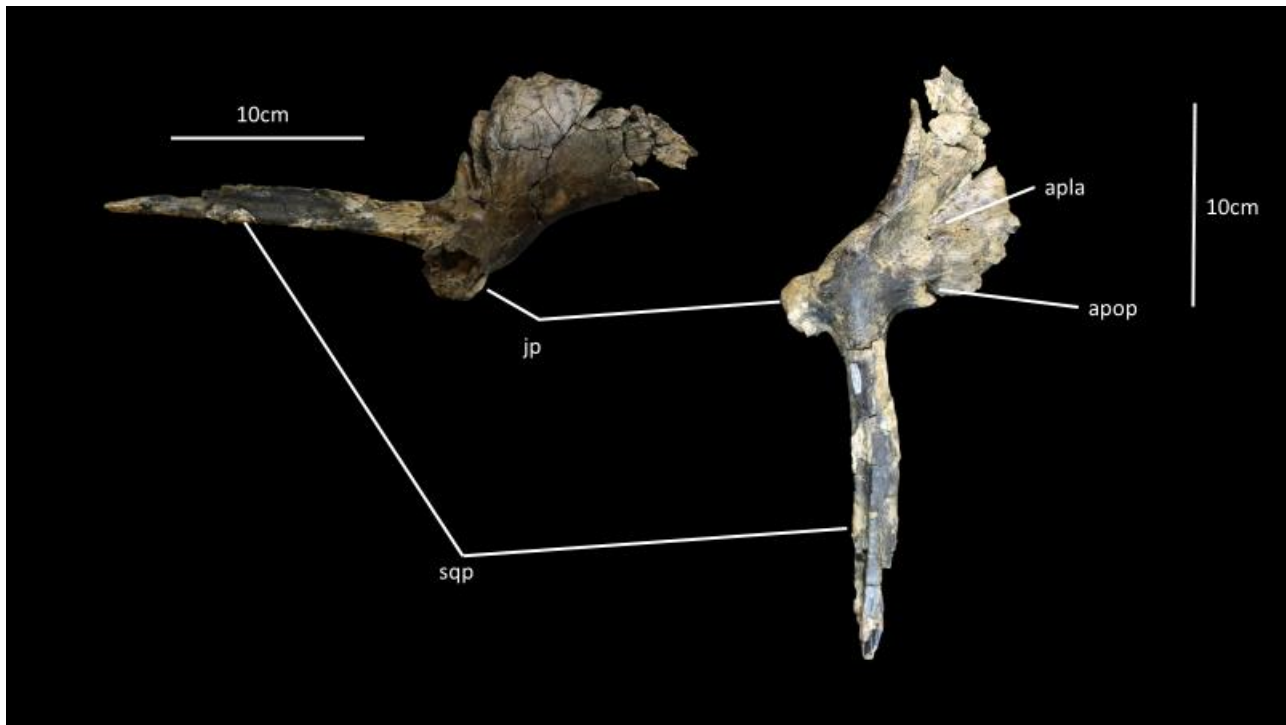


Figure 9. *Plioplatecarpus* sp. (MOR 10855) left postorbitofrontal in ventral (left) and dorsal (right) views. Abbreviations: *apla*, articulation for frontal posterolateral ala; *apop*, articulation for postorbital process of parietal; *jp*, jugal process; *sqp*, squamosal process. Scale bars are 10 cm.

Pterygoid:

Both pterygoids are complete and preserved in articulation with the rest of the skull (Figures 4 and 10). Similar to almost all other plioplatecarpines (with the exception of *Ectenosaurus*; William et al., 2021) the pterygoids of MOR 10855 each have a sigmoidal tooth

row with at least twelve tooth positions (Konishi and Caldwell, 2007, 2009, 2011). Like most species of *Plioplatecarpus*, the pterygoid teeth of MOR 10855 possess a uniform diameter along the length of the tooth row. Unlike *P. peckensis* and *L. willistoni*, the posterior-most tooth positions of MOR 10855 do not extend onto the basisphenoid process of either pterygoid (Cuthbertson and Holmes, 2015, Konishi and Caldwell, 2011). The anterior palatal rami are both complete in the pterygoids of MOR 10855 and terminate anteriorly at the seventh maxillary tooth position, identical to the condition noted in *P. primaevus* (Holmes, 1996). Like most plioplatecarpines, the suture between the pterygoids and palatines is long and diagonal. The ectopterygoid processes project laterally at a slight anterior angle from the body of the pterygoid and the longest portion of the ectopterygoid process projects to a point between the fifth and sixth pterygoid tooth positions. While the ectopterygoid is not preserved, the articulation points for these elements are concentrated on the anterior face of each ectopterygoid process, which also bears a prominent anterolateral sulcus near the distal tips of these processes. The lateral borders of the pterygoids in this specimen are convex and broadly curved. However, reanalysis of the prevalence of this feature suggests that this condition is more common across Plioplatecarpinae and not restricted to *Plioplatecarpus* as previously suggested by Cuthbertson and Holmes (2015). As in most plioplatecarpines, the pterygoids of MOR 10855 bear a pair of posteromedial basisphenoid processes immediately posterior to each pterygoid tooth row, which articulate with the basipterygoid process of the basisphenoid.

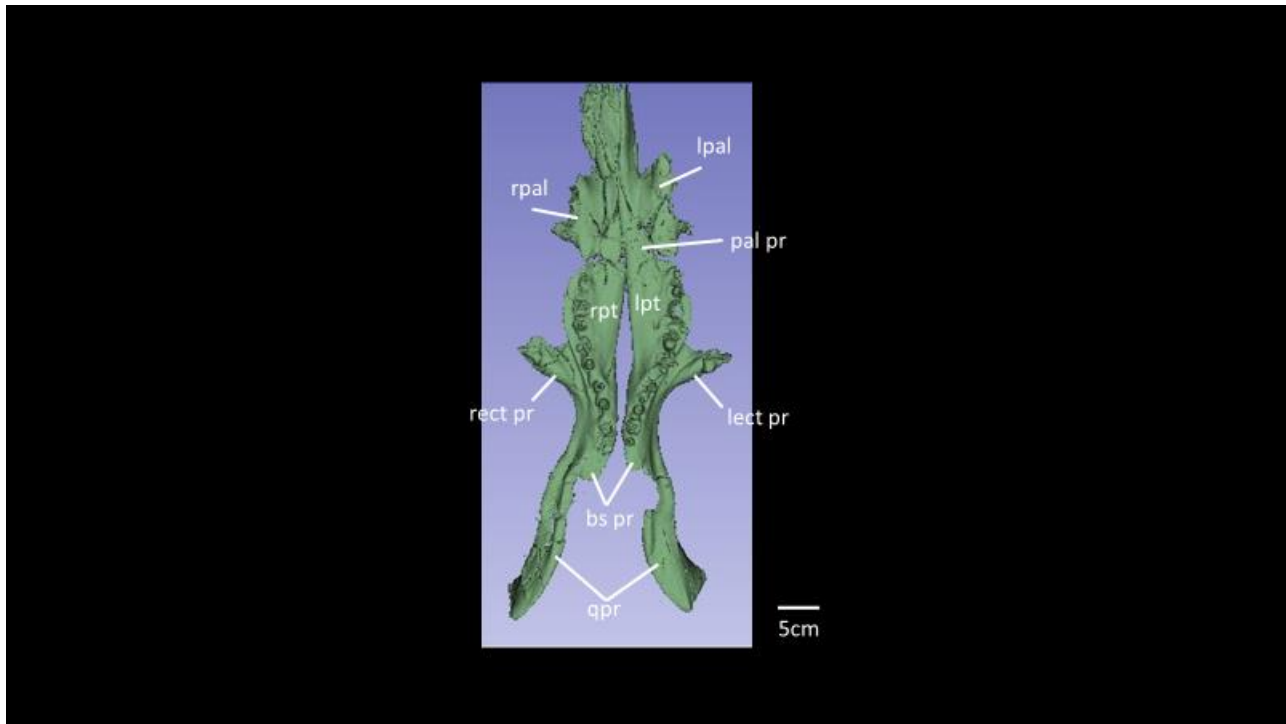


Figure 109. *Plioplatecarpus* sp. (MOR 10855) CT scan of palatal elements in ventral view. Abbreviations: *bs pr*, basisphenoid processes of the pterygoid; *lect pr*, ectopterygoid process of the left pterygoid; *lpal*, left palatine; *lpt*, left pterygoid; *qpr*, quadrate processes of the pterygoids; *rect pr*, ectopterygoid process of the right pterygoid; *rpal*, right palatine; *rpt*, right pterygoid. Scale bar is 5 cm.

Palatine:

Both palatines are preserved in MOR 10855 in articulation with the rest of the palate; however, the right palatine and pterygoid are slightly displaced dorsomedially while the left palatine and pterygoid are in the most likely life position (Figures 4 and 10). Similar to *L. willistoni*, the main body of each palatine in MOR 10855 extends from the eighth to the eleventh maxillary tooth positions. Like *L. willistoni* and *P. nichollsae*, both of MOR 10855's palatines possess a pronounced posterolateral notch. Unlike *L. willistoni*, this notch does not appear to make an impression on the ventral surface of either element and the posterior border is not evenly scalloped (Konishi and Caldwell, 2011).

Vomer:

In MOR 10855, the vomers are slender, paired elements restricted to the anterior portion of the palate. Unlike *P. planifrons*, the vomers do not contact the pterygoid at all (Konishi and Caldwell, 2007). Resembling *P. primaevus*, the palatine-vomer suture starts at the position of the fifth maxillary tooth (Holmes, 1996). The posterior flanges of the vomers in MOR 10855 are also convex and each bear an anteromedial sulcus. The vomerine processes are tightly spaced like in *P. nichollsae* (Konishi and Caldwell, 2009), and while marginally shorter, the ventral oblique crests of the vomers in MOR 10855 also extend the length of roughly three maxillary teeth anteriorly.

Squamosal:

Both squamosals are preserved and nearly complete with only a few minor fragments missing from the postorbitofrontal process of the left squamosal (Figure 11). As in *L. willistoni*, the postorbital process of the squamosal extends anteriorly along the entire length of the squamosal process of the postorbitofrontal and terminates just posterior to the jugal process of the postorbitofrontal (Konishi and Caldwell, 2011). This also indicates that the supratemporal fenestra was as long as this process, resembling the morphology of *P. nichollsae* and *L. willistoni* (Konishi and Caldwell, 2009, Konishi and Caldwell, 2011). The walls of the groove of the postorbital process get shorter anteriorly, with the medial wall being taller than the lateral wall as in *L. willistoni* and *P. nichollsae* (Konishi and Caldwell, 2009, 2011). Like *L. willistoni*, the parietal process of MOR 10855 is low and subtriangular. The lateral surface of the main body of the squamosal is slightly concave. On the medial surface of the main body of the squamosal, there is an antero-dorsally angled ridge projecting from the dorsal margin of the quadrate process, which articulates with the supratemporal. Resembling *P. peckensis*, this supratemporal

ridge is deeply fluted in both squamosals (Cuthbertson and Holmes, 2015). In ventral view each squamosal bears a large, elongate, and subtriangular quadrate process. The concave surface of this process is pitted and mildly ridged. The medial margin of this process is shorter than the lateral margin. The posterior border of the main body of the squamosal is nearly straight and slopes gently anteriorly.

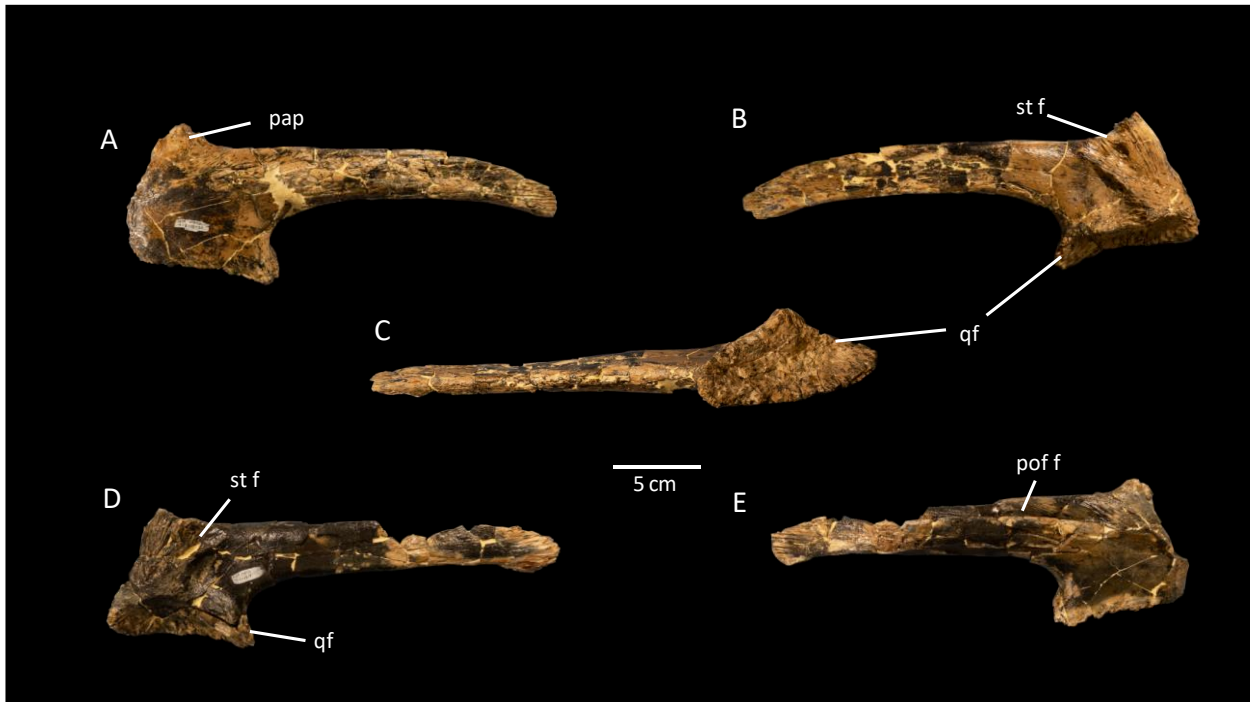


Figure 11. *Plioplatecarpus* sp (MOR 10855) left and right squamosals: A. Right squamosal lateral view, B. Right squamosal medial view, C. Right squamosal ventral view, D. Left squamosal medial view, E. Left squamosal lateral view. Abbreviations: pap, parietal process of squamosal; pof f, postorbitofrontal facet; qf, quadrate facet; st f, supratemporal facet; Scale bar is 5 cm.

Supratemporal:

Both supratemporals are preserved in articulation with the rest of the elements in the paraoccipital process (Figures 14 and 15). In *P. peckensis*, the dorsolateral portion of the supratemporal articulates with the squamosal, however, the same region in MOR 10855 does not appear to be deeply striated and instead appears to be mostly smooth suggesting this contact may not have been as extensive or mechanically significant compared to *P. peckensis* (Cuthbertson

and Holmes, 2015). However, like *P. peckensis*, the ventrolateral surface of this element lacks a deep concavity for accepting the medial surface of the posterodorsal portion of the suprastapedial process of the quadrate (Cuthbertson and Holmes, 2015). The parietal process of the right supratemporal process in MOR 10855 is preserved, but without the parietal, the interaction of this process and the suspensorial rami of the parietal cannot be evaluated. The dorsoventral lateral processes of the right supratemporal in MOR 10855 appear to be roughly subequal in height. The majority of the deep grooves and striae on the lateral surface of this element are concentrated near the middle and are parallel with the rest of the paraoccipital process.

Quadrate:

The left quadrate is completely preserved while the right quadrate only preserves the suprastapedial process and the mandibular condyle (Figure 12). The quadrate of MOR 10855, which is taller than it is wide, is the largest recorded for any plioplatecarpine to date at 17 cm tall. Like *L. willistoni*, the suprastapedial process bears two roughly parallel eminences posterior to the cephalic condyle, which form the lateral and medial dorsal borders of this process in posterior view (Konishi and Caldwell, 2011). The medial eminence is the larger of the two, but does not terminate in a distinct tubercle-like prominence at the end of the process as noted in *L. willistoni* and *P. peckensis* (Cuthbertson and Holmes, 2015, Konishi and Caldwell, 2011). Despite lacking this tubercle, there is still a large concavity on the supratemporal that accepts the distal end of the suprastapedial process. The lateral eminence has a low profile and is nearly indistinct from the dorso-lateral margin of the suprastapedial process. These parallel borders of the suprastapedial process come together to form a rounded end like *P. nichollsae* (Konishi and Caldwell, 2009).

As noted in most other members of Plioplatecarpinae, the quadrate is inclined anteriorly (Cuthbertson and Holmes, 2015, Konishi and Caldwell, 2011, Konishi et al., 2012). The rim of the tympanic ala is curved and completely preserved in MOR 10855. Resembling *P. peckensis*, the edge of the ala bears transversely oriented ridges along its entire height, suggesting it was an anchor point for the extracolumella (Cuthbertson and Holmes, 2015). The anterior edge of the tympanic ala bulges laterally from the quadrate shaft, forming a curved edge as in *P. nichollsae* (Konishi and Caldwell, 2009). The infrastapedial process in MOR 10855 is poorly preserved but appears parallel to the mandibular condyle rather than angled posteroventrally to it. This process therefore more closely resembles the infrastapedial processes of *Platecarpus* and *P. nichollsae* more so than other *Plioplatecarpus* species (Holmes, 1996, Konishi and Caldwell, 2009).

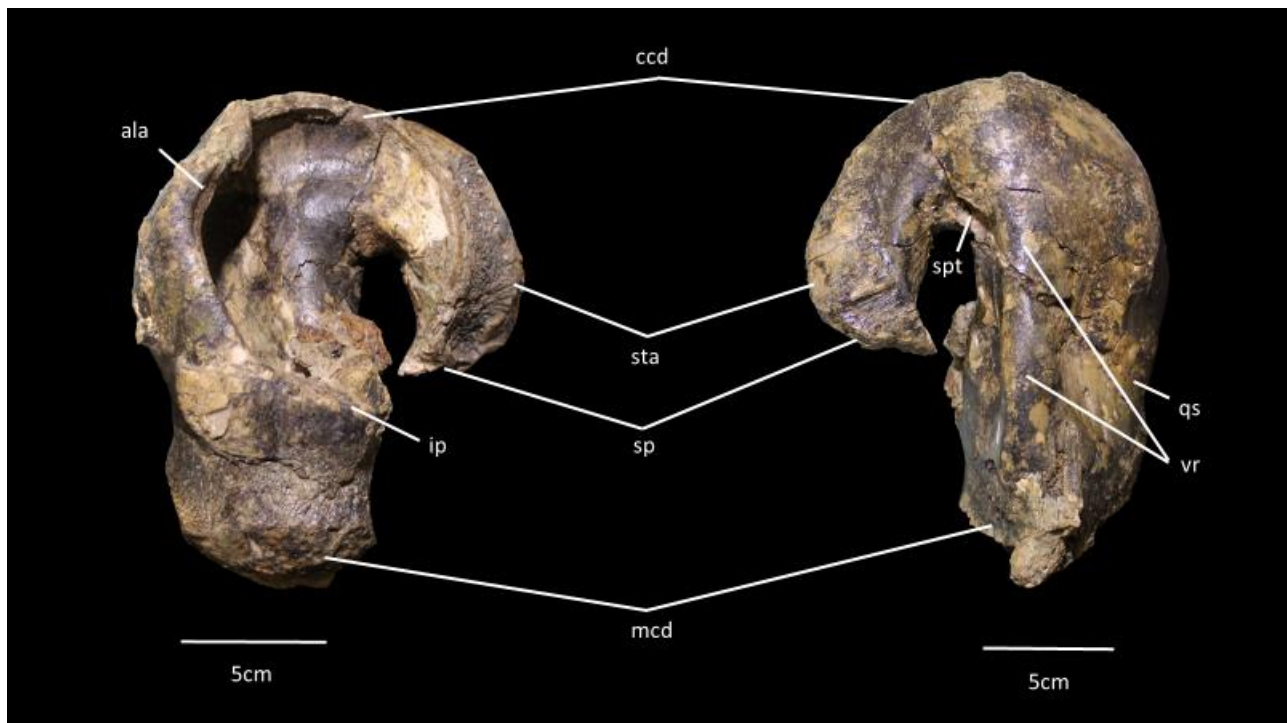


Figure 12. *Plioplatecarpus* sp. (MOR 10855) left quadrate in lateral (left) and medial (right) views. Abbreviations: ala, tympanic ala; ccd, cephalic condyle; ip, infrastapedial process; mcd, mandibular condyle; qs, quadrate shaft; sta, supratemporal articulation; sp, stapedial process; spt, stapedial pit; vr, vertical ridge. Scale bars are 5 cm.

The quadrate shaft of MOR 10855 lacks a posterior eminence like that found in other members of the genus *Plioplatecarpus* (Cuthbertson and Holmes, 2015, Holmes, 1996,

Lingham-Soliar, 1994) and instead has a straight posterior border like *Platecarpus* and *P. nichollsae* (Konishi and Caldwell, 2009). Similar to *P. planifrons*, the suprapedial process and quadrate shaft form an elongate stapedial notch. However, instead of the length of this notch equaling a third of the quadrate height as in *P. peckensis* (Cuthbertson and Holmes, 2015), in MOR 10855, this notch only makes up about one quarter of the quadrate's total height. The cephalic condyle of the quadrate of MOR 10855 lacks any form of posterior notch. Like *P. tympaniticus* and *P. nichollsae* (Konishi and Caldwell, 2009, Konishi et al., 2010), the anteromedial corner of this condyle is gently rounded. The stapedial pit of MOR 10855 forms an elongate oval with curved sides that is oriented obliquely to the quadrate shaft. Also, like *P. tympaniticus* and *P. nichollsae*, the quadrate of MOR 10855 bears a rounded medial dorsoventral ridge that extends up the quadrate shaft (Konishi and Caldwell, 2011, Konishi et al. 2010). Unlike *P. tympaniticus*, MOR 10855 lacks the medial excavation below this dorsoventral ridge (Konishi et al., 2010). The quadrate shaft's medial ridge is bounded on either side by two large depressions. The anterior depression, which coincides with the ventral base of the tympanic ala, is substantially larger and akin to the condition noted in *L. willistoni* and *P. nichollsae* (Konishi and Caldwell, 2011). In ventral view, the mandibular condyle is teardrop shaped as in *P. tympaniticus*, *P. nichollsae*, and *P. peckensis*, which tapers medially and has a slight posterior curvature at the tip (Konishi and Caldwell, 2009, Konishi et al., 2010). The contact between the posteroventral portion of the quadrate shaft and the mandibular condyle forms a small ridge that is tilted medioventrally. Above the medial portion of this ridge is a pronounced circular dimple.

Jugal:

Both jugals are preserved in MOR 10855, with the left jugal better preserved than the right (Figure 13). Overall, the morphology of MOR 10855's left jugal is very similar to *L.*

willistoni, *P. planifrons*, and *P. tympaniticus* (Konishi and Caldwell, 2007, 2011, Konishi et al., 2012). Like *L. willistoni*, the infraorbital ramus of the jugal in MOR 10855 is roughly twice as long as the postorbital ramus, gently curved, and distally expanded. The degree of distal curvature in the infraorbital ramus is slightly different between the two jugals of this specimen and may be a result of taphonomic distortion or pathology. As in *L. willistoni*, the medial side of this ramus bears a slight concavity approximately halfway along the length of the infraorbital ramus; this concavity accepts the posteroventral portion of the maxilla (Konishi and Caldwell, 2011). The ventrally opened ectopterygoid facet begins on the medio-ventral surface of the tapered posterior end of the maxillary facet of the infraorbital ramus. It then extends posteriorly until it terminates just before the base of the postorbital ramus. A pointed process projects medially just posterior to the termination of the ectopterygoid facet, as in *L. willistoni* (Konishi and Caldwell, 2011). Unlike the anterolateral articular facet for the postorbitofrontal found in *L. willistoni*, this facet is angled posterolaterally in MOR 10855 (Konishi and Caldwell, 2011). Again, like *L. willistoni*, this articular facet marks the narrowest preserved portion of the postorbital ramus in MOR 10855 (Konishi and Caldwell, 2011). However, the dorsal-most portions of both rami in this specimen are not preserved so the dorsal facet could theoretically taper further in a complete specimen as in other plioplatecarpines.

The posterior surface of the postorbital ramus in MOR 10855 lacks a distinct keel like that observed in *Platecarpus*, but the trailing edge of this ramus does form a rounded ridge. The jugals of MOR 10855 also lack the “roughened nubbin” on the dorsal surface of the posterior notch that is observed in *Plioplatecarpus marshi* (Lingham-Soliar, 1994: 184). There are transversely oriented grooves that may have served as a ligamentous attachment in this same

region. Unlike *P. houzeaui*, the infraorbital ramus of MOR 10855 is neither tubular nor dorsoventrally compressed anteriorly (Lingham-Soliar, 1994).



Figure 13. *Plioplatecarpus* sp. (MOR 10855) left Jugal in lateral view. Abbreviation: art po, articulation for jugal process of postorbitofrontal. Scale bar is 10 cm.

Prootic:

The left prootic is preserved but heavily fractured while the right element is considerably more complete (Figures 14 and 15). The anterodorsal rami of the prootics bear numerous deep and horizontal striations and each have a slight indentation on their lateral surface, likely for either an ossified or ligamentous attachment with the anterior descending lamina of the parietal. The posterior rami of the prootics each form a long posterolateral sutural contact that sheaths the supraoccipital and opisthotics and forms the anterior face of the paroccipital process, as seen in *P. peckensis* (Cuthbertson and Holmes, 2015). Also reminiscent of *P. peckensis*, the anteroventral process of MOR 10855 extends ventrally and overlaps the top of the basisphenoid ala. The ventral edge of the anterodorsal process is strongly hooked and almost contacts the

dorsal surface of the anteroventral process, making a considerably more restricted exit of the 5th cranial nerve than is noted in *P. peckensis* (Cuthbertson and Holmes, 2015). The exit for the 7th cranial nerve is recessed in MOR 10855. The lateral prootic-opisthotic contact is sutured shut along the paraoccipital process in MOR 10855, which also differs from the condition noted in *P. peckensis* (Cuthbertson and Holmes, 2015). Matrix and/or bone obstructs the area immediately ventral to the prootic-opisthotic suture and prevents the observation of any additional foramina.

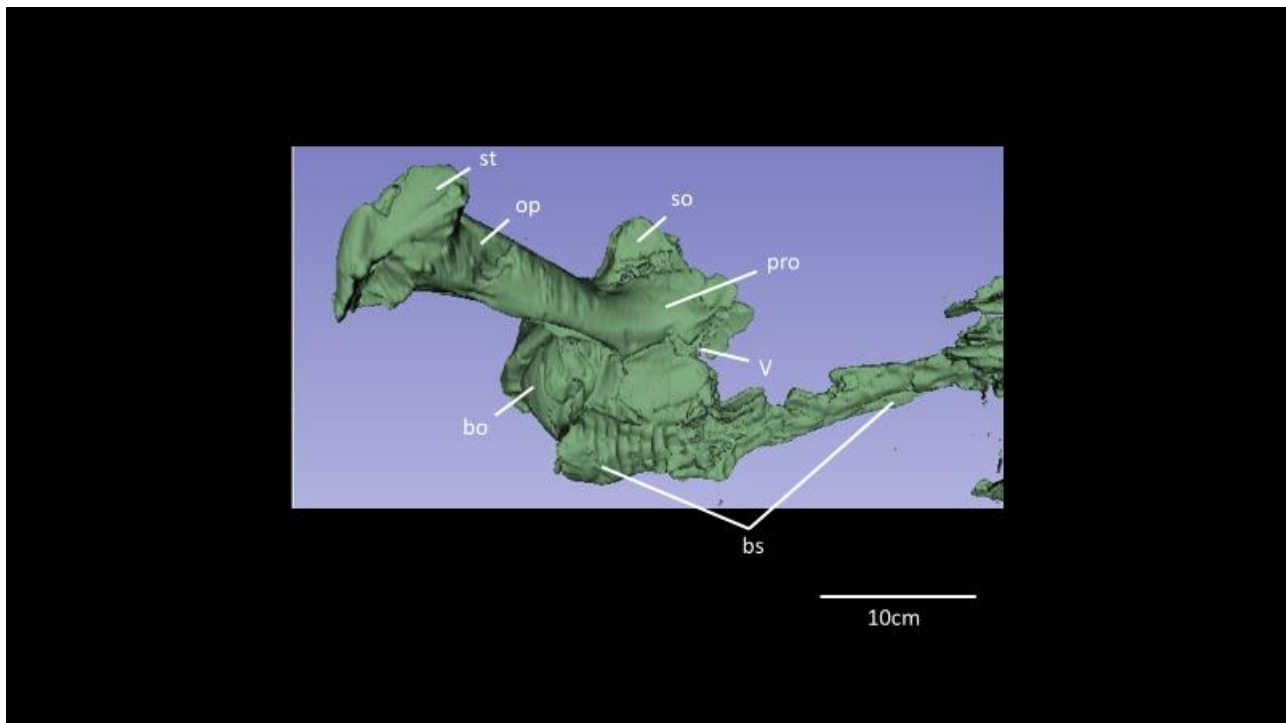


Figure 14. *Plioplatecarpus* sp. (MOR 10855) CT scan of braincase in right lateral view. Abbreviations: bo, basioccipital; bs, basisphenoid; op, opisthotic; pro, prootic; so, supraoccipital; st, supratemporal; V, exit for cranial nerve V. Scale bar is 10 cm.

Opisthotic-Exoccipital:

The opisthotic and exoccipital appear to be indistinguishably fused as in *P. peckensis* (Cuthbertson and Holmes, 2015); additionally, MOR 10855 has a similar posteroventrally oriented suture between the exoccipital and the basioccipital. The medial wall of the left opisthotic is pierced by a large anterior foramen in the position of the 9th cranial nerve, similar to the noted morphology of *P. peckensis* (Cuthbertson and Holmes, 2015). There is a long

bifurcated trough that runs along the suture of the prootic and opisthotic. The deeper of the two troughs is just ventral to the contact of the prootic and opisthotic, while the shallower trough runs along the prootic immediately dorsal to this contact. Both of these troughs extend from the external auditory meatus roughly half the length of the opisthotic.

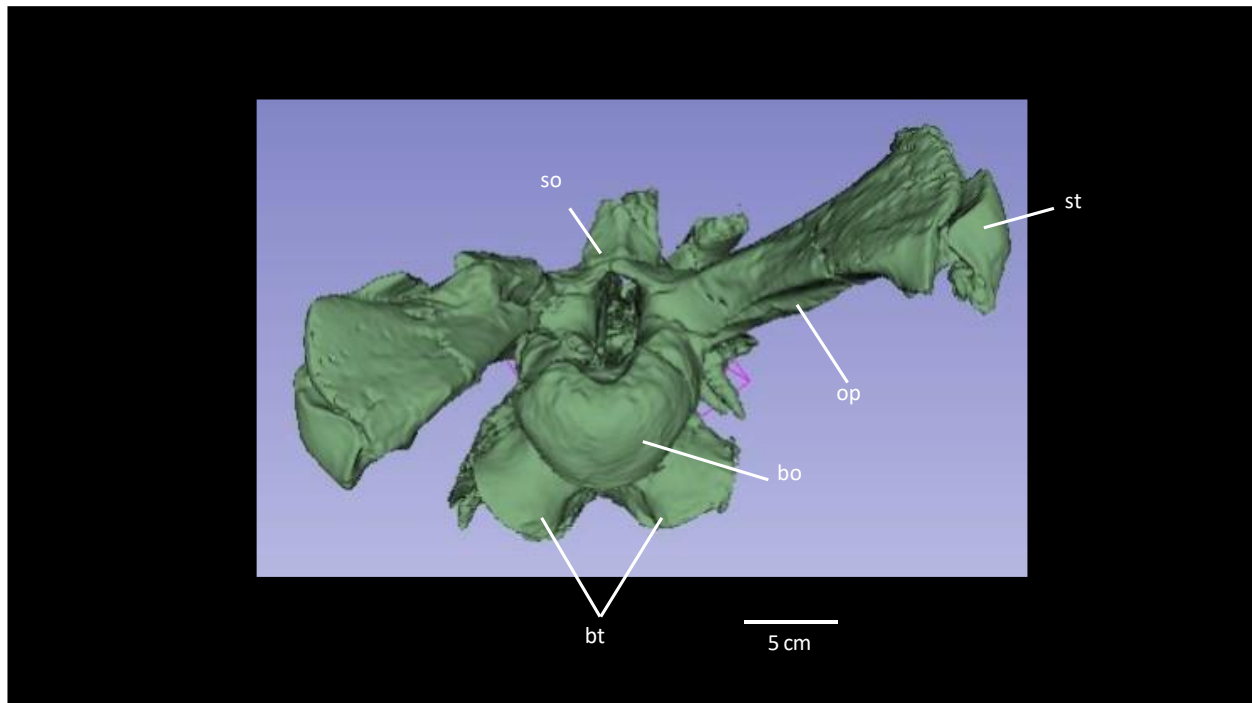


Figure 15. *Plioplatecarpus* sp. (MOR 10855) CT scan of braincase in poster view. Abbreviations: bo, basioccipital; bt, basal tubera; op, opisthotic; so, supraoccipital; st, supratemporal. Scale is 5 cm.

Supraoccipital:

The supraoccipital forms a horizontal suture with the dorsal surface of the prootic and opisthotic-exoccipital elements (Figures 14 and 15). It projects posterolaterally onto the paraoccipital processes and terminates slightly past the lateral extent of the basioccipital. Due to the slight lateral compression of the braincase of MOR 10855, the supraoccipital's contribution to the medial wall of the otic capsule cannot be adequately assessed. As seen in *P. peckensis*, the supraoccipital of MOR 10855 bears a substantial sagittal crest (Cuthbertson and Holmes, 2015). However, unlike *P. peckensis*, whose sagittal crest slopes posteriorly (Cuthbertson and Holmes,

2015), the posterior portion of the sagittal crest in MOR 10855 is very tall and its posterior edge makes a nearly flat surface with a slight medial ridge. The anterior surface of the sagittal crest in MOR 10855 is too fragmentary to assess for the presence of an articulation facet for the posterior descending lamina of the parietal.

Basioccipital:

The basilar artery canal starts as a single trough on the dorsal surface of the basioccipital at the floor of the medullary cavity, but internally appears to branch into two narrow but distinct canals as viewed in CT scans of the specimen. Although this is reminiscent of the condition noted in *P. marshi* and *P. houzeaui* (Lingham-Soliar, 1994), Cuthbertson and Holmes (2015) state that a partially bifurcated or incomplete basilar artery canal may be a preservational and/or ontogenetic artifact. The stout basal tubera project ventrolaterally like *P. planifrons* and the *P. peckensis* holotype (Cuthbertson and Holmes, 2015, Konishi and Caldwell, 2007). Again, like *P. peckensis*, the ventral surface of the basioccipital of MOR 10855 is solid and unpierced by the basilar canals and its surface has a small anteroposteriorly elongate depression with nutrient canals (Cuthbertson and Holmes, 2015).

Basisphenoid-Parasphenoid:

Like the observed morphology in *P. peckensis* (Cuthbertson and Holmes, 2015), the diverging posterior processes of the basisphenoid loosely sheath the anterior surfaces of the basal tubera (Figure 14). However, the size of the gap between these processes and the basal tubera is different on each side and is likely taphonomically influenced. Like *P. peckensis* and *P. primaevus*, the basisphenoid of MOR 10855 bears a pair of ventrolateral basiptyergoid processes that are elongated anteroposteriorly (Cuthbertson and Holmes, 2015, Holmes, 1996). The troughs

for the vena capitis lateralis, found immediately dorsal to the basiptyergoid processes, are especially broad and posteriorly terminate around the level of the external auditory meatus. The vidian canals, which are each about half the width of the troughs for the vena capitis lateralis, are ventral to the anteroventral rami of the prootics. While the vidian canals of MOR 10855 are laterally open like *P. peckensis*, the overhanging ala and ventral crests of the vidian canals are much more substantial in MOR 10855 and maintain a roughly equal distance from one another along the length of this canal (Cuthbertson and Holmes, 2015). The anterior opening of the vidian canal arches dorsally along the basisphenoid but otherwise provides little to no evidence regarding whether this canal is bifurcated or not. The parasphenoid is complete and preserved in articulation in MOR 10855. This elongate element originates from the ventral surface of the basisphenoid between the basiptyergoid processes and extends anteriorly until it terminates at the second pterygoid tooth positions. To date, MOR 10855 represents the only figured specimen of *Plioplatecarpus* that preserves a complete parasphenoid.

Sclerotic Ring:

MOR 10855 preserves a single three-dimensional partial sclerotic ring with 11-12 individual ossicles (Figure 16). Like all other studied mosasaur sclerotic rings (Yamashita et al., 2015), MOR 10855 lacks any sigmoidal flexure. Unlike *P. tympaniticus*, the external surface of the scleral ossicles of MOR 10855 appears to be completely smooth with no visible grooves or striae (Yamashita et al., 2015). The fragmented nature of the scleral ossicles obscures the margins of the individual ossicles, making the precise identification of Yamashita et al. (2015: 3)'s "plus, minus, and imbricating" types difficult. Despite this, the imbricating type ossicles appear to be the most abundant in the ring, with three definitively identified imbricating types. While less in number, the plus and minus type ossicles may be equal to each other in

abundance with at least two definitely identified plus types; a similar trend is noted in nearly all of the sclerotic rings included in the study by Yamashita et al. (2015).

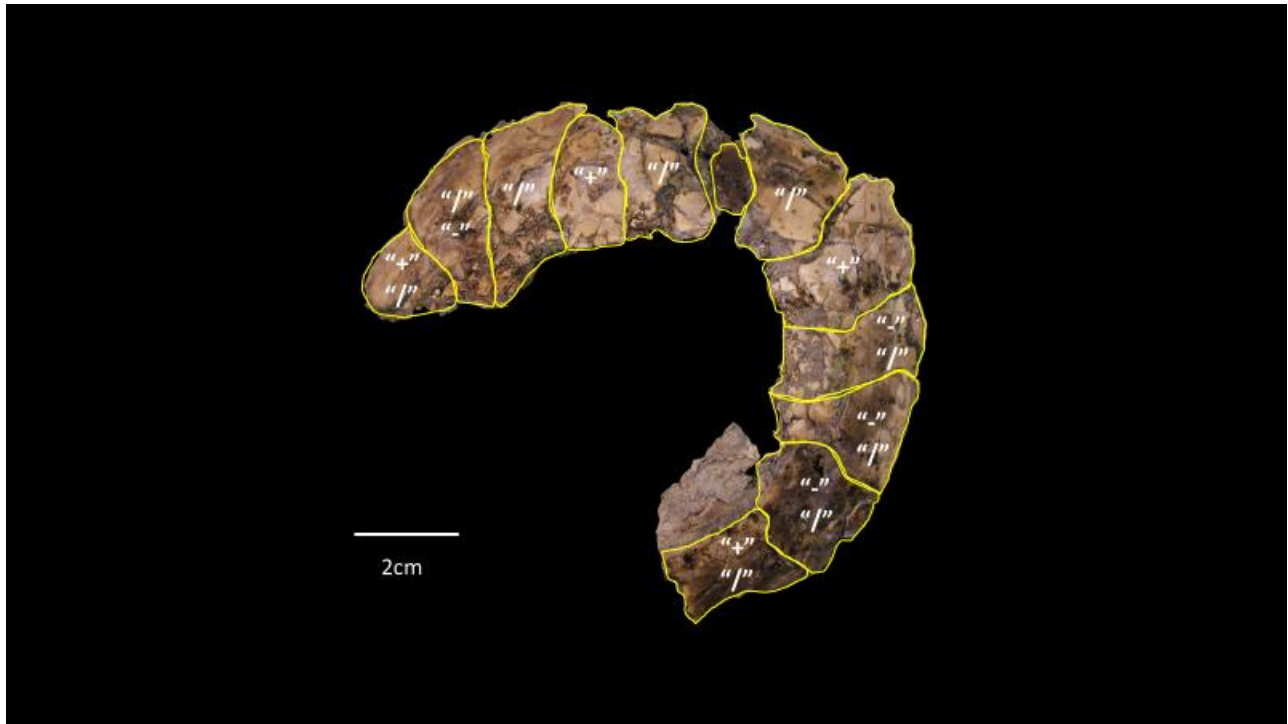


Figure 16. *Plioplatecarpus* sp. (MOR 10855) left sclerotic ring in lateral view. The "+", "-", and "/", symbols correspond with the "plus", "minus", and "imbricating" type ossicles respectively outlined in Yamashita et al., (2015). Scale bar is 2 cm.

Lower Jaw:

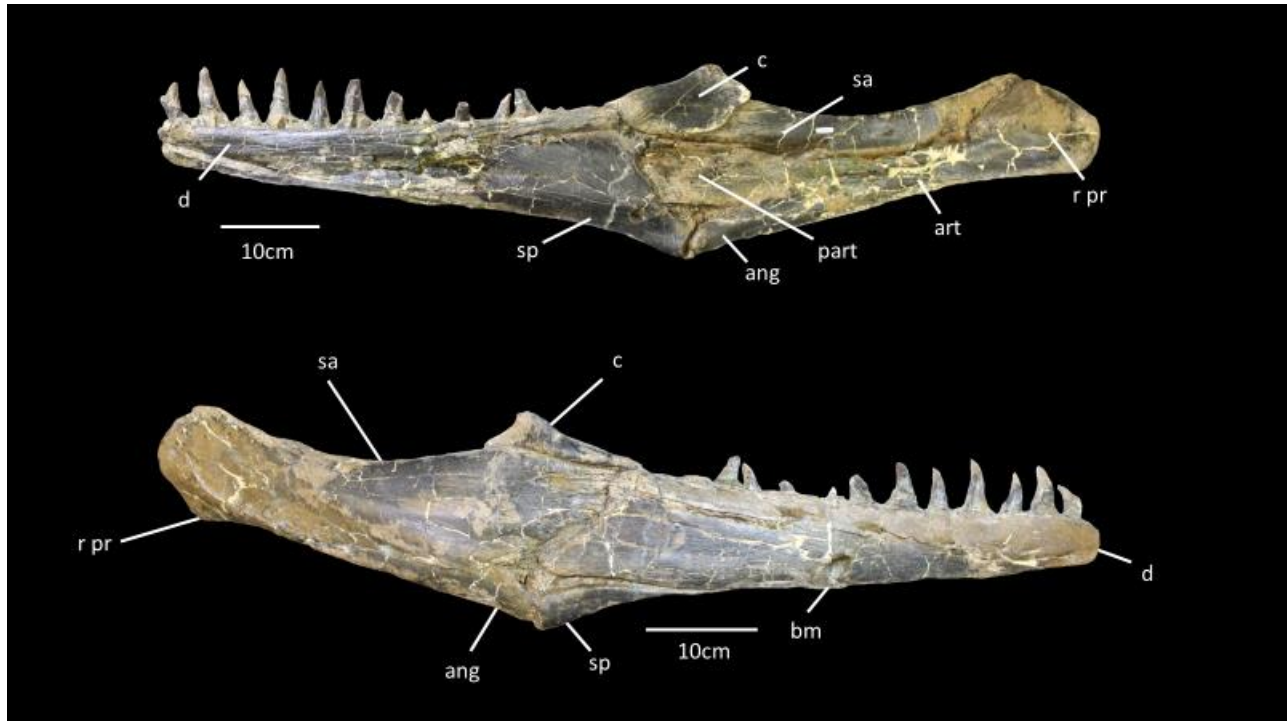


Figure 17. *Plioplatecarpus* sp. (MOR 10855) right mandible in medial (top) and lateral (bottom) views. Abbreviations: ang, angular; art, articular; bm, bite mark; c, coronoid; d, dentary; part, prearticular; r pr, retroarticular process; sa, surangular; sp, splenial. Scale bars are 10 cm.

Dentary:

Both dentaries are preserved in MOR 10855 and the left dentary is articulated with the rest of the mandibular elements (Figure 17). Like *L. willistoni*, *P. planifrons*, *P. tympaniticus*, and *Plioplatecarpus*, the dentaries of MOR 10855 each bear twelve alveoli (Konishi and Caldwell, 2007, 2011, Konishi et al., 2012). Unlike most other known plioplatecarpine mosasaurs, there is a small squared predental ramus that extends about 1 cm in front of the first dentary tooth. As in most plioplatecarpines, the meckelian groove becomes narrower anteriorly and reaches the medial symphysis of both mandibles.

Similar to *P. planifrons*, the mandibular teeth of MOR 10855 are bicarinate and curve posteromedially at about the mid-height of each crown (Konishi and Caldwell, 2007). Given the curvature of the teeth, it is unlikely that the teeth of MOR 10855 were capable of occlusion. The first seven dentary teeth curve lingually towards the symphysis of the mandibles. While the apices of the posterior dentary teeth are not preserved, their bases appear to preserve a similar trend to the condition noted in *P. nichollsae* in which the tips curve lingually (Cuthbertson et al., 2007). Only the first three dentary teeth appear to project slightly anteriorly while the rest of the teeth project dorsally from their alveoli. The missing crowns of the posterior dentary teeth prevent accurate anterior-posterior comparisons of crown height. Based on the diameter of the alveoli, it appears that tooth width was conserved throughout the length of the jaw, averaging between 1.6 and 2.2 cm. As in *P. planifrons* (Konishi and Caldwell, 2007), resorption pits are evident on the postero-lingual side of the teeth of MOR 10855.

The right dentary possesses at least nine foramina and the left dentary has approximately 10 foramina on the lateral surface for the mandibular branches of the fifth cranial nerve; the highest concentration of foramina appears between the first and fourth dentary teeth as in *P. tympaniticus* (Konishi et al., 2012). The dorsal ala of the splenial covers the posterior four fifths of the dentary, but like *P. planifrons*, leaves the anterior most section of the meckelian groove exposed (Konishi and Caldwell, 2007). Just above the dorsal edge of the splenial, approximately 2 cm of the medial side of the dentary is not covered by the splenial along its length. The dentaries of MOR 10855 lack the horizontal sulcus immediately ventral to the posterior edentulous portion of the dentary noted in *P. tympaniticus* (Konishi et al., 2012). The medial parapet is shorter than the lateral wall in the anterior portion of the dentary, but after the seventh to ninth tooth positions, the posterior medial parapet is roughly equal in height to the lateral wall

like *P. nichollsae* (Konishi and Caldwell, 2009). At its shallowest point, the dentary is around 3.5 cm deep and at its deepest point it is 9 cm deep.

Splénial:

Both splénials are preserved articulated with the rest of the mandibular elements (Figure 17). Each splénial extends below the posterior terminus of the third dentary alveolus. The posterior border of the splénial is undulatory and the dorsal and ventral corners of this margin are hooked. In overall morphology, the posterior border of each splénial is inclined anterodorsally as in most other plioplatecarpines. Similar to *L. willistoni*, the splénials of MOR 10855 each bear a conspicuous ellipsoid foramen for the inferior alveolar nerve near the ventral portion of the intramandibular joint (Konishi and Caldwell, 2011). Like *L. willistoni*, the dorsal borders of the lateral wing of both splénials are straight and taper anteriorly, consistently leaving a 2 cm margin between this border and the tooth row (Konishi and Caldwell, 2011). The cotyle of MOR 10855's splénial is a semicircular depression that bears multiple faint oblique ridges like *P. peckensis*, *P. primaevus*, and *P. houzeau* (Holmes, 1996, Lingham-Soliar, 1994). Approximately the bottom third of the splénial's total height extends beyond the ventral border of the dentary. The posterodorsal corner of the splénial buttresses the articular just below the anterior-most medial portion of the coronoid; the two elements do not touch like in *P. planifrons* (Konishi and Caldwell, 2007). Like *P. tympaniticus*, *P. primaevus*, and *P. peckensis*, the intramandibular joint is ventral to the posterior portion of the anterior surangular foramen (Holmes, 1996, Konishi et al., 2012). In contrast, the intramandibular joint occurs past the posterior extent of this foramen in *L. willistoni* and *P. houzeau* (Konishi and Caldwell, 2011, Lingham-Soliar, 1994).

Angular:

The right angular is nearly complete, save for the mediodorsal flange of bone that buttresses the medial side of the articular (Figure 17). The right angular is preserved in articulation with the rest of the mandible. Meanwhile, only the condyle of the disarticulated left angular is preserved. Like *P. peckensis*, *P. primaevus*, and *P. houzeaui*, the angular condyle bears multiple oblique ridges (Holmes, 1996, Lingham-Soliar, 1994). The medial wing of the angular is not preserved in MOR 10855. While the posteroventral-most portion of the angular is incomplete, based on the surface texture of the ventral margin of the articular, it appears to have extended to a point immediately ventral to the start of the glenoid fossa, as in *P. planifrons* and *P. houzeaui* (Konishi and Caldwell, 2007, Lingham-Soliar, 1994).

Surangular:

Both surangulars are preserved in MOR 10855 (Figure 17). The right surangular is complete and preserved in articulation with the rest of the mandible while the left surangular is an isolated element that is missing only a small portion of its anteroventral border. As in *L. willistoni* and *P. tympaniticus*, the surangular deepens anteriorly in MOR 10855 (Konishi and Caldwell, 2011, Konishi et al., 2012). The deepest point of the element is located just below the posterior end of the coronoid suture; anterior to this point, the surangular tapers similar to *P. nichollsae* (Konishi and Caldwell, 2009). The dorsal border of the surangular is concave between the coronoid suture and the glenoid fossa. As in *L. willistoni*, the anterior surangular foramen and corresponding fossa are located directly under the first third of the length of the coronoid suture.

This seems to corroborate Konishi and Caldwell's (2011) hypothesis that an anterior extension of the surangular in derived plioplatecarpines drives the increased relative length of the anterior surangular foramen and fossa. Again, like *L. willistoni*, more than one third of the coronoid suture projects anteriorly to the intramandibular joint (Konishi and Caldwell, 2011). The surangulars of MOR 10855 lack the plateau-like structure anterior to the glenoid fossa found in *P. planifrons* (Konishi and Caldwell, 2007). Resembling *P. peckensis*, the meckelian groove on the medial surface of the surangular extends to about half the element's total length.

Coronoid:

Both coronoids are preserved in MOR 10855 (Figure 17). The left coronoid is preserved as a disarticulated element and the right is preserved articulated with the rest of the mandible. In overall morphology, these elements resemble other plioplatecarpine coronoids and share a generally low profile. The ventral and dorsal borders of the lateral wings are curved and meet anteriorly to form a small upward projecting wedge, unlike the straight edges on the lateral face of *P. houzeaui*'s coronoids (Konishi and Caldwell, 2011, Lingham-Soliar 1994). The posterior process of the coronoid of MOR 10855 is rounded like *L. willistoni* and *P. peckensis*, but the angle of this process resembles *P. peckensis* and not *L. willistoni* (Konishi and Caldwell, 2011). Like *L. willistoni*, the posterior coronoid process is rounded and both the curvature and angle of this process is nearly identical to *P. peckensis*. The dorsal border of MOR 10855's coronoid more closely resembles the concave and saddle like coronoids of *Platecarpus*, *L. willistoni*, *P. nichollsae*, and *P. peckensis* than the straighter coronoids of *P. primaevus* and *P. houzeaui* (Holmes, 1996, Konishi and Caldwell, 2007, 2009, 2011, Lingham-Soliar, 1994).

Articular-Prearticular:

Both articulators are complete and articulated with the rest of each mandible (Figure 17). Like *L. willistoni*, *P. tympaniticus*, and *P. peckensis*, the posterior border of the retroarticular of MOR 10855 is rounded and becomes planar at the posteromedial corner (Konishi and Caldwell, 2007, 2011). Like *L. willistoni*, *P. nichollsae*, and *P. peckensis*, the surangular-articular suture of the glenoid fossa reaches the postero-lateral corner of the articular, which generates a similar crescent shaped articular portion of this fossa (Konishi and Caldwell, 2009, 2011). The prearticular of MOR 10855 is long, slender, and medial to the surangular while also projecting anteriorly between the splenial and dentary. This character is observed in *L. willistoni* and *P. peckensis* (Konishi and Caldwell, 2011). The articular portion of the glenoid fossa is raised from the rest of the retroarticular body in MOR 10855. The retroarticular process of MOR 10855 is not as medially extensive as *L. willistoni*, *P. planifrons*, and *P. tympaniticus* and instead bears a more symmetrical spatulate posterior margin resembling *P. primaevus* and *P. peckensis* (Holmes, 1996, Konishi and Caldwell, 2007, 2011, Konishi et al., 2012).

Post Cranial Skeleton:

Scapula:

Both scapulae and a small amount of suprascapular cartilage are preserved in MOR 10855, however the right element is better preserved than the left one (Figure 18). Like most other plioplatecarpines, the scapulae are flat and the dorsal edge of the scapular blades of MOR 10855 are curved and semicircular. The anterior portion of the scapular blade has a steep almost compressed curvature, which flattens out on its dorsal surface and then comes to a more gradual

taper at the rear of the element. The ventral surface of the scapular blade immediately posterior to the articular condyle possesses the same embayment seen in *L. willistoni*, *P. tympaniticus*, *P. houzeaui*, *P. primaevus*, and *P. peckensis* (Holmes, 1996, Konishi and Caldwell, 2011, Konishi et al., 2012, Lingham-Soliar, 1994). Further along the ventral surface of the scapula, at its posterior terminus, is a small rod of bone that is present on both scapulae and projects anteriorly. The exact function of this rod is unknown, as the gap between this cylindrical process and the ventral surface of the scapular blade is considerably narrow. The scapula and coracoid are not interdigitated and contact each other on a facet of the larger articular surface of the condyle of the glenoid fossa. From the articular condyle to the dorsal surface of the scapular blade, the scapula is 21.86 cm tall. From the anteroventral corner of the scapular blade to the posteroventral corner, the scapula is 36.27 cm wide. From the articular condyle to the dorsal surface of the coracoidal fan, the coracoid is 23.50 cm tall; and from the anteroventral corner of the anterior process of the coracoid to the posteroventral corner of the coracoidal fan, the coracoid is 28.20 cm wide. This makes the scapula and coracoid roughly equal in height, but the scapula is wider than the coracoid.

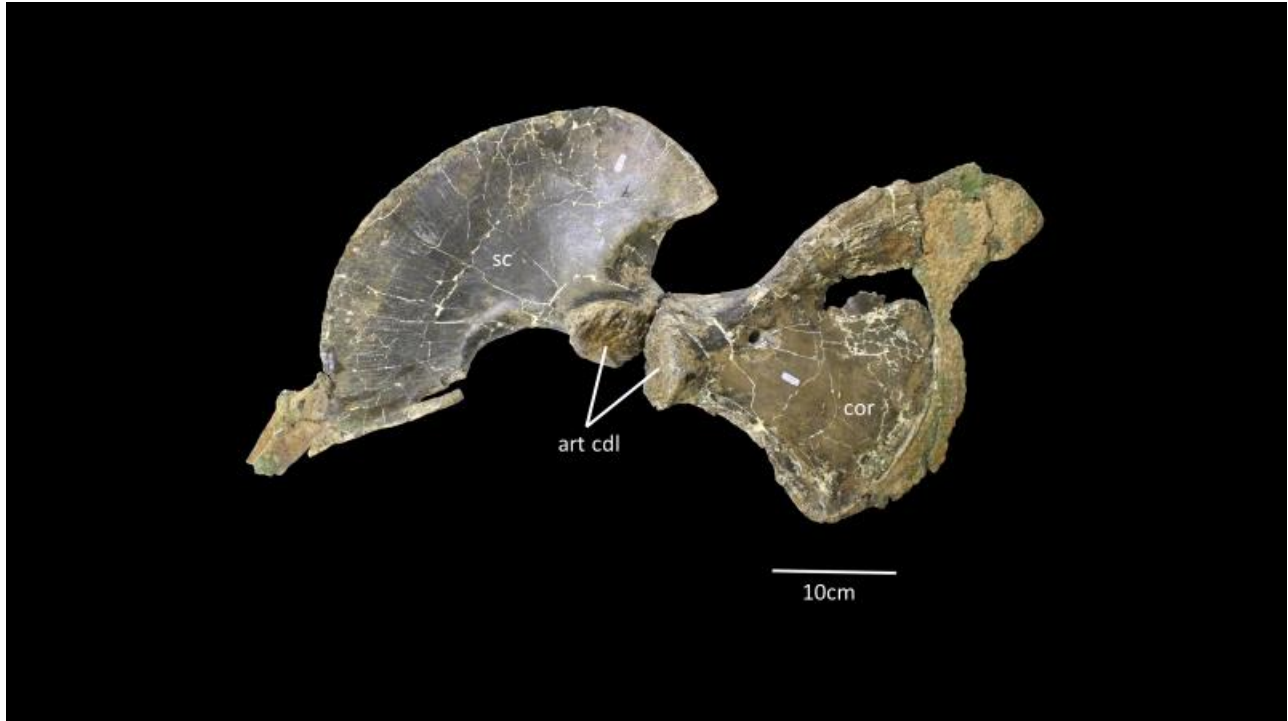


Figure 18. *Plioplatecarpus* sp. (MOR 10855) right scapula (left) and coracoid (right) in lateral view. Abbreviations: art cdl, articular condyle; cor, coracoid; sc, scapula. Scale bar is 10 cm.

Coracoid:

Both coracoids and a significant amount of sternal cartilage are preserved in MOR 10855; like the scapulae, the right element is more complete than the left (Figure 18). The anteroventral excavation on the coracoids of MOR 10855 are among the widest in any figured plioplatecarpine; the only comparable coracoids are from *P. marshi* (Lingham-Soliar, 1994). As stated above, the coracoids do not interdigitate with the scapula and instead bear a pair of large, relatively smooth, offset articular facets where they meet the scapulae and humeri. Unlike *P. primaevus* and *P. peckensis*, the anterior border of the coracoid is approximately equal in length to the posterior border (Holmes, 1996). The coracoid foramen is not notable in size and is proportionately similar compared to the foramina observed in most North American plioplatecarpines.

Ribs:

Numerous cervical and dorsal rib and rib fragments are preserved in MOR 10855. Similar to *P. peckensis*, the ribs of MOR 10855 are flat near the head of each rib and become more circular in distal cross sections (Cuthbertson and Holmes, 2015). The longest of the dorsal ribs is 45 cm from the proximal head to distal end.

PHYLOGENETIC ANALYSIS

Methods:

Because MOR 10855 displays the main *Plioplatecarpus* synapomorphies (see Diagnosis above) (Cuthbertson et al., 2007), it is confidently diagnosed as belonging to the genus, *Plioplatecarpus*. To determine how MOR 10855 relates to previously described plioplatecarpine species, this study further modified the character-taxon matrix from Cuthbertson and Holmes (2015) which is a modification of the Konishi and Caldwell (2011) dataset. *Clidastes*, *Kourisodon*, *Tylosaurus*, *Russellosaurus*, *Selmasaurus*, *Angolasaurus*, and *Tethysaurus* were all excluded from the modified character matrix for this study in order to remove less informative outgroups such as mosasaurines, tylosaurines, and plioplatecarpines that did not inhabit the Western Interior Seaway. *Plesioplatecarpus*, *Platecarpus*, *Latoplatecarpus*, and *Plioplatecarpus* were retained to reconstruct the relationship between plioplatecarpine genera from the Western Interior Seaway. “*Platecarpus somenensis*” was regarded as a junior synonym of *Plioplatecarpus nichollsae* (sensu Konishi and Caldwell 2011) and was removed from the analysis. Accordingly, 20 characters and multiple character states that coded specifically for the taxa excluded from the matrix were removed (See APPENDIX for list of removed characters and edited character states). Including MOR 10855, a total of eleven taxa were evaluated with two species,

Yaguarasuaurs columbianus and *Ectenosaurus clidastoides*, used as outgroups. MOR 10855 could be coded for 60 out of the 77 possible characters. Paup version 4.0a169 was used to run a branch-and-bound bootstrap analysis. All characters were unweighted and unordered and utilized both ACCTRAN and DELTRAN character optimizations. 77 morphological characters were used in branch and bound and bootstrap analyses using full heuristic and branch and bound searches with strict, 75%, and 90% majority rule consensus parameters. Aside from these specified parameters, all other settings relied on Paup version 4.0a169's defaults.

Results:

Both the ACCTRAN and DELTRAN optimized branch and bound analyses produced six MPT's each (see APPENDIX). A strict consensus tree with bootstrap values was generated with an ACCTRAN optimized length of 139 steps (Figure 19). The following index values were recovered for this phylogeny: consistency index (CI) = 0.8345, the retention index (RI) = 0.8034 and the rescaled consistency index (RCI) = 0.6705. Topologically, the trees recovered in this study are nearly identical to those recovered by Konishi and Caldwell (2011) and Cuthbertson and Holmes (2015). The main difference is that here, *Latoplatecarpus willistoni* is recovered as a sister to *P. nichollsae* which are both placed just outside the rest of the genus *Plioplatecarpus*. The removal of numerous extraneous taxa and associated characters from this analysis combined with the addition of MOR 10855, a basal representative of the genus *Plioplatecarpus* which displays both basal and derived features, are the likely factors driving *Latoplatecarpus*' more derived placement within the plioplatecarpine phylogenetic tree.

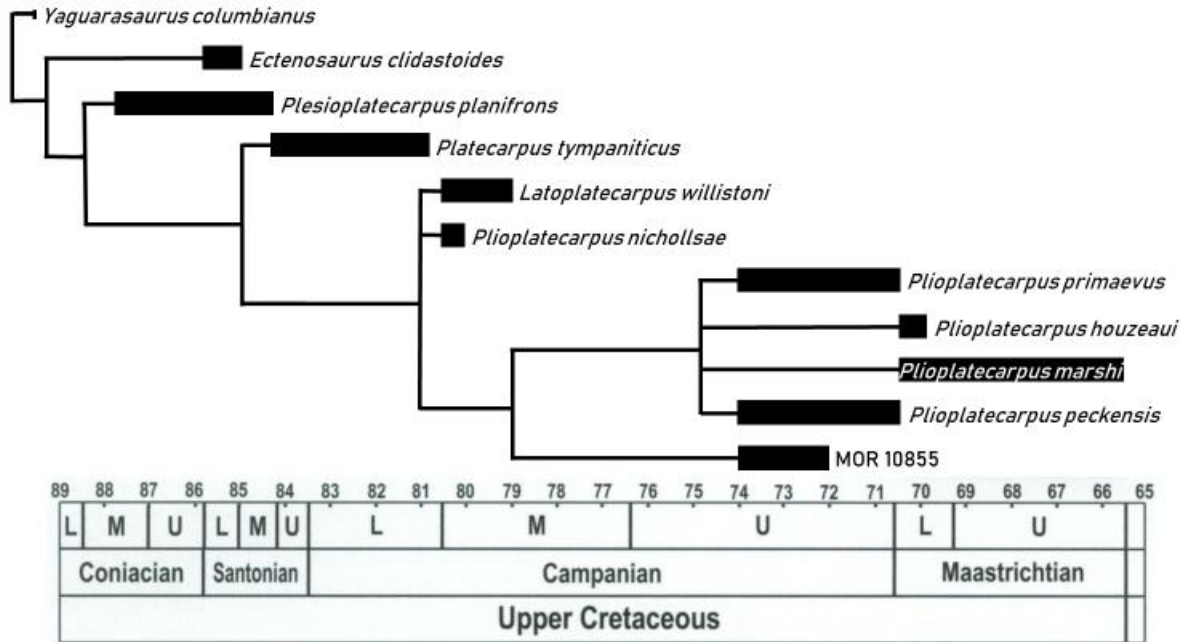


Figure 19. Strict consensus tree of Plioplatecarpinae including biostratigraphic ranges of each species.

The placement of MOR 10855 is consistent with both the stratigraphy of the evaluated taxa and the assignment to the genus *Plioplatecarpus* based on preserved diagnostic characters including, a pineal foramen whose anterior margin extends across the frontoparietal suture, the presence of a frontal plate which widens anterior to the orbits, and the lack of an otosphenoidal crest on the prootic, among other features. (see “Diagnosis” section). A unique combination of anatomical features from more basal plioplatecarpines such as *Latoplatecarpus* from the middle Campanian, including the presence of a straight frontal in lateral view (Figure A11), frontal ala whose posterior borders are transversely oriented (Figure A12), and quadrates with teardrop shaped mandibular condyles are present in MOR 10855. Simultaneously, features of the more derived species of *Plioplatecarpus* from the upper Campanian and lower Maastrichtian which includes features such as: quadrates whose cephalic condyles have straight borders that form obtuse angles with the long axis of the suprastapedial process, suprastapedial processes that are shorter than two-thirds the total quadrate’s height (Figure A15), and scapula whose condylar surfaces are

less than 30% the length of the scapular blade are also present in MOR 10855. This blend of basal and derived characters reflects MOR 10855's basal position within the more derived genus, *Plioplatecarpus*. Despite the distinct phylogenetic placement of MOR 10855 within the genus *Plioplatecarpus*, the author was unable to identify autapomorphies that would confidently distinguish this specimen from other basal species within the genus. However, the mosaic of basal and derived plioplatecarpine features present in MOR 10855 prevent its solid placement in any of the currently established species of *Plioplatecarpus*. Additionally, a number of unpublished specimens from other species such as *Latoplatecarpus willistoni* and *Plioplatecarpus peckensis* reveal the need for separate investigations assessing the degrees of individual and ontogenetic variation amongst plioplatecarpine mosasaurs. Given these factors, the author has decided not to identify MOR 10855 beyond *Plioplatecarpus sp.*

DISCUSSION

The phylogenetic analysis in this study corroborates the well documented diversity of plioplatecarpines in the Western Interior Seaway and suggests that this speciose clade of mosasaurus thrived in these habitats. While there is still a gap in the fossil record of mid Campanian plioplatecarpines, MOR 10855 serves as a close approximation of what these taxa may have looked like with a combination of basal and derived characters (Figure 19). This phylogeny also reveals the complexity of plioplatecarpine evolution which may simultaneously be obfuscated by a poor understanding of individual and ontogenetic variation in these animals. Additionally, the size and completeness of MOR 10855 grants a unique perspective into the functional morphology and ecological specializations of this taxon. The articulated nature of the skull of this specimen permits the assessment of cranial kinesis in this individual. Comparisons of cranial dimensions with other coeval mosasaurs preserved in the Bearpaw Shale facilitate

ecological interpretations regarding niche partitioning and further understanding the complexities of the this ecosystem's food web during the Late Cretaceous.

Cranial Kinesis:

Squamates are unique among tetrapods for being one of the few terrestrial vertebrates with highly kinetic skulls. Unlike other tetrapods which may exhibit varying degrees of flexibility at specific cranial sutures, many squamate clades possess numerous mobile elements that can operate on multiple kinetic axes simultaneously (Cundall, 1983, 1995, Handschuh et al., 2019, Herrel et al., 1999, 2000, Iordansky, 1996, 2011, Mezzasalma et al., 2014, Montuelle and Williams, 2015). There are three main types of kinesis commonly investigated in mosasaurs and most other squamates: mesokinesis, metakinesis, and streptostyly. The mesokinetic joint primarily consists of the frontal, prefrontal, and postorbitofrontal and allows dorso-ventral flexion of the cranium dorsal to the orbit. Next is the metakinetic joint, which consists of the parietal and supraoccipital and allows the dermatocranium overlying the braincase to flex dorso-ventrally. The last is streptostyly, which involves the quadrate and its interaction with the squamosal, supratemporal, and retroarticular that facilitates antero-posterior rotation of the quadrate and in turn, antero-posterior movement of the entire mandible. Given the phylogenetic position of mosasaurs within Squamata, historical studies have assumed mosasaurs had skulls as equally kinetic as various extant lizards and snakes (Callison, 1967, Frazetta, 1962, Russell, 1967, Williston, 1898). However, several analyses from the last two decades have demonstrated that many mosasaurs possessed considerably less kinetic, and in some cases completely akinetic, skulls that were likely rigid and inflexible (LeBlanc et al., 2013, 2019).

The anteriorly rotated quadrates that are “locked” in place by the interaction of the supratemporal and the disto-medial portion of the suprastapedial process of the quadrate likely prevented streptostyly in MOR 10855 (figures 3 and 14), as suggested for the coeval *P. peckensis* (Cuthbertson and Holmes 2015). The tall supraoccipital and large parietal articular facets on the prootic and supraoccipital, suggest a lack of metakinesis, as the contacts of these elements would have prevented dorso-ventral flexion of the skull at this axis. Additionally, the prefrontals and postorbitofrontals contact each other on the ventral surface of the frontal, suggesting a lack of mesokinesis which would have been caused by the lack of dorso-ventral flexion of these elements above the orbits. The lack of mesokinesis, metakinesis, and streptostyly in the cranium of MOR 10855 support that this taxon possessed an akinetic skull. Akinetic skulls are more common in derived mosasaurs, such as *Globidens*, *Gnathomortis*, *Plotosaurus*, and *Selmasaurus*, and likely was an adaptation for increased feeding efficiency in aquatic environments (LeBlanc et al., 2013, 2019, Lively, 2020, Wright and Shannon, 1988). The prevalence of akinetic crania among derived mosasaurs suggests a functional shift across mosasauroida towards increasingly well adapted aquatic apex predators. While not unexpected, the trend towards akinesis in a larger taxon of plioplatecarpine such as MOR 10855 mirrors the same mechanically conservative trend seen among other large members of various mosasaur clades such as the tylosaurines and mosasaurines [LeBlanc et al., 2013, 2019, Lively, 2020]. plioplatecarpines are typically considered to have less robust skulls than other mosasaurs, as suggested by features such as their small coronoids, delicate teeth, and poorly ossified braincases, however the convergence of akinetic crania among these distantly related mosasaur clades corroborates the idea of mechanical advantage provided by this loss of mobility by

preventing prey items from being deflected out of the oral cavity due to feeding in a viscous underwater environment (Callison, 1967, LeBlanc et al., 2013, Russell, 1967).

A different type of cranial kinesis, unique to squamates is intramandibular mobility where the ball and socket joint of the splenial and angular bones divide the mandible into two distinct halves. The morphology of the splenial condyles and angular cotyles suggest varying degrees of lateral and dorso-ventral motion in different mosasaur taxa. The mandibles of MOR 10855 may have been capable of bowing out laterally to a degree, as evidenced by the presence of multiple oblique ridges and grooves on the splenials and angulars of the specimen. In life this may have provided a limited advantage to suction feeding—a widespread adaptation found in multiple marine tetrapod clades including, odontocete whales, pinnipeds, auks, and turtles (Bardet et al., 2013, Enstipp et al., 2018, Gumpenberger et al., 2010, Hocking et al., 2013, 2014, Johnston and Berta, 2011, Joyce et al., 2021, Kienle et al., 2018, Lemell et al., 2002, Marshall et al., 2008, 2014, Van Damme and Aerts, 1997, Werth, 2000, 2004, 2006a, 2006b). Among extant suction feeding marine tetrapods, most taxa use this method of prey capture to consume smaller and more maneuverable prey such as cephalopods and small fish, which is consistent with the reconstructed diet of plioplatecarpines (including *Plioplatecarpus*) based on tooth morphology, stomach contents, and isotopic data (Giltaij et al., 2021, Harrell and Pérez-Huerta, 2015, Konishi et al., 2014, Massare, 1987, Schulp et al., 2013).

Plioplatecarpine Size and Ecology:

Given the size of the skull, MOR 10855 was likely twice the size of all other known species of *Plioplatecarpus* from the Bearpaw Shale (Cuthbertson and Holmes, 2015, Holmes, 1996); it was one of the largest plioplatecarpine mosasaurs in the Western Interior Seaway and possibly the entire Campanian. When scaled to other plioplatecarpines with associated

postcrania, such as *Plioplatecarpus primaevus* and *Platecarpus tympaniticus*, MOR 10855 is estimated to have a total body length between 4.5 and 6 meters. It should be noted, however, that without any vertebrae for direct comparison, the comparative scaling of MOR 10855 to *P. primaevus* and *P. tympaniticus* relies solely on cranial dimensions, namely skull length from snout to posterior termination of the squamosal.

While the size of this specimen is noteworthy, the size disparity in coeval plioplatecarpines in the Bearpaw Shale is perhaps more interesting. Adult specimens of *P. peckensis* and *P. primaevus* possess skulls that are barely half the size of MOR 10855. This size disparity between the smaller species of *Plioplatecarpus* in the Bearpaw Shale (*P. peckensis* and *P. primaevus*) and the considerably larger species MOR 10855 represents, is similar to the observed trends in extant delphinids (dolphins, pilot whales, and orcas) and physeteroids (sperm, dwarf, and pygmy sperm whales) where substantially larger orcas and sperm whales share habitats and feed alongside smaller dolphins, pygmy, and dwarf sperm whales (Silva et al., 2014). Likewise, Konishi and Caldwell (2014) have suggested niche partitioning among mosasaurs in the Bearpaw Shale before, which is corroborated by this discovery of MOR 10855 which would have coexisted with even larger mosasaurs such as *Prognathodon*, *Tylosaurus*, and *Mosasaurus* (Ikejiri and Lucas, 2015, Jiménez-Huidobro et al., 2019, Konishi et al., 2011, 2014). Based on preserved stomach contents, tooth morphology, and dental isotopes, larger tylosaurines and mosasaurines are thought to have been macropredators that regularly fed on other marine reptiles and larger fish (Konishi et al., 2011, 2014, Massare, 1987, Schulp et al., 2013). Meanwhile, smaller plioplatecarpines are evidenced as feeding on smaller fish and cephalopods (Konishi et al., 2014, Lindgren et al., 2010, Massare, 1987, Schulp et al., 2013). This niche partitioning in the Bearpaw Shale and broader Western Interior Seaway, was likely driven by a

combination of differences in diet as well as foraging depth and habitat preference with regards to distance from shorelines.

The tooth crowns of MOR 10855 are similar in overall size to those observed in *Mosasaurus conodon* and *Tylosaurus saskatchewanensis* (Ikejiri and Lucas, 2015 and Jiménez-Huidobro et al., 2019), the recurved nature of these teeth and their generally circular cross-sectional areas remain identical to the condition noted in other smaller plioplatecarpine mosasaurs, which are considered to be teuthivores and small piscivores (Massare, 1987, Schulp et al., 2013). By the end of the Campanian, there are a number of large coleoid cephalopods which had evolved and inhabited the Western Interior Seaway (Carpenter, 1996, Fuchs et al., 2020, Green, 1977, Larson and Fuchs, 2010, Miller, 1957, Miller and Walker, 1968, Nicholls and Isaak, 1987). It is possible that MOR 10855 represents an evolutionary lineage within plioplatecarpines that specialized in feeding on the larger cephalopods of the Western Interior Seaway, while the smaller, and perhaps more agile, species such as *P. peckensis* and *P. primaevus* and juveniles of larger mosasaurine and tylosaurine species fed on the diminutive and more maneuverable coleoids and belemnites. Similar trends in diet and body size disparity are observed in extant physeteroids, with the smaller species of the extant genera, *Kogia*, typically eating smaller prey items than the much larger *Physeter* (Beatson, 2007, Clarke et al., 1993, Evans and Hindell, 2004, Gaskin and Cawthorn, 1967, Gómez-Villota, 2007, Kawakami, 1980, Roberts, 2003, Santos et al., 2006, Staudinger et al., 2014, Wang et al., 2002, West et al., 2009,). While MOR 10855 represents an individual whose increased size may have afforded it a broader diet more similar to larger coeval mosasaurines and tylosaurines, its cranial and dental morphology suggest a diet that would have been consistent with other smaller and more closely

related members of *Plioplatecarpus*. In this instance, larger body and dental size does not automatically denote macropredatory tendencies in MOR 10855.

Non-Lethal Face Biting:

MOR 10855 bears two conspicuous semi-circular bite marks, both on the right side of the skull (Figure 20). One pierces into the posteroventral surface of the dentary and the other completely pierces the suborbital ramus of the jugal (Figures 20 and 21). Given the lack of any other bite marks on the skull, the presence of these two bites on the lateral-most edge of the right side of these elements, and the complimentary orientation of each bite mark (the jugal wound being angled ventrally and the dentary wound being angled dorsally), the author suggests these wounds were inflicted at the same time in a single event. The external margins of the bite mark on the dentary exhibit rounded edges, which serves as evidence of healing of a non-lethal bite (Bastiaans et al., 2020). However, the position and depth of the bite on the jugal suggests that the globe of MOR 10855's right eye may have been completely ruptured by the bite, which in turn may have directly contributed to this individual's death by impeding its hunting ability. The ellipsoidal nature of the bite marks rules out a bite caused by sharks, and the dimensions (2.7 cm wide by 1.7 cm tall by 3.1 cm deep) of the bite marks seem unlikely for any coeval osteichthyans or plesiosaurs. Specifically, the diameter of the bite marks exceed the average diameter of most polycotylid and elasmosaurid plesiosaur teeth that existed in this portion of the Western Interior Seaway. Likewise, the reconstructed gape and estimated bite forces of the larger osteichthyans that existed in the Bearpaw Shale are hypothesized by the author to have been insufficient to inflict the specific wounds observed in MOR 10855. However, the marks do compare favorably with the average measurements of the teeth of MOR 10855. Mosasaurs are known to engage in both lethal and non-lethal face biting (Bastiaans et al., 2020, Everhart, 2008) and the wounds in

MOR 10855 suggest that another large mosasaur, possibly another large plioplatecarpine, caused these bite marks. The shallow angle of these bite marks suggests that the individual which bit MOR 10855 was nearly parallel to MOR 10855 and likely slightly behind the animal when it bit (Figure 22). This may have been a failed predation attempt, territorial dispute, or possibly part of a mating or courtship ritual in which the biting individual was attempting to grab a hold of MOR 10855 in order to better position itself. Regardless of the exact scenario leading to the wounds, while this individual appears to have survived this bite, how long it continued to live after the encounter is unknown. In a scenario where the right eyeball was ruptured and the animal was rendered blind on its right side, this animal would have been unlikely to successfully hunt for itself and may have ended up starving to death.

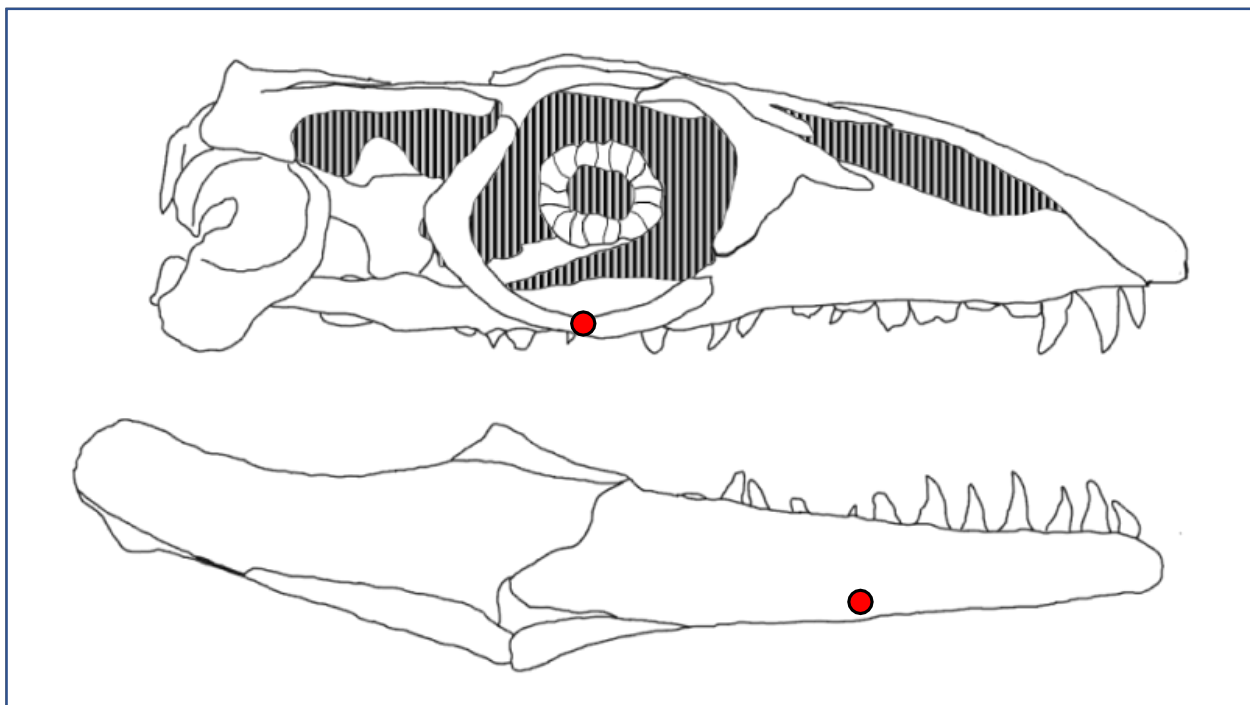


Figure 20. Right lateral view of the reconstructed skull of MOR 10855 with red circles indicating location of bite marks on the specimen.

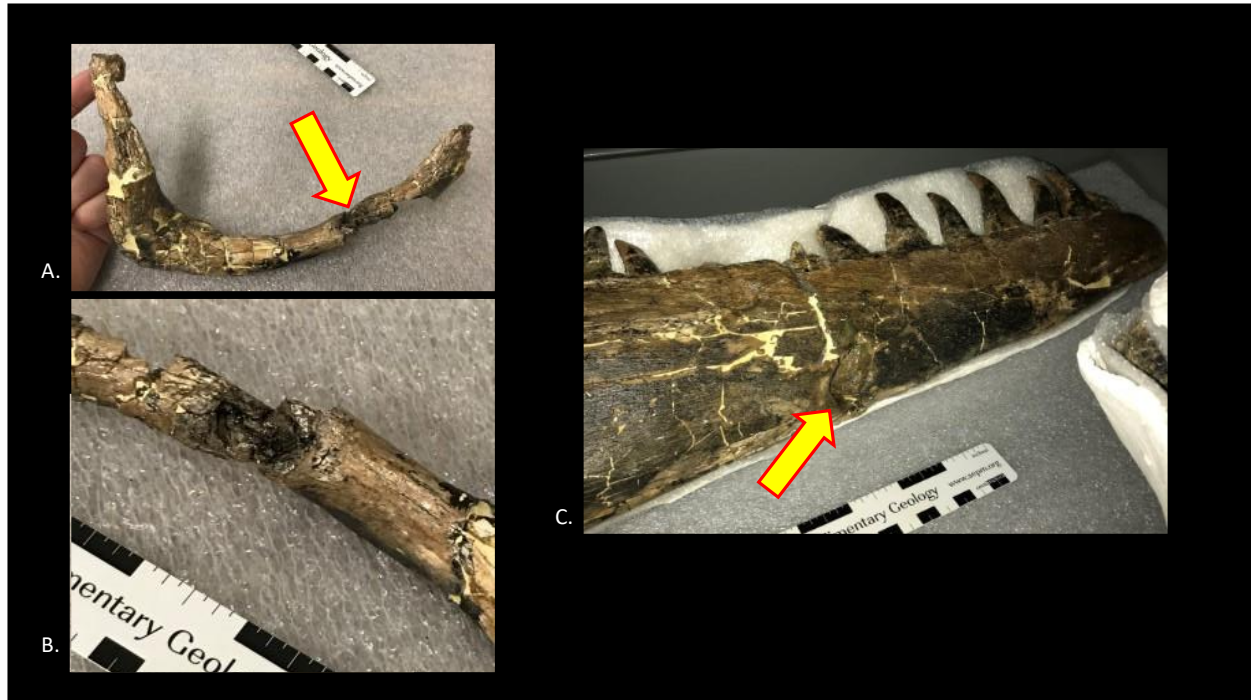


Figure 21. Photos of the right jugal and right dentary of MOR 10855 highlighting the two preserved bite marks. A. Lateral view of the right jugal with an arrow highlighting the location of the puncture wound. B. Dorsal view of the puncture wound on the right jugal. C. Oblique view of the right dentary with an arrow highlighting the location of the dorsally angled puncture wound.

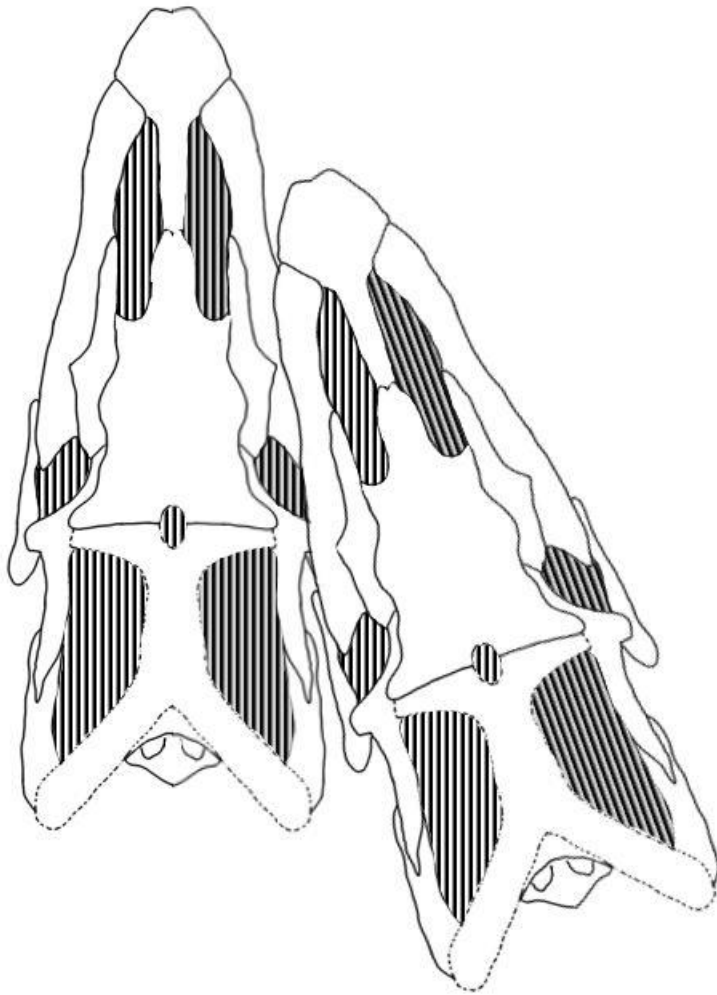


Figure 22. Hypothetical arrangement of *Plioplatecarpus* sp. skulls based on position of bite marks on MOR 10855.

CONCLUSIONS:

The discovery of MOR 10855 highlights the heightened diversity of Plioplatecarpinae in the Western Interior Seaway and suggests that the environment preserved in the Bearpaw Shale was extremely productive and capable of supporting a diverse array of large mosasaur species simultaneously. While the alpha taxonomy of this specimen remains uncertain, its confident placement in the genus *Plioplatecarpus* implies the need for a more thorough understanding of the morphologic and ontogenetic variability within the genus and clade as a whole. This study

provides insight into the morphologic combinations that could be expected from mid Campanian plioplatecarpines, of which MOR 10855 may be a late surviving exemplar. Functionally, MOR 10855 mirrors trends observed in other larger members of various mosasaur clades in the possession of an akinetic cranium which reflects an overall trend among most post-Santonian mosasaurs towards increasingly efficient feeding strategies in aquatic environments. The tooth morphology of MOR 10855 further supports the idea of niche partitioning among late Campanian mosasaurs in the Western Interior Seaway. Functionally distinct from larger coeval mosasaurs like *Prognathodon* and *Tylosaurus*, the recurved dentition of MOR 10855 suggests this specimen maintained a similar diet to smaller coeval species of *Plioplatecarpus*, consisting of cephalopods and fish. Lastly, the size disparity of this specimen and coeval relatives draws fascinating parallels to today's marine ecosystems and further demonstrates the complexity of marine food webs in the Late Cretaceous.

References:

- Bardet, N., Jalil, N. E., de Lapparent de Broin, F., Germain, D., Lambert, O., & Amaghazaz, M. (2013). A giant chelonioid turtle from the Late Cretaceous of Morocco with a suction feeding apparatus unique among tetrapods. *PLoS One*, *8*(7), e63586.
- Bastiaans, D., Kroll, J. J., Cornelissen, D., Jagt, J. W., & Schulp, A. S. (2020). Cranial palaeopathologies in a Late Cretaceous mosasaur from the Netherlands. *Cretaceous Research*, *112*, 104425.
- Beatson, E. (2007). The diet of pygmy sperm whales, *Kogia breviceps*, stranded in New Zealand: implications for conservation. *Reviews in Fish Biology and Fisheries*, *17*(2), 295-303.
- Bergstresser, T. J., & Krebs, W. N. (1983). Late Cretaceous (Campanian-Maastrichtian) diatoms from the Pierre Shale, Wyoming, Colorado and Kansas. *Journal of Paleontology*, 883-891.
- Brinkman, D., Hart, M., Jamniczky, H., & Colbert, M. (2006). *Nichollsemys baieri* gen. et sp. nov, a primitive chelonioid turtle from the late Campanian of North America. *Paludicola*, *5*(4), 111-124.
- Callison, G. 1967 Intracranial mobility in mosasaurs. *Univ. Kansas Paleont. Contr.* 26, 1–15

- Carpenter, K. (1996). *Sharon Springs Member, Pierre Shale (lower Campanian): depositional environment and origin of its vertebrate fauna, with a review of North American Cretaceous Plesiosaurs*. University of Colorado at Boulder.
- Clarke, M. R., Martins, H. R., & Pascoe, P. (1993). The diet of sperm whales (*Physeter macrocephalus* Linnaeus 1758) off the Azores. *Philosophical Transactions of the Royal Society of London. Series B: Biological Sciences*, 339(1287), 67-82.
- Cobban, W. A., Walaszczyk, I., Obradovich, J. D., & McKinney, K. C. (2006). A USGS zonal table for the Upper Cretaceous middle Cenomanian-Maastrichtian of the Western Interior of the United States based on ammonites, inoceramids, and radiometric ages. *US Geological Survey open-file report, 1250*, 46.
- Cook, T. D., Brown, E., Ralrick, P. E., & Konishi, T. (2017). A late Campanian euselachian assemblage from the Bearpaw Formation of Alberta, Canada: some notable range extensions. *Canadian Journal of Earth Sciences*, 54(9), 973-980.
- Cundall, D. (1983). Activity of head muscles during feeding by snakes: a comparative study. *American Zoologist*, 23(2), 383-396.
- Cundall, D. (1995). Feeding behaviour in *Cylindrophis* and its bearing on the evolution of alethinophidian snakes. *Journal of Zoology*, 237(3), 353-376.
- Cuthbertson, R. S., & Holmes, R. B. (2015). A new species of *Plioplatecarpus* (Mosasauridae, Plioplatecarpinae) from the Bearpaw Formation (Campanian, Upper Cretaceous) of Montana, USA. *Journal of Vertebrate Paleontology*, 35(3), e922980.
- Cuthbertson, R. S., Mallon, J. C., Campione, N. E., & Holmes, R. B. (2007). A new species of mosasaur (Squamata: Mosasauridae) from the Pierre Shale (lower Campanian) of Manitoba. *Canadian Journal of Earth Sciences*, 44(5), 593-606.
- Dollo, L. 1882. Note sur l'osteologie des Mosasauridae. Bulletin du Musee Royal d'Histoire Naturelle de Belgique 1:55-80.
- Driscoll, D. A., Dunhill, A. M., Stubbs, T. L., & Benton, M. J. (2019). The mosasaur fossil record through the lens of fossil completeness. *Palaeontology*, 62(1), 51-75.
- Enstipp, M. R., Descamps, S., Fort, J., & Grémillet, D. (2018). Almost like a whale—first evidence of suction feeding in a seabird. *Journal of Experimental Biology*, 221(13), jeb182170.
- Evans, K., & Hindell, M. A. (2004). The diet of sperm whales (*Physeter macrocephalus*) in southern Australian waters. *ICES Journal of Marine Science*, 61(8), 1313-1329.
- Everhart, M. J. (2008). A bitten skull of *Tylosaurus kansasensis* (Squamata: Mosasauridae) and a review of mosasaur-on-mosasaur pathology in the fossil record. *Transactions of the Kansas Academy of Science*, 111(3), 251-262.

- Feldmann, R. M., Franțescu, A., Franțescu, O. D., Klompmaker, A. A., Logan Jr, G., Robins, C. M., ... & Waugh, D. A. (2012). Formation of lobster-bearing concretions in the Late Cretaceous Bearpaw Shale, Montana, United States, in a complex geochemical environment. *Palaios*, 27(12), 842-856.
- Frazzetta, T. H. (1962). A functional consideration of cranial kinesis in lizards. *Journal of Morphology*, 111(3), 287-319.
- Fuchs, D., Iba, Y., Heyng, A., Iijima, M., Klug, C., Larson, N. L., & Schweigert, G. (2020). The Muensterelloidea: phylogeny and character evolution of Mesozoic stem octopods. *Papers in Palaeontology*, 6(1), 31-92.
- Gaskin, D. E., & Cawthorn, M. W. (1967). Diet and feeding habits of the sperm whale (*Physeter catodon* L.) in the Cook Strait region of New Zealand. *New Zealand Journal of Marine and Freshwater Research*, 1(2), 156-179.
- Gervais, P. 1853. Observations relatives aux reptiles fossiles de France. Comptes-rendus hebdomadaires des seances de l'Academie des Sciences, Paris 36:374–377, 470–474.
- Giltaij, T., van der Lubbe, J. H., Lindow, B., Schulp, A. S., & Jagt, J. W. (2021). Carbon isotope trends in north-west European mosasaurs (Squamata; Late Cretaceous). *Bulletin of the Geological Society of Denmark*, 69, 59-70.
- Gómez-Villota, F. (2007). *Sperm whale diet in New Zealand* (Doctoral dissertation, Auckland University of Technology).
- Green, R. G. (1977). *Niobrarateuthis walkeri*, a new species of teuthid from the Upper Cretaceous Niobrara Formation of Kansas. *Journal of Paleontology*, 992-995.
- Gumpenberger, M., Gemel, R., Lemell, P., Snelderwaard, P., Weisgram, J., & Beisser, C. J. (2010). The feeding apparatus of *Chelus fimbriatus* (Pleurodira; Chelidae)—adaptation perfected?. *Amphibia-Reptilia*, 31(1), 97-107.
- Handschuh, S., Natchev, N., Kummer, S., Beisser, C. J., Lemell, P., Herrel, A., & Vergilov, V. (2019). Cranial kinesis in the miniaturised lizard *Ablepharus kitaibelii* (Squamata: Scincidae). *Journal of Experimental Biology*, 222(9), jeb198291.
- Harrell, T. L., & Pérez-Huerta, A. (2015). Habitat preference of mosasaurs indicated by rare earth element (REE) content of fossils from the Upper Cretaceous marine deposits of Alabama, New Jersey, and South Dakota (USA). *Netherlands Journal of Geosciences*, 94(1), 145-154.
- Herrel, A., De Vree, F., Delheusy, V., & Gans, C. (1999). Cranial kinesis in gekkonid lizards. *Journal of Experimental Biology*, 202(24), 3687-3698.
- Herrel, A., Aerts, P., & De Vree, F. (2000). Cranial kinesis in geckoes: functional implications. *Journal of Experimental Biology*, 203(9), 1415-1423.

- Hocking, D. P., Evans, A. R., & Fitzgerald, E. M. (2013). Leopard seals (*Hydrurga leptonyx*) use suction and filter feeding when hunting small prey underwater. *Polar Biology*, 36(2), 211-222.
- Hocking, D. P., Salverson, M., Fitzgerald, E. M., & Evans, A. R. (2014). Australian fur seals (*Arctocephalus pusillus doriferus*) use raptorial biting and suction feeding when targeting prey in different foraging scenarios. *PloS one*, 9(11), e112521.
- Holmes, R. (1996). *Plioplatecarpus primaevus* (Mosasauridae) from the Bearpaw Formation (Campanian, Upper Cretaceous) of the North American Western Interior Seaway. *Journal of Vertebrate Paleontology*, 16(4), 673-687.
- Ikejiri, T., & Lucas, S. G. (2015). Osteology and taxonomy of *Mosasaurus conodon* Cope 1881 from the Late Cretaceous of North America. *Netherlands Journal of Geosciences*, 94(1), 39-54.
- Iordansky, N. N. (1996). The temporal ligaments and their bearing on cranial kinesis in lizards. *Journal of Zoology*, 239(1), 167-175.
- Iordansky, N. N. (2011). Cranial kinesis in lizards (Lacertilia): origin, biomechanics, and evolution. *Biology Bulletin*, 38(9), 868-877.
- Jiménez-Huidobro, P., Caldwell, M. W., Paparella, I., & Bullard, T. S. (2019). A new species of tylosaurine mosasaur from the upper Campanian Bearpaw Formation of Saskatchewan, Canada. *Journal of Systematic Palaeontology*, 17(10), 849-864.
- Johnston, C., & Berta, A. (2011). Comparative anatomy and evolutionary history of suction feeding in cetaceans. *Marine Mammal Science*, 27(3), 493-513.
- Joyce, W. G., Rollot, Y., Evers, S. W., Lyson, T. R., Rahantarisoa, L. J., & Krause, D. W. (2021). A new pelomedusoid turtle, *Sahonachelys mailakavava*, from the Late Cretaceous of Madagascar provides evidence for convergent evolution of specialized suction feeding among pleurodires. *Royal Society open science*, 8(5), 210098.
- Kawakami, T. A. K. E. H. I. K. O. (1980). A review of sperm whale food. *Sci. Rep. Whales Res. Inst*, 32, 199-218.
- Kienle, S. S., Hermann-Sorensen, H., Costa, D. P., Reichmuth, C., & Mehta, R. S. (2018). Comparative feeding strategies and kinematics in phocid seals: suction without specialized skull morphology. *Journal of Experimental Biology*, 221(15), jeb179424.
- Konishi, T., Brinkman, D. (2016). Non-lethal face biting between mosasaurs (Squamata: Mosasauridae): The first unequivocal evidence from an exceptional skeleton of *Mosasaurus* sp. from Southern Alberta, Canada. Society of Vertebrate Paleontology Annual Conference 2016 abstract book.
- Konishi, T., Brinkman, D., Massare, J. A., & Caldwell, M. W. (2011). New exceptional specimens of *Prognathodon overtoni* (Squamata, Mosasauridae) from the upper Campanian

of Alberta, Canada, and the systematics and ecology of the genus. *Journal of Vertebrate Paleontology*, 31(5), 1026-1046.

Konishi, T., & Caldwell, M. W. (2007). New specimens of *Platecarpus planifrons* (Cope, 1874)(Squamata: Mosasauridae) and a revised taxonomy of the genus. *Journal of Vertebrate Paleontology*, 27(1), 59-72.

Konishi, T., & Caldwell, M. W. (2009). New material of the mosasaur *Plioplatecarpus nichollsae* Cuthbertson et al., 2007, clarifies problematic features of the holotype specimen. *Journal of Vertebrate Paleontology*, 29(2), 417-436.

Konishi, T., & Caldwell, M. W. (2011). Two new plioplatecarpine (Squamata, Mosasauridae) genera from the Upper Cretaceous of North America, and a global phylogenetic analysis of plioplatecarpines. *Journal of Vertebrate Paleontology*, 31(4), 754-783.

Konishi, T., Caldwell, M. W., Nishimura, T., Sakurai, K., & Tanoue, K. (2016). A new halisaurine mosasaur (Squamata: Halisaurinae) from Japan: the first record in the western Pacific realm and the first documented insights into binocular vision in mosasaurs. *Journal of Systematic Palaeontology*, 14(10), 809-839.

Konishi, T., Lindgren, J., Caldwell, M. W., & Chiappe, L. (2012). *Platecarpus tympaniticus* (Squamata, Mosasauridae): osteology of an exceptionally preserved specimen and its insights into the acquisition of a streamlined body shape in mosasaurs. *Journal of Vertebrate Paleontology*, 32(6), 1313-1327.

Konishi, T., Newbrey, M. G., & Caldwell, M. W. (2014). A small, exquisitely preserved specimen of *Mosasaurus missouriensis* (Squamata, Mosasauridae) from the upper Campanian of the Bearpaw Formation, western Canada, and the first stomach contents for the genus. *Journal of Vertebrate Paleontology*, 34(4), 802-819.

Kubo, T., Mitchell, M. T., & Henderson, D. M. (2012). *Albertonectes vanderveldei*, a new elasmosaur (Reptilia, Sauropterygia) from the Upper Cretaceous of Alberta. *Journal of Vertebrate Paleontology*, 32(3), 557-572.

Larson, N. L., & Fuchs, D. (2010). Fossil coleoids from the Late Cretaceous (Campanian & Maastrichtian) of the Western Interior. *Ferrantia*, 59, 78-113.

LeBlanc, A. R., Caldwell, M. W., & Lindgren, J. (2013). Aquatic adaptation, cranial kinesis, and the skull of the mosasaurine mosasaur *Plotosaurus bennisoni*. *Journal of Vertebrate Paleontology*, 33(2), 349-362.

Leblanc, A. R., Mohr, S. R., & Caldwell, M. W. (2019). Insights into the anatomy and functional morphology of durophagous mosasaurines (Squamata: Mosasauridae) from a new species of *Globidens* from Morocco. *Zoological Journal of the Linnean Society*, 186(4), 1026-1052.

- Lemell, P., Lemell, C., Snelderwaard, P., Gumpenberger, M., Woche-sländer, R., & Weisgram, J. (2002). Feeding patterns of *Chelus fimbriatus* (Pleurodira: Chelidae). *Journal of Experimental Biology*, 205(10), 1495-1506.
- Lindgren, J., Caldwell, M. W., Konishi, T., & Chiappe, L. M. (2010). Convergent evolution in aquatic tetrapods: insights from an exceptional fossil mosasaur. *PLoS one*, 5(8), e11998.
- Lindgren, J., Everhart, M. J., & Caldwell, M. W. (2011). Three-dimensionally preserved integument reveals hydrodynamic adaptations in the extinct marine lizard *Ectenosaurus* (Reptilia, Mosasauridae). *PLoS One*, 6(11), e27343.
- Lingham-Soliar, T. 1994. The mosasaur *Plioplatecarpus* (Reptilia, Mosasauridae) from the Upper Cretaceous of Europe. *Bulletin de L'Institute Royal des Sciences Naturelles de Belgique*. 64: 177–211.
- Lively, J. R. (2020). Redescription and phylogenetic assessment of 'Prognathodon' *stadtmani*: implications for Globidensini monophyly and character homology in Mosasaurinae. *Journal of Vertebrate Paleontology*, 40(3), e1784183.
- Marshall, C. D., Kovacs, K. M., & Lydersen, C. (2008). Feeding kinematics, suction and hydraulic jetting capabilities in bearded seals (*Erignathus barbatus*). *Journal of Experimental Biology*, 211(5), 699-708.
- Marshall, C. D., Wieskotten, S., Hanke, W., Hanke, F. D., Marsh, A., Kot, B., & Dehnhardt, G. (2014). Feeding kinematics, suction, and hydraulic jetting performance of harbor seals (*Phoca vitulina*). *PLoS One*, 9(1), e86710.
- Massare, J. A. (1987). Tooth morphology and prey preference of Mesozoic marine reptiles. *Journal of Vertebrate Paleontology*, 7(2), 121-137.
- Mezzasalma, M., Maio, N., & Guarino, F. M. (2014). To move or not to move: cranial joints in European gekkotans and lacertids, an osteological and histological perspective. *The Anatomical Record*, 297(3), 463-472.
- Miller, H. W. (1957). *Niobrarateuthis bonneri*, a new genus and species of squid from the Niobrara Formation of Kansas. *Journal of Paleontology*, 809-811.
- Miller, H. W., & Walker, M. V. (1968). *Enchoteuthis melanae* and *Kansasteuthis lindneri*, New Genera and Species of Teuthids, and a Sepiid from the Niobrara Formation of Kansas. *Transactions of the Kansas Academy of Science (1903-)*, 71(2), 176-183.
- Montuelle, S. J., & Williams, S. H. (2015). In vivo measurement of mesokinesis in Gekko gecko: the role of cranial kinesis during gape display, feeding and biting. *PLoS One*, 10(7), e0134710.
- Nicholls, E. L., & Isaak, H. (1987). Stratigraphic and taxonomic significance of *Tusoteuthis longa* Logan (Coleoidea, Teuthida) from the Pembina Member, Pierre Shale (Campanian), of Manitoba. *Journal of Paleontology*, 61(4), 727-737.

- Oelrich, T. M. (1956). The anatomy of the head of *Ctenosaura pectinata* (Iguanidae).
- Oppel, M. 1811. Die Ordnungen, Familien, und Gattungen der Reptilien als Prodrum einer Naturgeschichte derselben, J. Lindauer, Munich, 86 pp.
- Palamarczuk, S., & Landman, N. H. (2011). Dinoflagellate cysts from the upper Campanian Pierre Shale and Bearpaw shale of the US Western Interior. *Rocky Mountain Geology*, 46(2), 137-164.
- Palci, A., Konishi, T., & Caldwell, M. W. (2020). A comprehensive review of the morphological diversity of the quadrate bone in mosasauroids (Squamata: Mosasauridae), with comments on the homology of the infrastapedial process. *Journal of Vertebrate Paleontology*, 40(6), e1879101.
- Polcyn, M. J., and G. L. Bell. 2005. *Russellosaurus coheni* n. gen., n. sp., a 92 million year old mosasaur from Texas (USA), and the definition of the parafamily Russellosaurina. *Netherlands Journal of Geosciences* 84:321–333.
- Polcyn, M. J., & Everhart, M. J. (2008). Description and phylogenetic analysis of a new species of *Selmasaurus* (Mosasauridae: Plioplatecarpinae) from the Niobrara Chalk of western Kansas. In *Proceedings of the Second Mosasaur Meeting* (Vol. 2008, pp. 13-28). Fort Hayes Studies, Special.
- Polcyn, M. J., Jacobs, L. L., Araújo, R., Schulp, A. S., & Mateus, O. (2014). Physical drivers of mosasaur evolution. *Palaeogeography, Palaeoclimatology, Palaeoecology*, 400, 17-27.
- Roberts, S. M. (2003). Examination of the stomach contents from a Mediterranean sperm whale found south of Crete, Greece. *Journal of the Marine Biological Association of the United Kingdom*, 83(3), 667-670.
- Russell, D. A. 1967 Systematics and morphology of American mosasaurs. *Bull. Peabody Mus. nat. Hist.* 23, 1–237.
- Santos, M. B., Pierce, G. J., Lopez, A., Reid, R. J., Ridoux, V., & Mente, E. (2006). Pygmy sperm whales *Kogia breviceps* in the Northeast Atlantic: New information on stomach contents and strandings. *Marine Mammal Science*, 22(3), 600-616.
- Sato, T. (2003). Description of plesiosaurs (Reptilia: Sauropterygia) from the Bearpaw Formation (Campanian-Maastrichtian) and a phylogenetic analysis of the Elasmosauridae.
- Sato, T. (2005). A new polycotyloid plesiosaur (Reptilia: sauropterygia) from the Upper Cretaceous Bearpaw Formation in Saskatchewan, Canada. *Journal of Paleontology*, 79(5), 969-980.
- Schulp, A. S., Vonhof, H. B., Van der Lubbe, J. H. J. L., Janssen, R., & Van Baal, R. R. (2013). On diving and diet: resource partitioning in type-Maastrichtian mosasaurs. *Netherlands Journal of Geosciences*, 92(2-3), 165-170.

- Serratos, D. J., Druckenmiller, P., & Benson, R. B. (2017). A new elasmosaurid (Sauropterygia, Plesiosauria) from the Bearpaw Shale (Late Cretaceous, Maastrichtian) of Montana demonstrates multiple evolutionary reductions of neck length within Elasmosauridae. *Journal of Vertebrate Paleontology*, 37(2), e1278608.
- Silva, M. A., Prieto, R., Cascão, I., Seabra, M. I., Machete, M., Baumgartner, M. F., & Santos, R. S. (2014). Spatial and temporal distribution of cetaceans in the mid-Atlantic waters around the Azores. *Marine Biology Research*, 10(2), 123-137.
- Staudinger, M. D., McAlarney, R. J., McLellan, W. A., & Ann Pabst, D. (2014). Foraging ecology and niche overlap in pygmy (*Kogia breviceps*) and dwarf (*Kogia sima*) sperm whales from waters of the US mid-Atlantic coast. *Marine Mammal Science*, 30(2), 626-655.
- Sternberg, C. M. (1933). XXIX.—Relationships and habitat of *Troödon* and the Nodosours. *Annals and Magazine of Natural History*, 11(62), 231-235.
- Street, H. P., Bamforth, E. L., & Gilbert, M. M. (2019). The formation of a marine bonebed at the Upper Cretaceous Dinosaur Park-Bearpaw transition of west-central Saskatchewan, Canada. *Frontiers in Earth Science*, 7, 209.
- Tourtelot, H. A. (1962). *Preliminary investigation of the geologic setting and chemical composition of the Pierre Shale, Great Plains region*. US Government Printing Office.
- Van Damme, J., & Aerts, P. (1997). Kinematics and functional morphology of aquatic feeding in Australian snake-necked turtles (Pleurodira; Chelodina). *Journal of Morphology*, 233(2), 113-125.
- Wang, M. C., Walker, W. A., Shao, K. T., & Chou, L. S. (2002). Comparative Analysis of the Diets of Pygmy Sperm Whales and Dwarf Sperm Whales in Taiwanese Waters. *Acta Zoologica Taiwanica*, 13(2), 53-62.
- Werth, A. (2000). A kinematic study of suction feeding and associated behavior in the long-finned pilot whale, *Globicephala melas* (Traill). *Marine Mammal Science*, 16(2), 299-314.
- Werth, A. J. (2004). Functional morphology of the sperm whale (*Physeter macrocephalus*) tongue, with reference to suction feeding. *Aquatic Mammals*, 30(3), 405-418.
- Werth, A. J. (2006a). Mandibular and dental variation and the evolution of suction feeding in Odontoceti. *Journal of Mammalogy*, 87(3), 579-588.
- Werth, A. J. (2006b). Odontocete suction feeding: experimental analysis of water flow and head shape. *Journal of Morphology*, 267(12), 1415-1428.
- West, K., Walker, W., Baird, R., White, W., Levine, G., Brown, E., & Schofield, D. (2009). Diet of pygmy sperm whales (*Kogia breviceps*) in the Hawaiian Archipelago. *Publications, Agencies and Staff of the US Department of Commerce*, 18.

Wright, K. R., & Shannon, S. W. (1988). *Selmasaurus rosselli*, a new plioplatecarpine mosasaur (Squamata, Mosasauridae) from Alabama. *Journal of Vertebrate Paleontology*, 8(1), 102-107.

Williston, S. W. 1897. Range and distribution of the mosasaurs. *Kansas University Quarterly* 6:39–41.

Williston, S. W. 1898. Mosasaurs. University Geological Survey of Kansas 4:83–221.

APPENDIX:

Matrix Addendums: The following characters were removed from the original Konishi and Caldwell (2011) matrix: 8, 22, 34, 46, 49, 63, 66, 69, 70, 72, 73, 79, 81, 83, 87, 89, 92, 94, 95, and 96. The following character states have been edited in the following characters: Character 1 (state 3 was removed), 2 (state 2 was removed), 3 (states 3 and 5 were removed: state 4 is now 3), 19 (states 5 and 6 were removed), 21 (states 0 and 5 were removed: state 1 is now 0, state 2 is now 1, state 3 is now 2, and state 4 is now 3), 23 (state 2 was removed: state 3 is now state 2 and state 4 is now state 3), 26 (states 3 and 4 were removed), 30 (state 2 was removed), 35 (state 0 was removed: state 1 is now state 0 and state 2 is now state 1), 37 (states 0 and 3 were removed: state 1 is now state 0, state 2 is now state 1, and state 4 is now state 2), 38 (state 1 was removed: state 2 is now state 1 and state 3 is now state 2), 40 (state 0 was removed: state 1 is now state 0 and state 2 is now state 1), 41 (states 0, 2, 3, and 7 were removed: state 1 is now state 0, state 4 is now state 1, state 5 is now state 2, and state 6 is now state 3), 42 (state 3 was removed), 47 (state 4 was removed), 48 (state 2 was removed), 50 (state 2 was removed), 55 (states 2 and 3 were removed), 56 (state 1 was removed: state 2 is now state 1), 60 (state 3 was removed), 62 (states 0 and 2 were removed: state 1 is now state 0 and state 3 is now state 1), 78 (states 0 and 1 were removed: state 2 became state 0 and state 3 became state 1), 84 (state 1 was removed: state 2 became state 1), 88 (states 1 and 3 were removed: state 2 became state 1), 97 (state 0 was removed: state 1 became state 0, state 2 became state 1, and state 3 became state 2).

Character Matrix:

Character matrix modified from Cuthbertson and Holmes, 2015:

'Yaguarasaurus columbianus'

10000 11100 01111 20000 0??11 10?0? 0010? 00?10 010?0 00??0 ??00? ????? 0???? ?????
???01 00

'Ectenosaurus clidastoides'

(12)0310 20101 01111 00100 0??00 200?? 0?22? ?1000 000?0 ?0011 1?000 00?00 0?100 ?00?1
01001 0?

'Plesioplatecarpus planifrons '

00000 01010 01111 10200 100?0 20000 00010 11110 000?1 10010 00000 00000 1?000 000??
0??01 01

'Platecarpus tympaniticus'

00100 01011 01001 (01)131(03) 10000 20000 1001(01) 21211 10111 10010 00110 01000 ?0100
10000 00011 12

'Latoplatecarpus willistoni'

00201 01022 01300 123(12)0 20?00 10000 10000 21311 10311 10010 00(12)10 11110 1?100
1???? ???21 ?2

'Plioplatecarpus nichollsae'

00201 01022 00201 12321 20100 ?????1 10001 21211 103?1 10??0 0?21? ??110 11100 1101?
???21 ??

'Plioplatecarpus primaevus'

00201 ?1022 11301 22422 31120 0????1 21202 31221 10300 11010 01222 21110 211(12)(12)
21120 10121 ?2

'Plioplatecarpus houzeau'

???01 0?022 11301 22422 31?00 01?21 21202 31321 10101 20?(01)? ?1222 11111 2?123 2????
???2(01) 12

'Plioplatecarpus marshi'

0120? 1?022 ?0201 0???? ?1??? ?1?21 21??1 3?3?1 1?20? ??120 02222 ?????1 21123 ??12?
???2(01) 12

'Plioplatecarpus peckensis'

?1?01 01022 11301 22422 31120 ?????1 2?202 31321 10311 10??? ????? ?????1 ????? ?????
???21 11

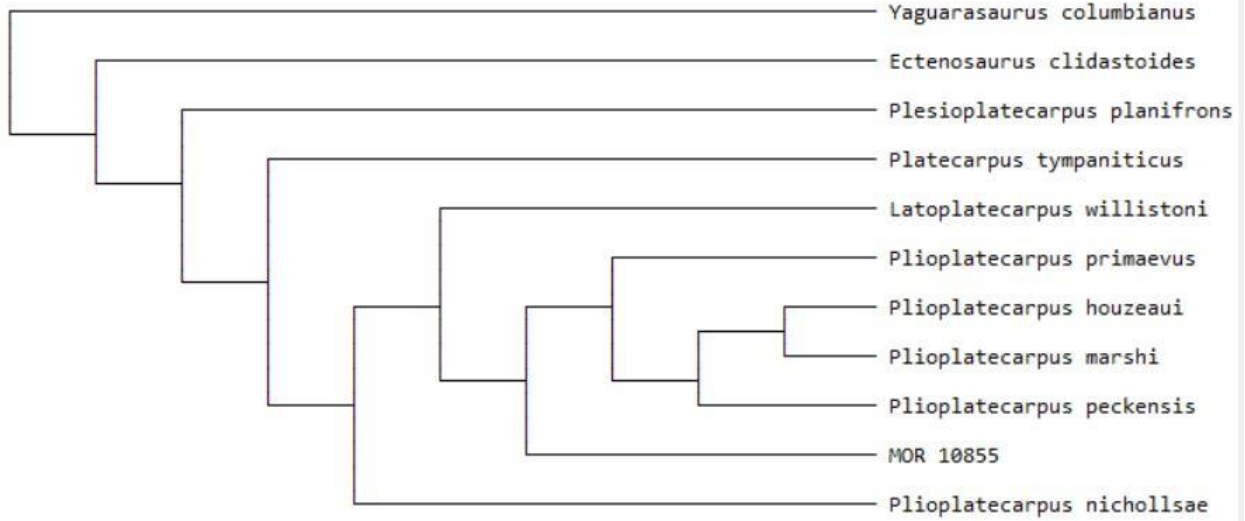
'MOR 10855'

00201 01022 01301 12??? ??120 1?021 21200 21311 00301 1001(01) 01221 2101? ??120 2????
???21 1?

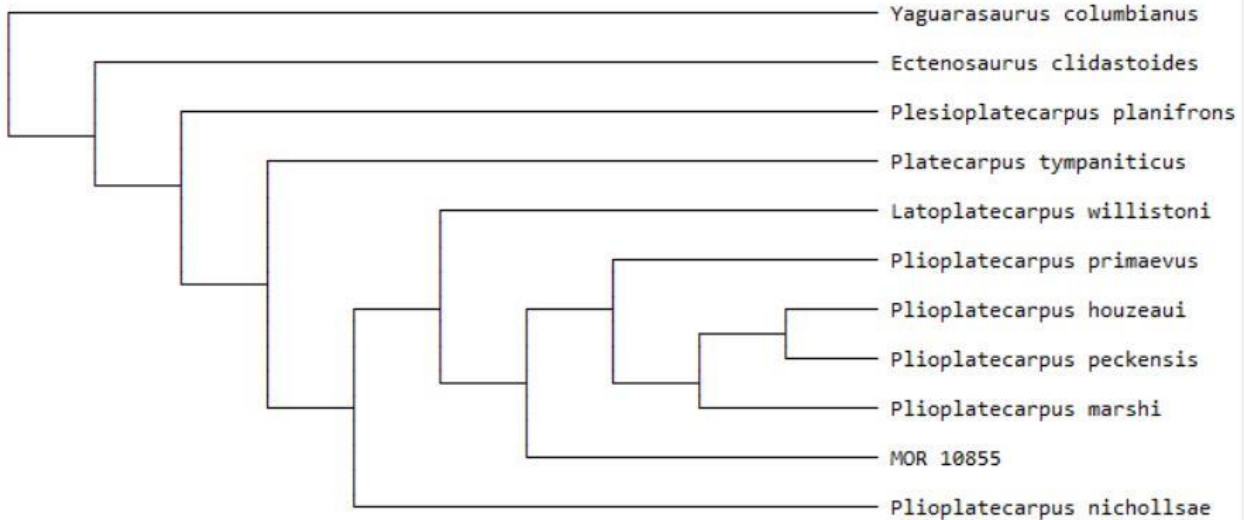
Recovered Trees:

Figure A1. Results of Branch and Bound Analysis with ACCTRAN optimization

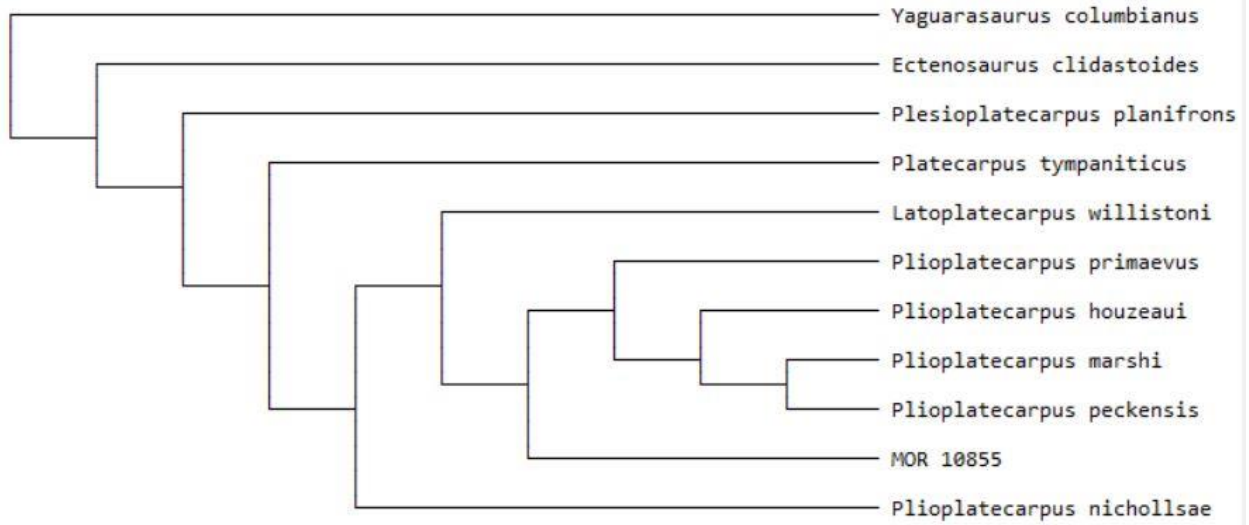
Tree 1 (rooted using default outgroup)



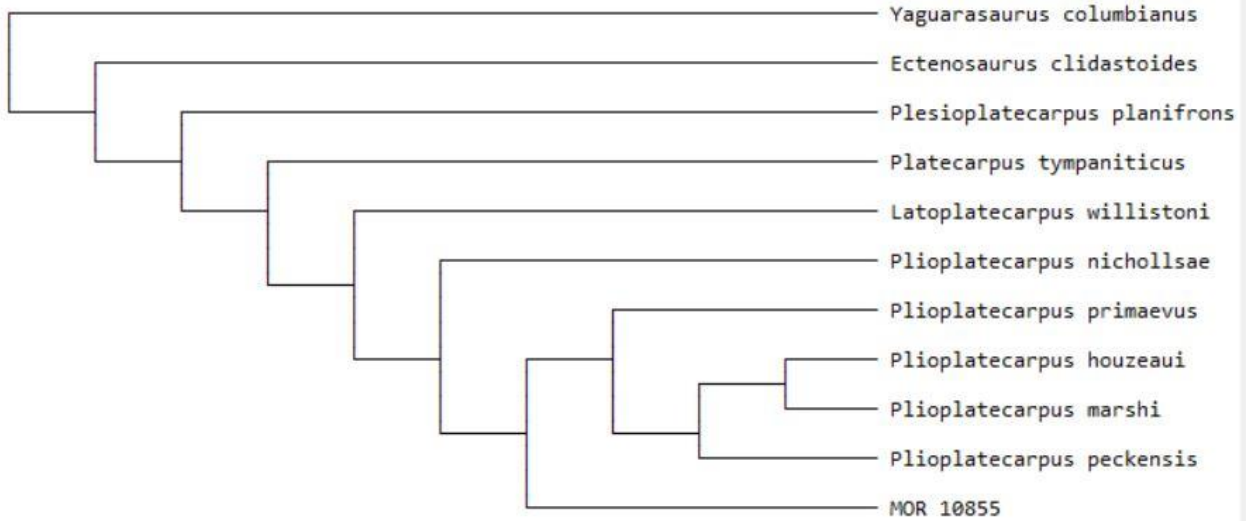
Tree 2 (rooted using default outgroup)



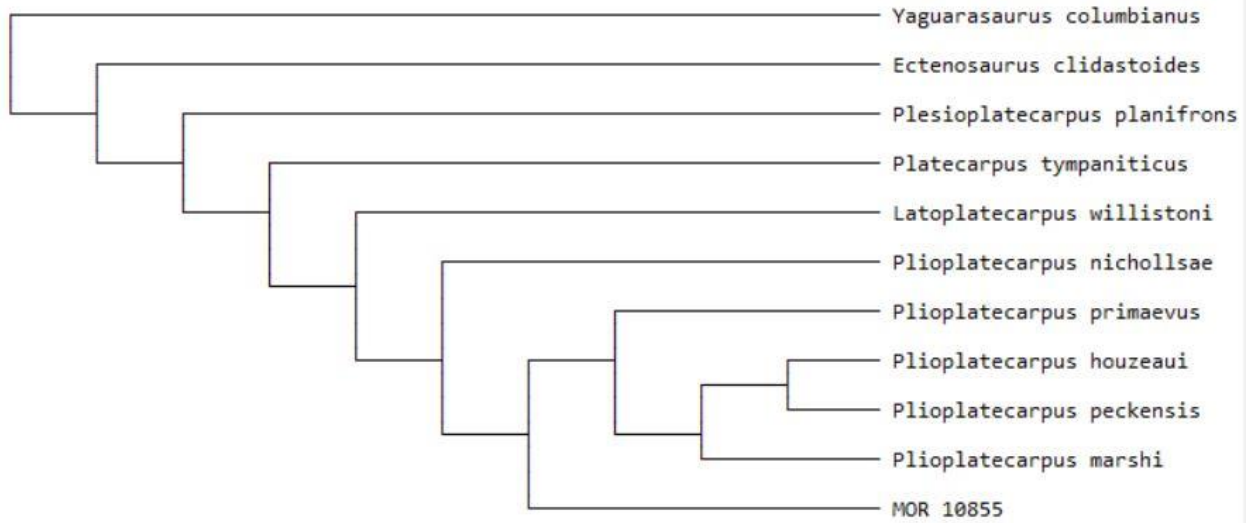
Tree 3 (rooted using default outgroup)



Tree 4 (rooted using default outgroup)



Tree 5 (rooted using default outgroup)



Tree 6 (rooted using default outgroup)

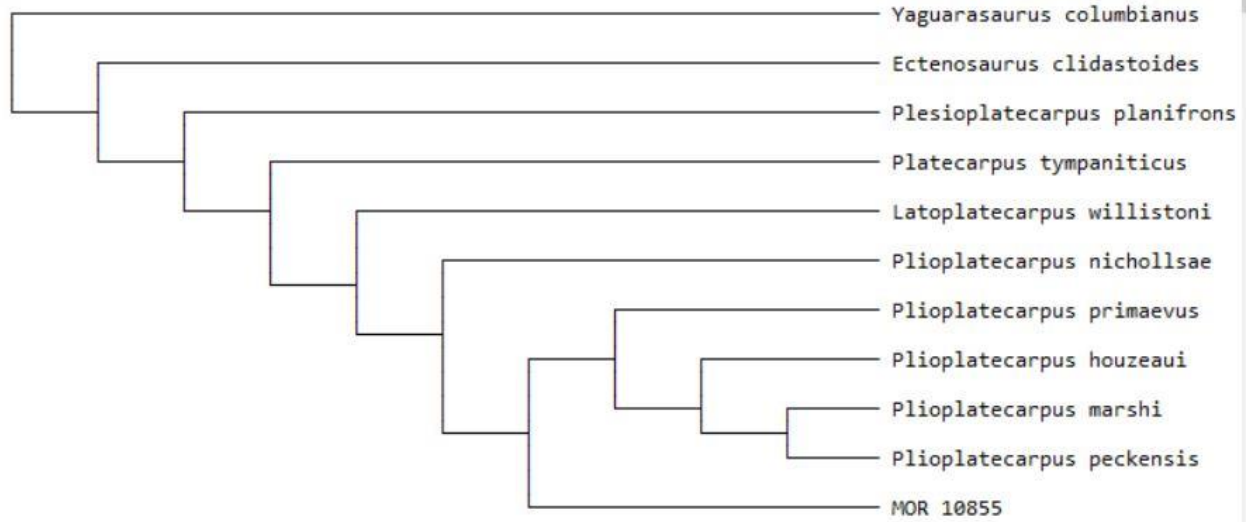
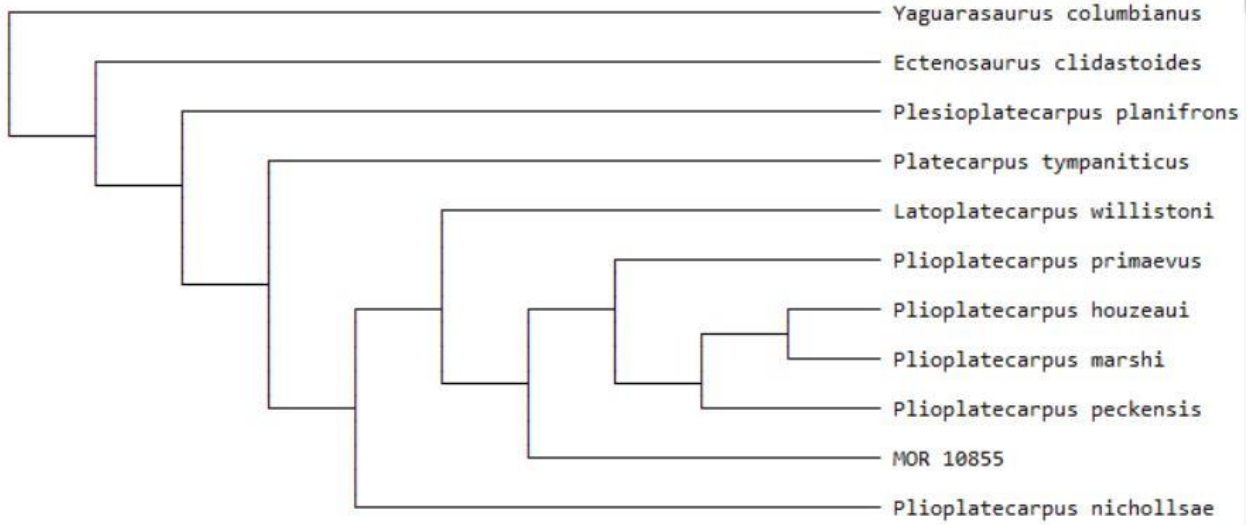
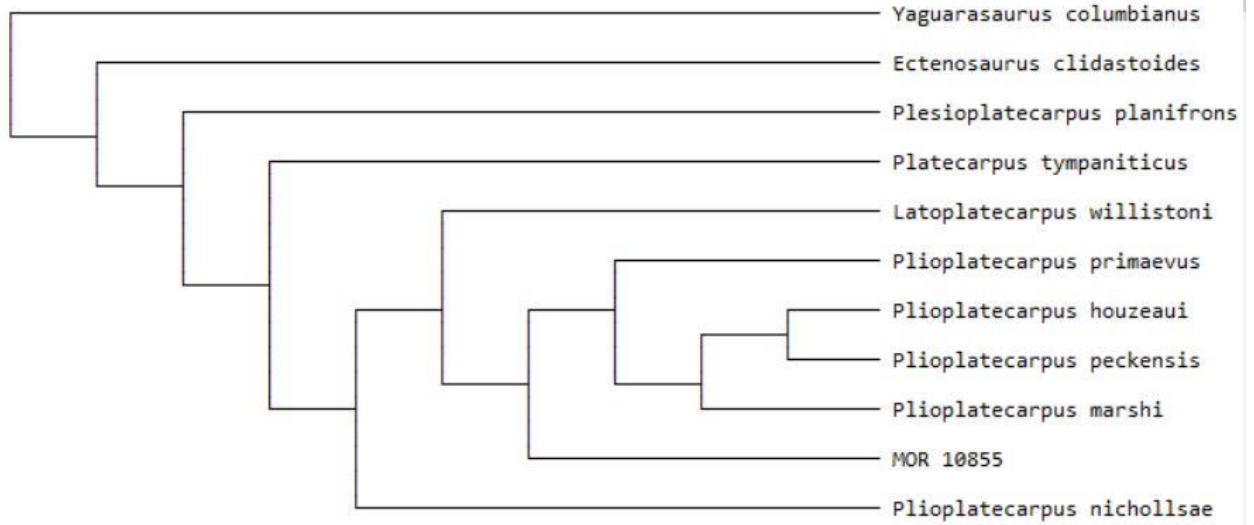


Figure A2. Results of Branch and Bound Analysis with DELTRAN optimization

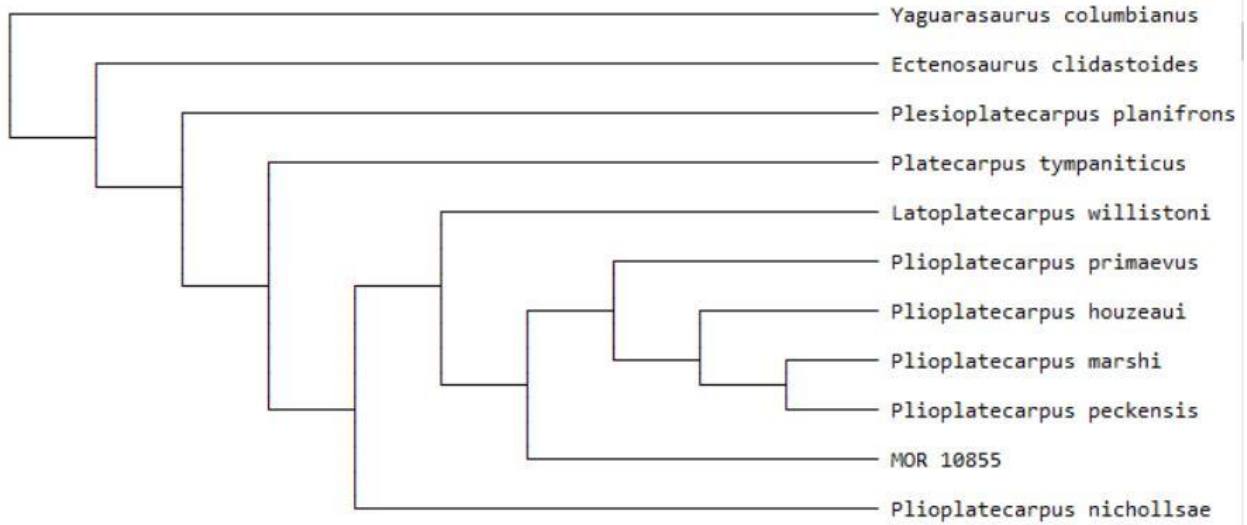
Tree 1 (rooted using default outgroup)



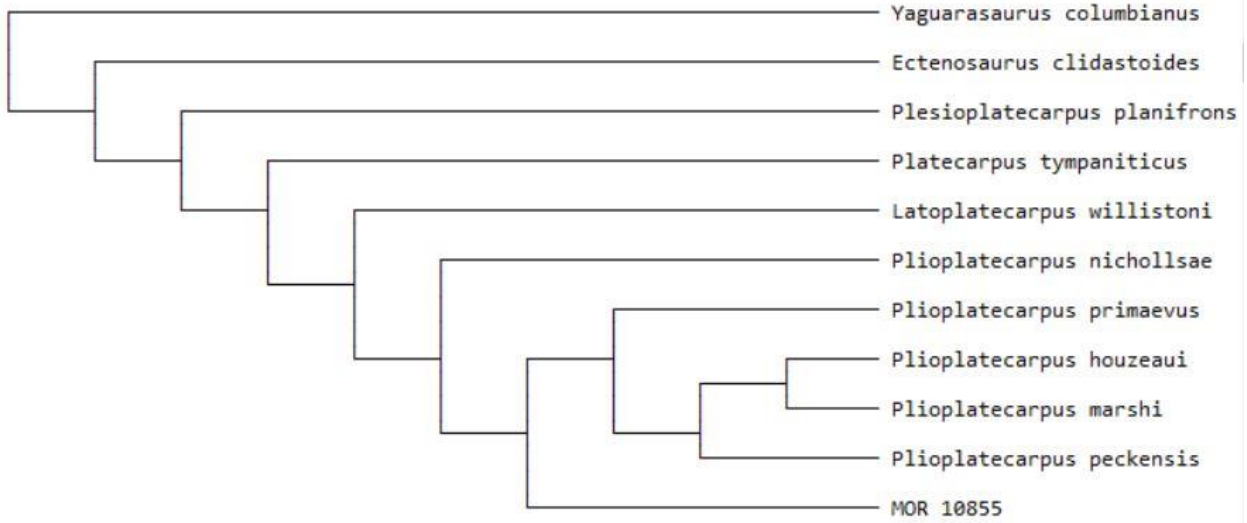
Tree 2 (rooted using default outgroup)



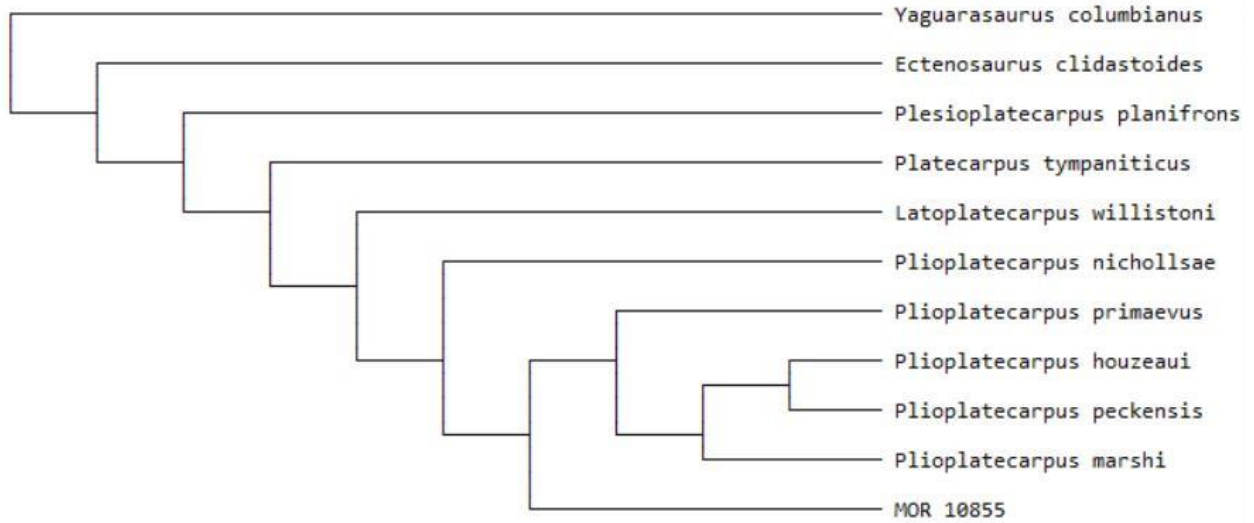
Tree 3 (rooted using default outgroup)



Tree 4 (rooted using default outgroup)



Tree 5 (rooted using default outgroup)



Tree 6 (rooted using default outgroup)

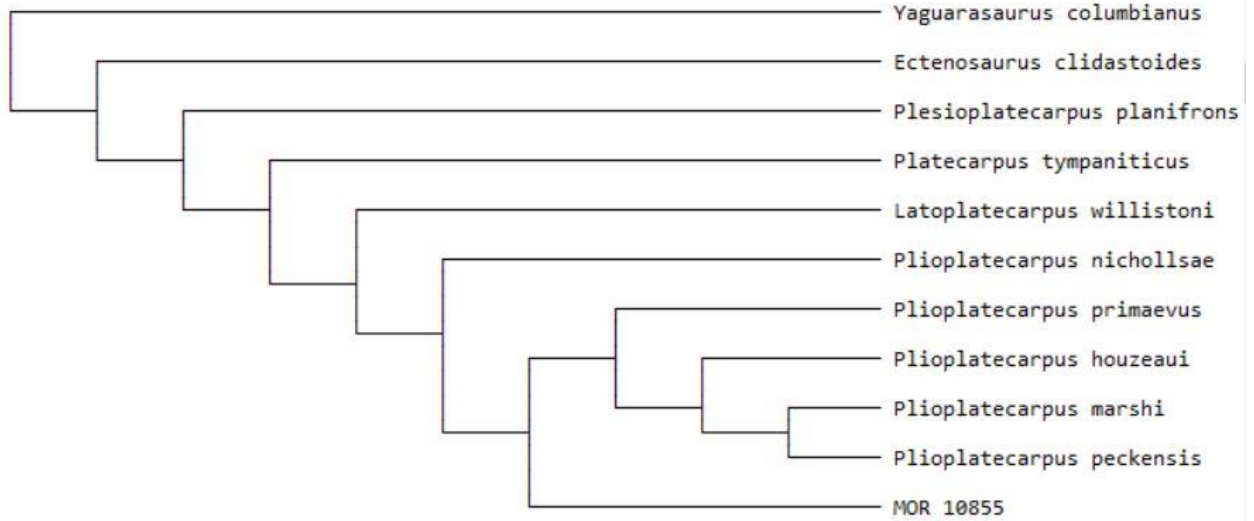


Figure A3. Results of full heuristic bootstrap analysis with 75% consensus and ACCTRAN optimization

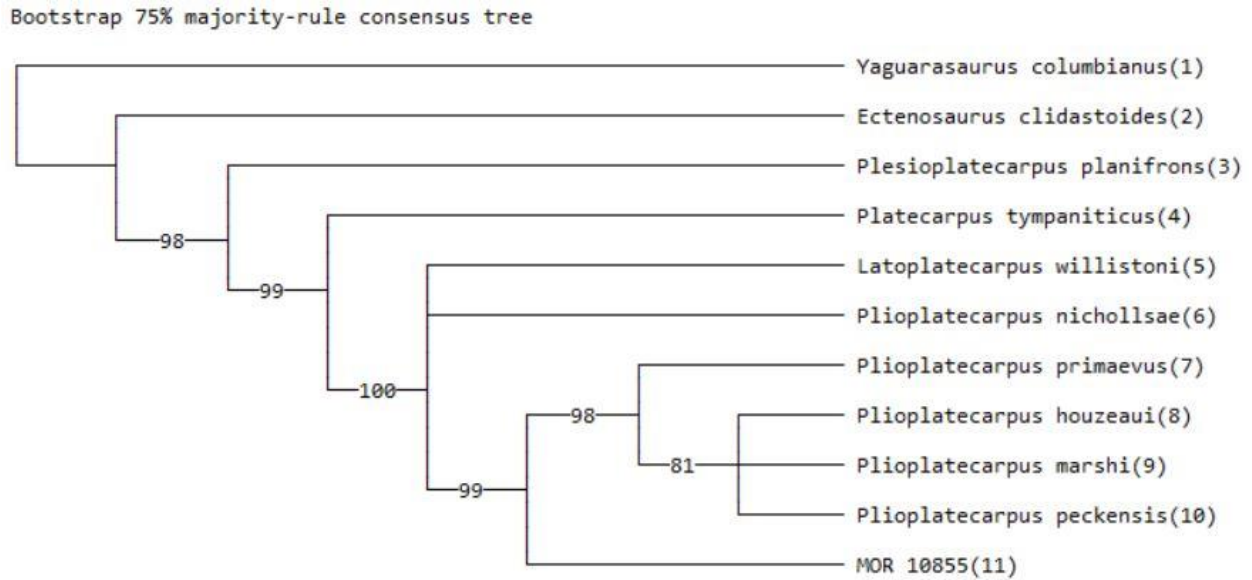


Figure A4. Results of branch and bound bootstrap analysis with 75% consensus and ACCTRAN optimization

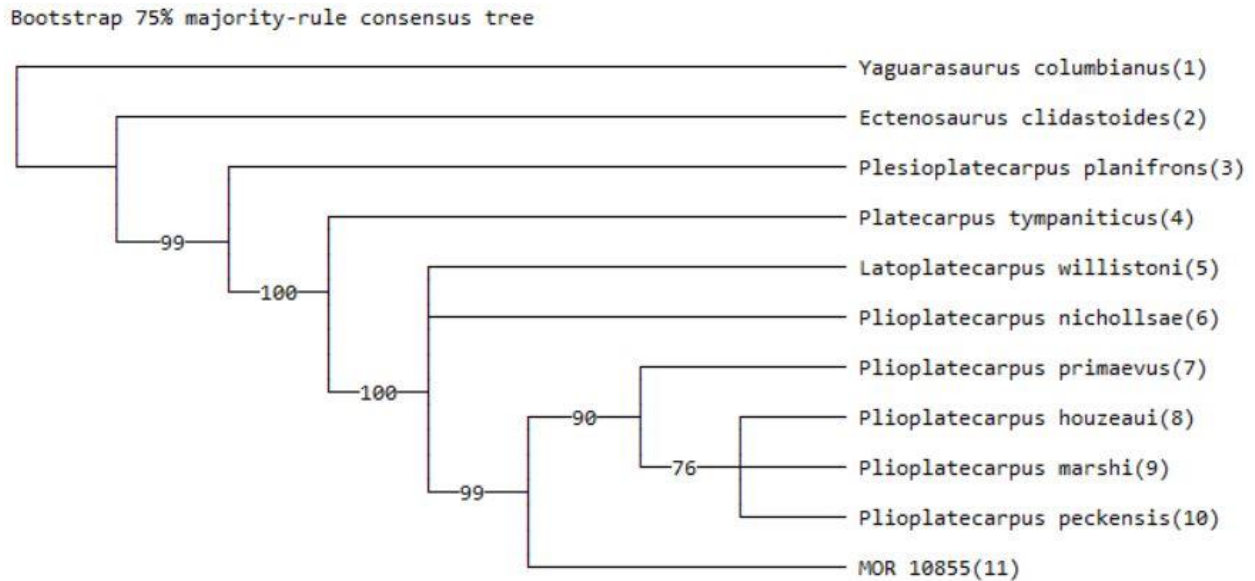


Figure A5. Results of full heuristic bootstap analysis with 90% consensus and ACCTRAN optimization

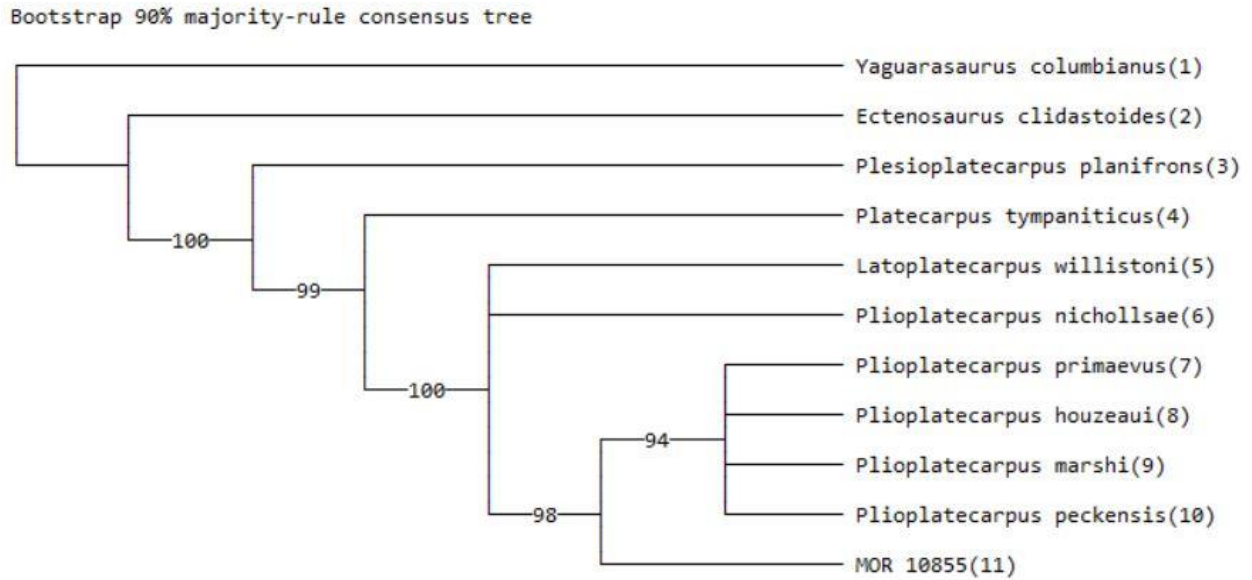


Figure A6. Results of branch and bound bootstrap analysis with 90% consensus and ACCTRAN optimization

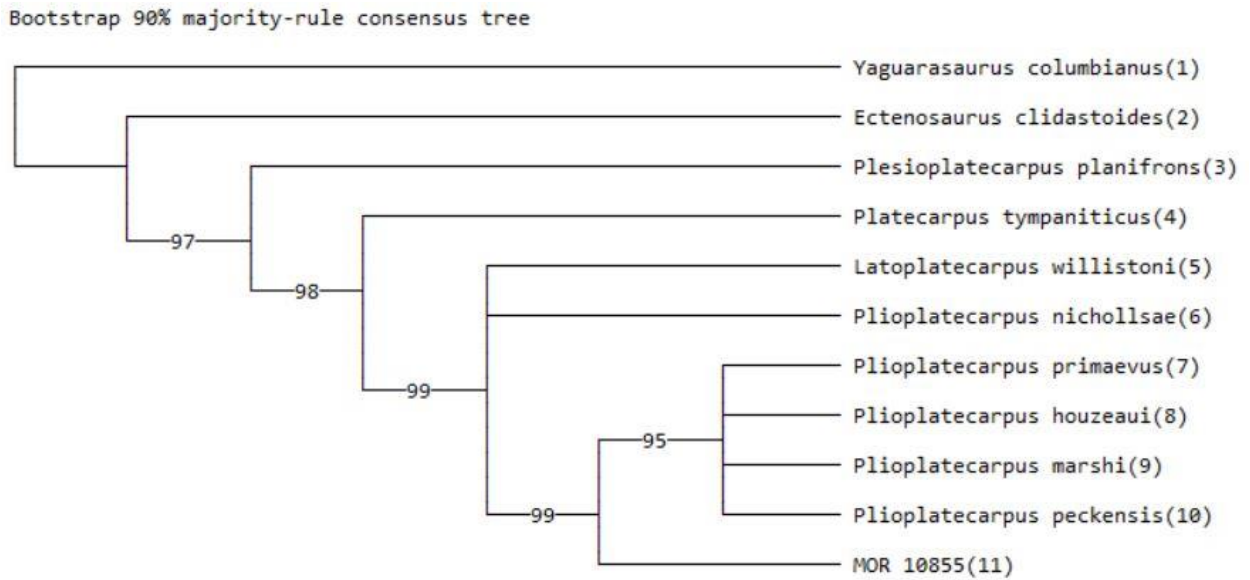


Figure A7. Results of full heuristic bootstrap analysis with 70% consensus and DELTRAN optimization

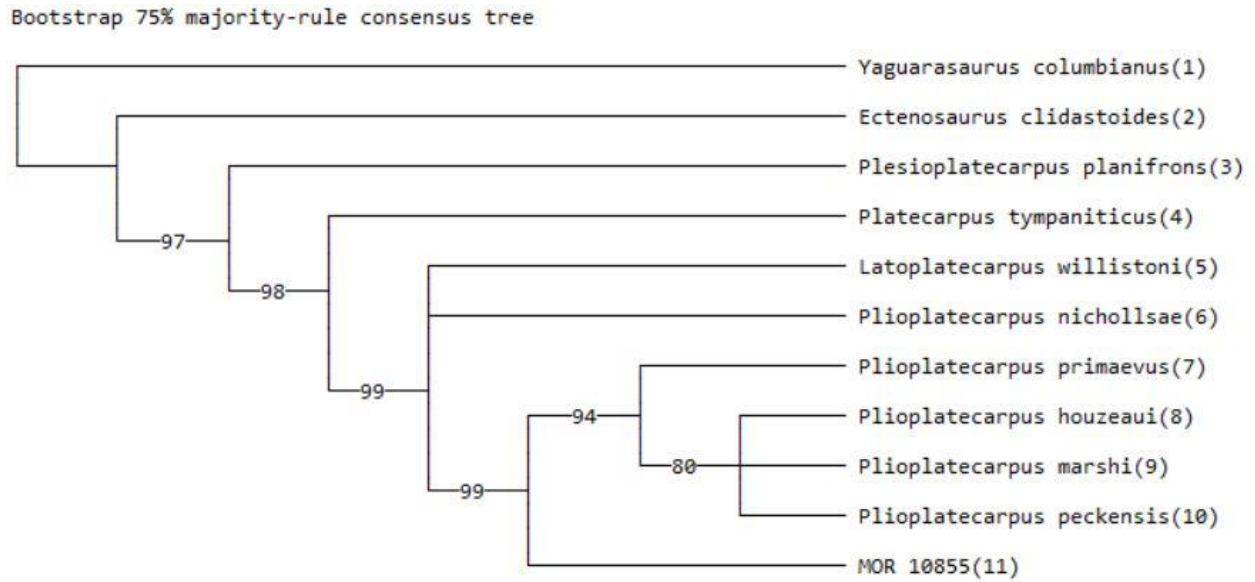


Figure A8. Results of branch and bound bootstrap analysis with 75% consensus and DELTRAN optimization

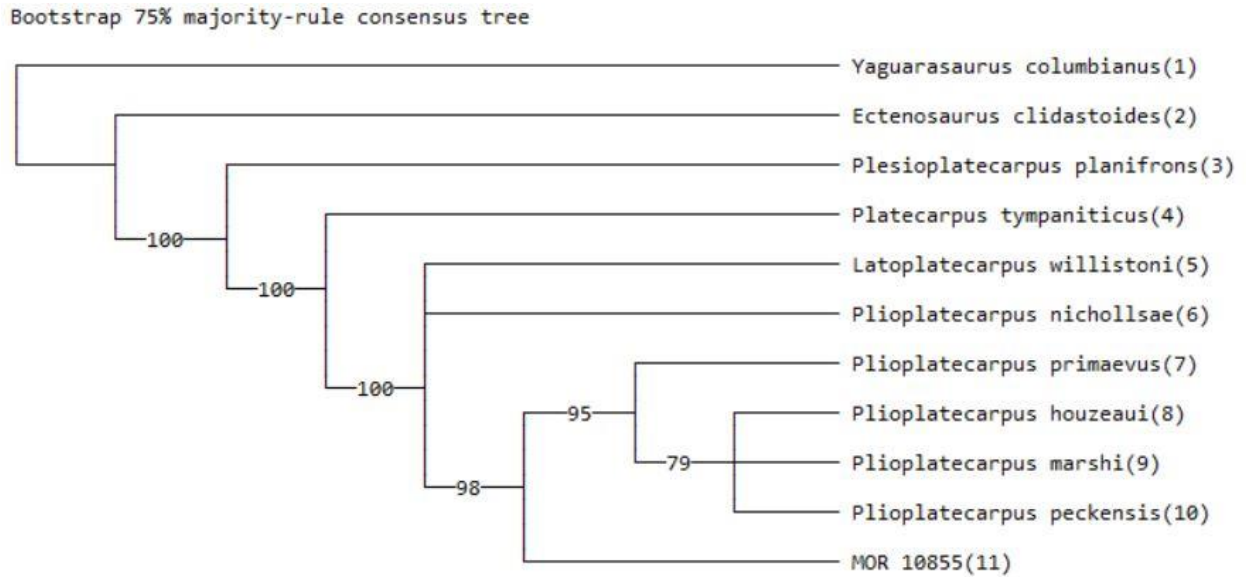


Figure A9. Results of full heuristic bootstap analysis with 90% consensus and DELTRAN optimization

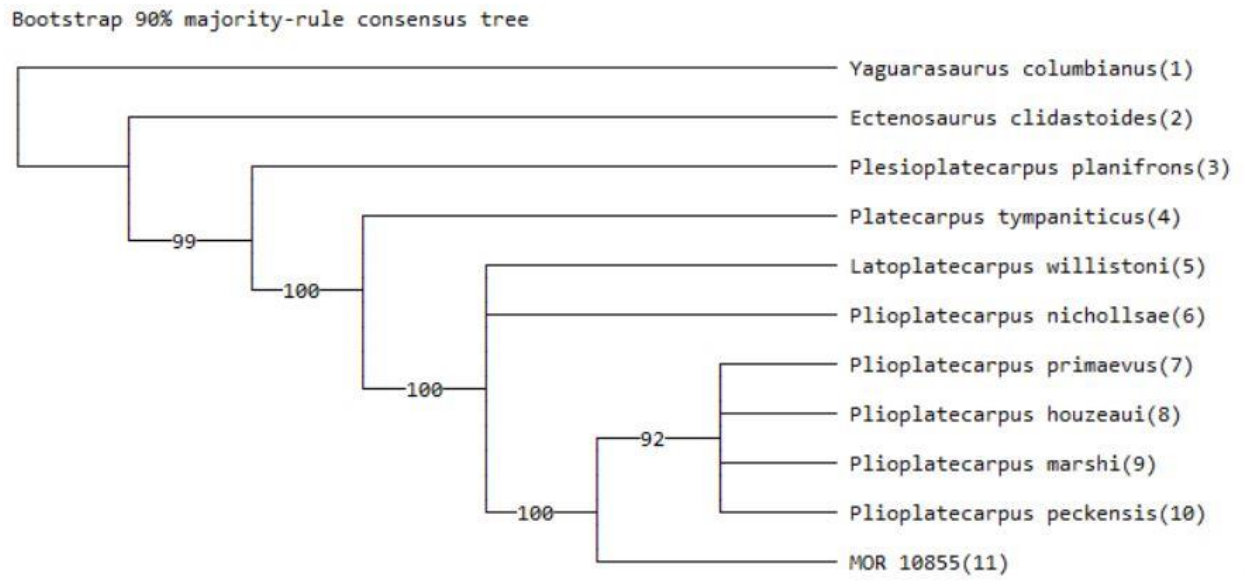
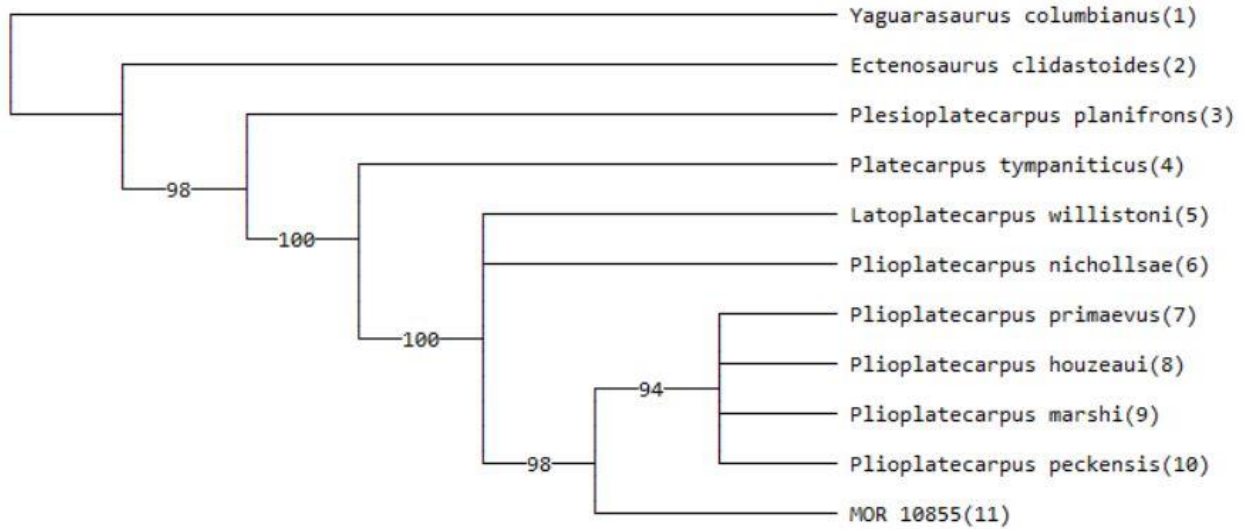


Figure A10. Results of branch and bound bootstrap analysis with 90% consensus and DELTRAN optimization

Bootstrap 90% majority-rule consensus tree



Unique Combination of Features:

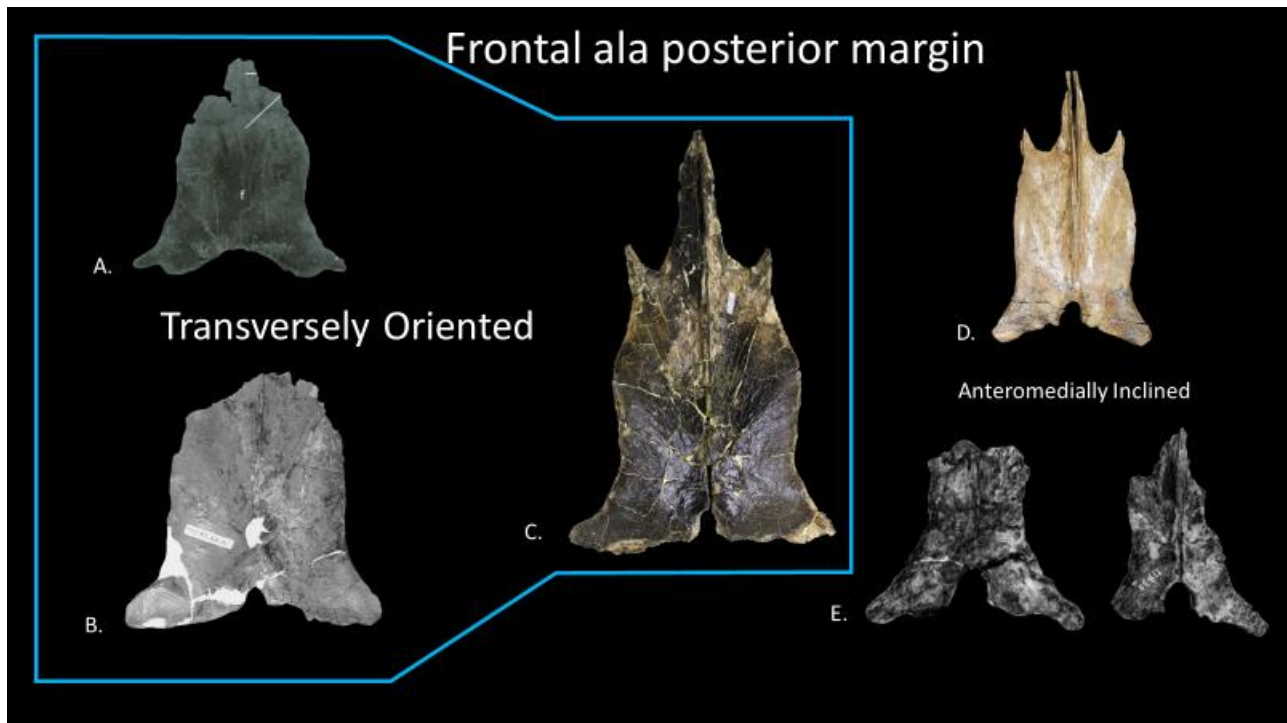


Figure A11. Orientation of the frontal ala's posterior margin in A. *Latoplatecarpus willistoni* (modified from Konishi and Caldwell, 2011), B. *Plioplatecarpus nichollsae* (modified from Konishi and Caldwell, 2009), C. MOR 10855, D. *Plioplatecarpus peckensis*, and E. *Plioplatecarpus primaevus* (modified from Holmes, 1996). A-C are transversely oriented, D and E are anteromedially inclined. Elements are not to scale.

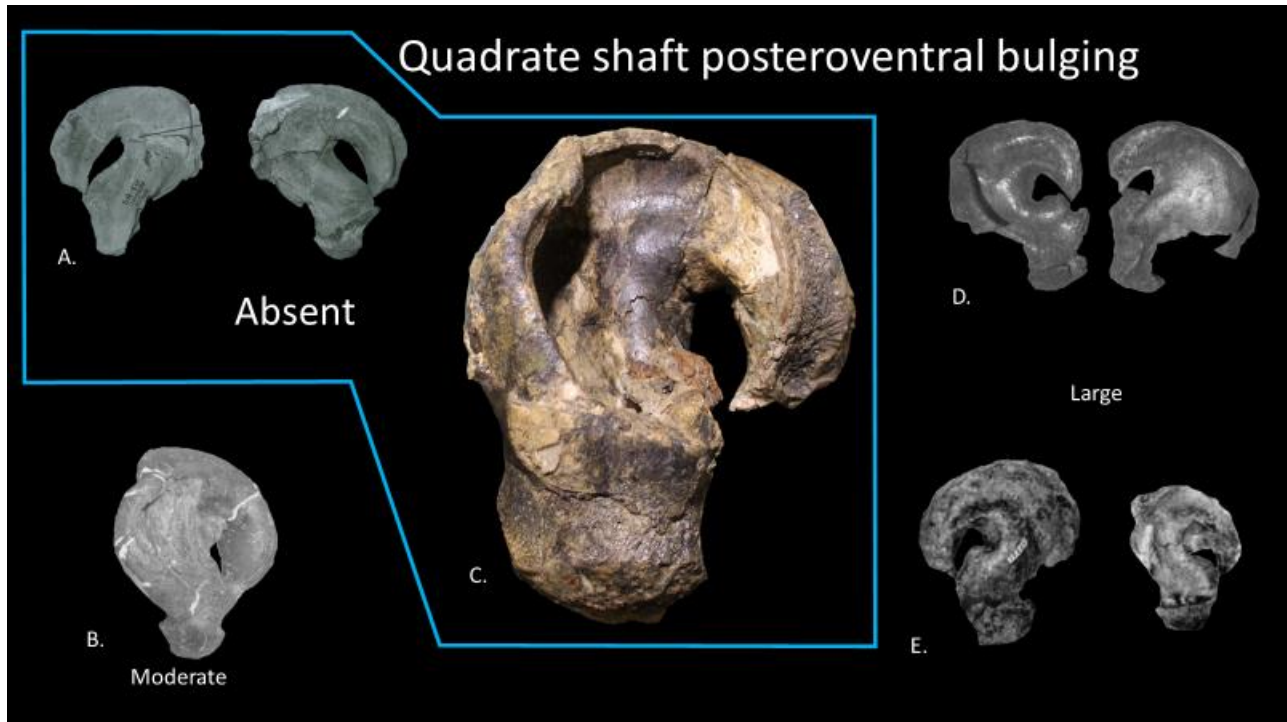


Figure A12. Degree of posteroventral bulging on the quadrate shaft of A. *Latoplatecarpus willistoni* (modified from Konishi and Caldwell, 2011), B. *Plioplatecarpus nichollsae* (modified from Konishi and Caldwell, 2009), C. MOR 10855, D. *Plioplatecarpus peckensis* (modified from Cuthbertson and Holmes, 2015), E. *Plioplatecarpus primaevus* (modified from Holmes, 1996). A and C lack this bulging, the bulging is moderate in B, and large in D and E. These elements are not to scale.

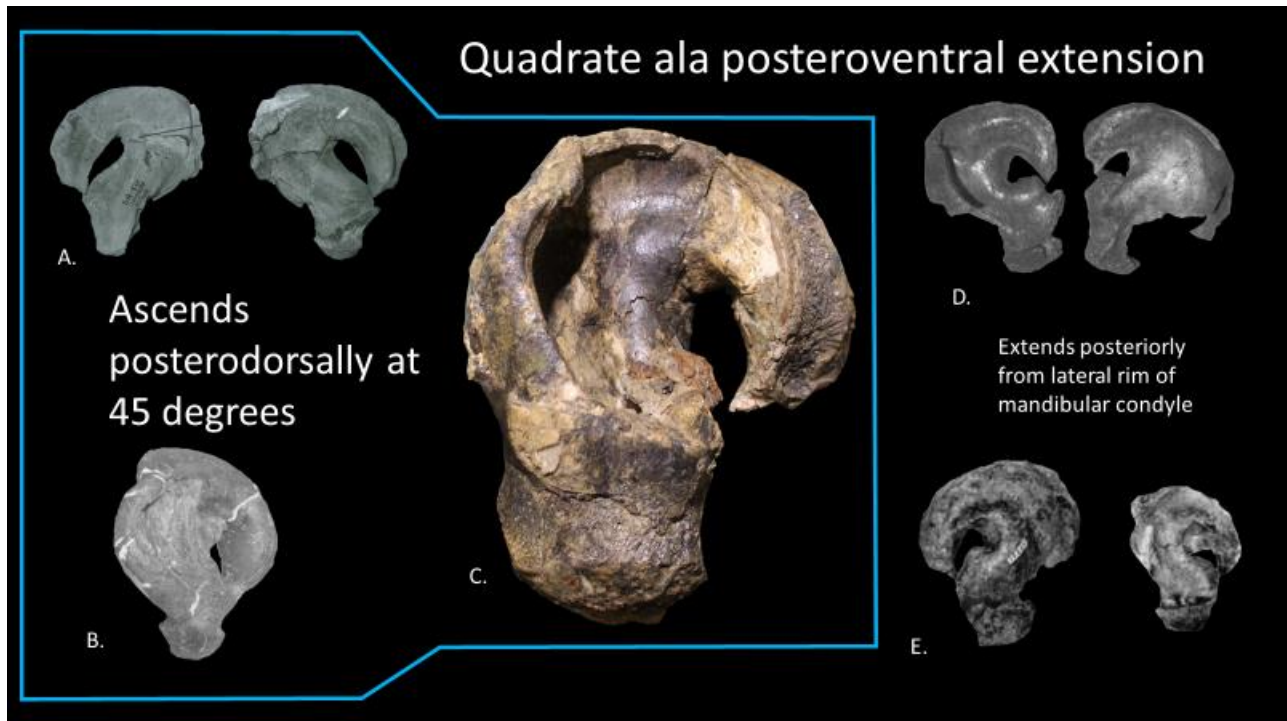


Figure A13. Degree of posteroventral extension of the quadrate ala in A. *Latoplatecarpus willistoni* (modified from Konishi and Caldwell, 2011), B. *Plioplatecarpus nichollsae* (modified from Konishi and Caldwell, 2009), C. MOR 10855, D. *Plioplatecarpus peckensis* (modified from Cuthbertson and Holmes, 2015), E. *Plioplatecarpus primaevus* (modified from Holmes, 1996). The ala ascends posterodorsally at 45 degrees in A-C, and extends posteriorly from the lateral rim of the mandibular condyle in D and E. These elements are not to scale.

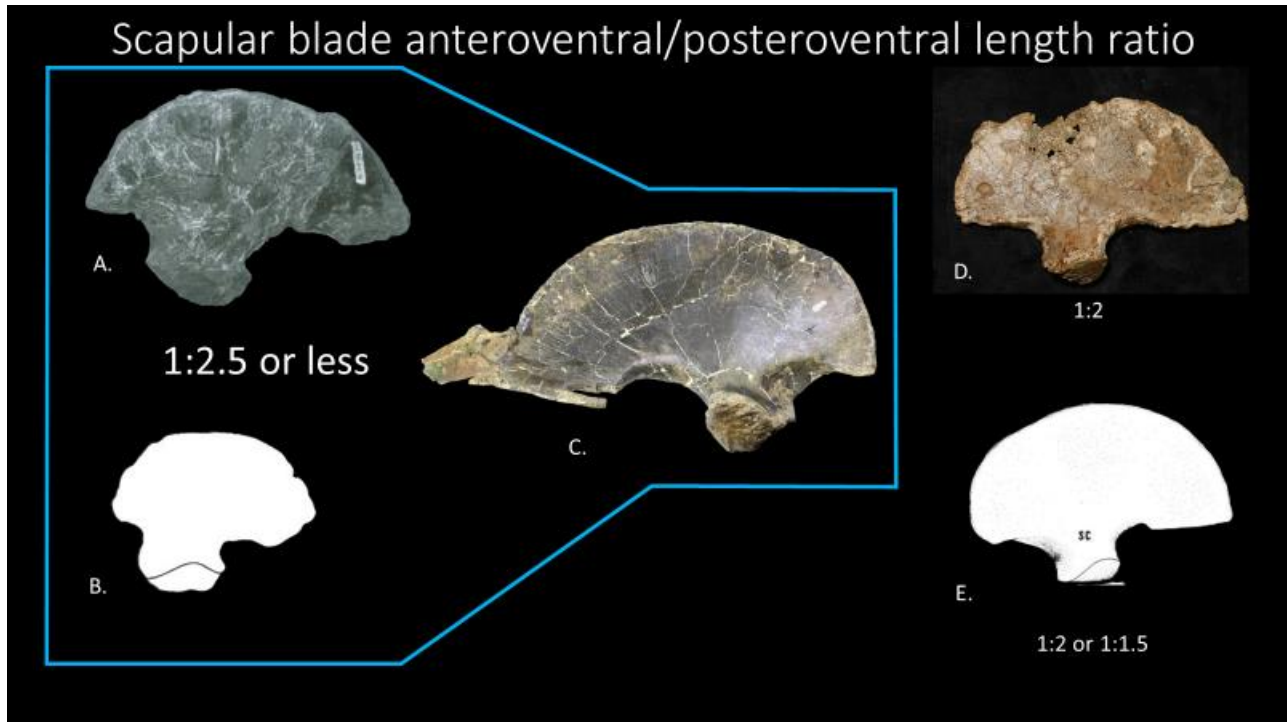


Figure A14. Length ratio of the anteroventral and posteroventral margins of the scapular blade in A. *Latoplatecarpus willistoni* (modified from Konishi and Caldwell, 2011), B. *Plioplatecarpus nichollsae* (modified from Konishi and Caldwell, 2009), C. MOR 10855, D. *Plioplatecarpus peckensis*, E. *Plioplatecarpus primaevus* (modified from Holmes, 1996). This ratio is 1:2.5 or less in A-C, 1:2 in D, and between 1:2 and 1:1.5 in E. These elements are not to scale.

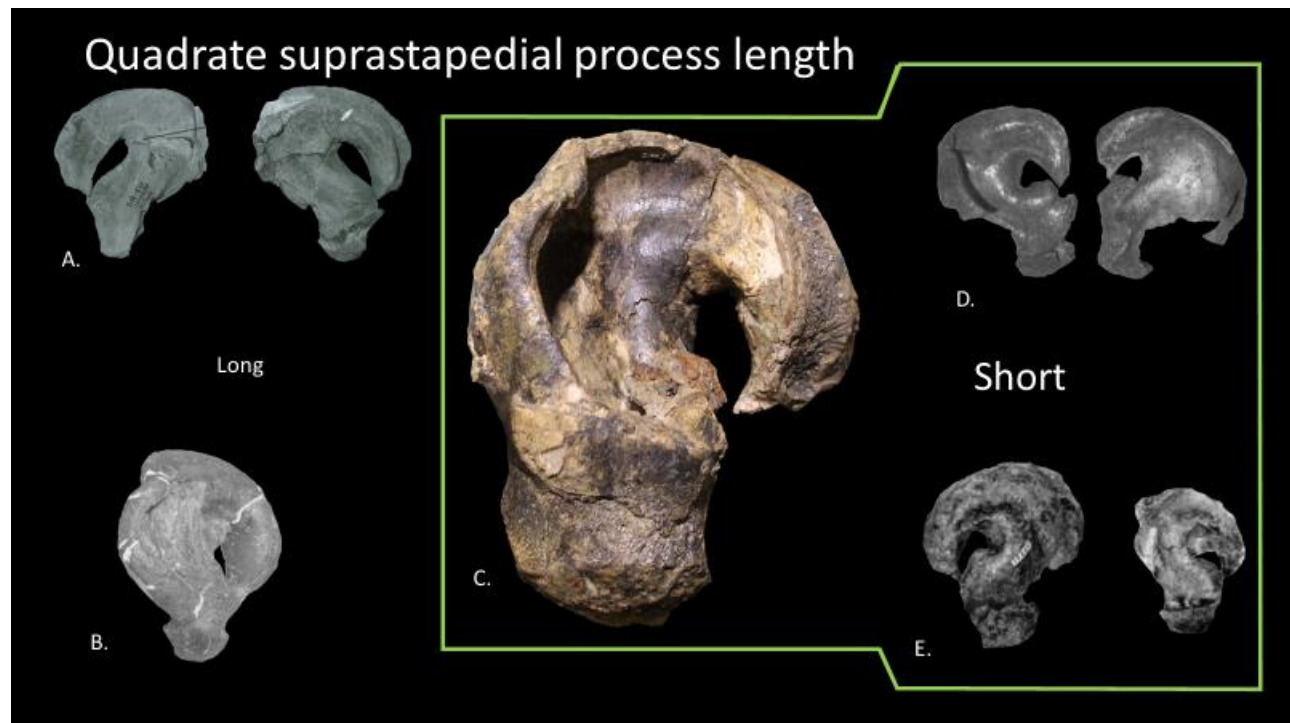


Figure A15. Length of the quadrate's suprastapedial process in A. *Latoplatecarpus willistoni* (modified from Konishi and Caldwell, 2011), B. *Plioplatecarpus nichollsae* (modified from Konishi and Caldwell, 2009), C. MOR 10855, D. *Plioplatecarpus peckensis* (modified from Cuthbertson and Holmes, 2015), E. *Plioplatecarpus primaevus* (modified from Holmes, 1996). This process is long in A and B and short in C-E. These elements are not to scale.

Coronoid posterodorsal process development

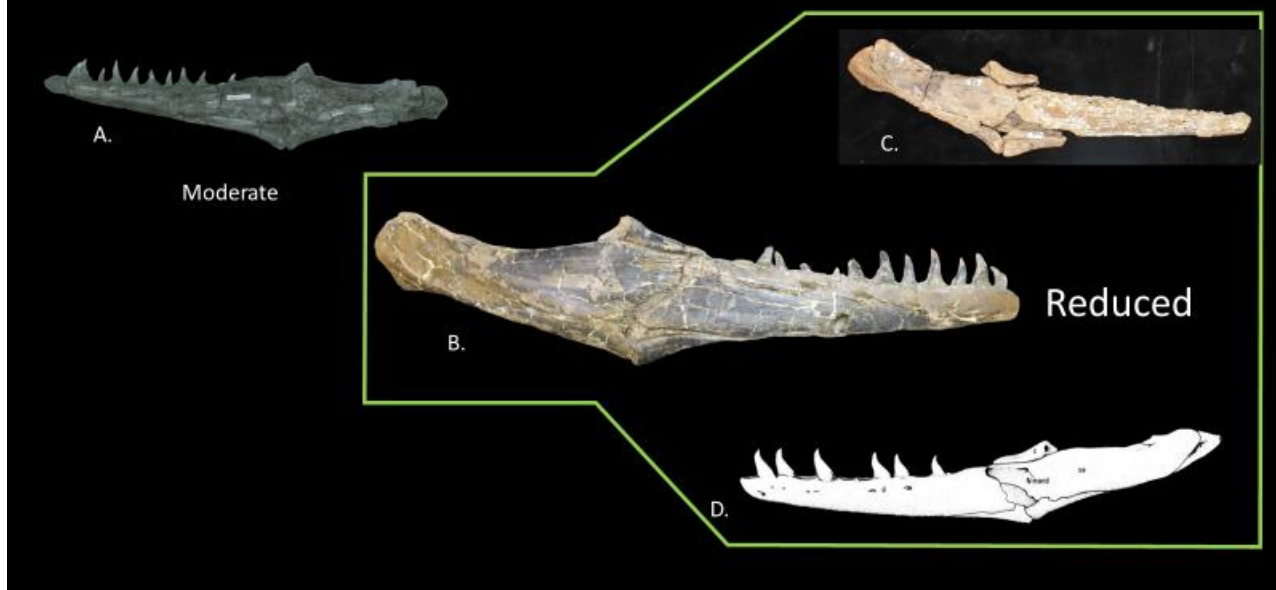


Figure A16. Development of the posterodorsal process of the coronoid in A. *Latoplatecarpus willistoni* (modified from Konishi and Caldwell, 2011), B. MOR 10855, C. *Plioplatecarpus peckensis*, D. *Plioplatecarpus primaevus* (modified from Holmes, 1996). This process is moderately developed in A and reduced in B-D. These elements are not to scale.

Percentage of Glenoid Fossa made by the Surangular

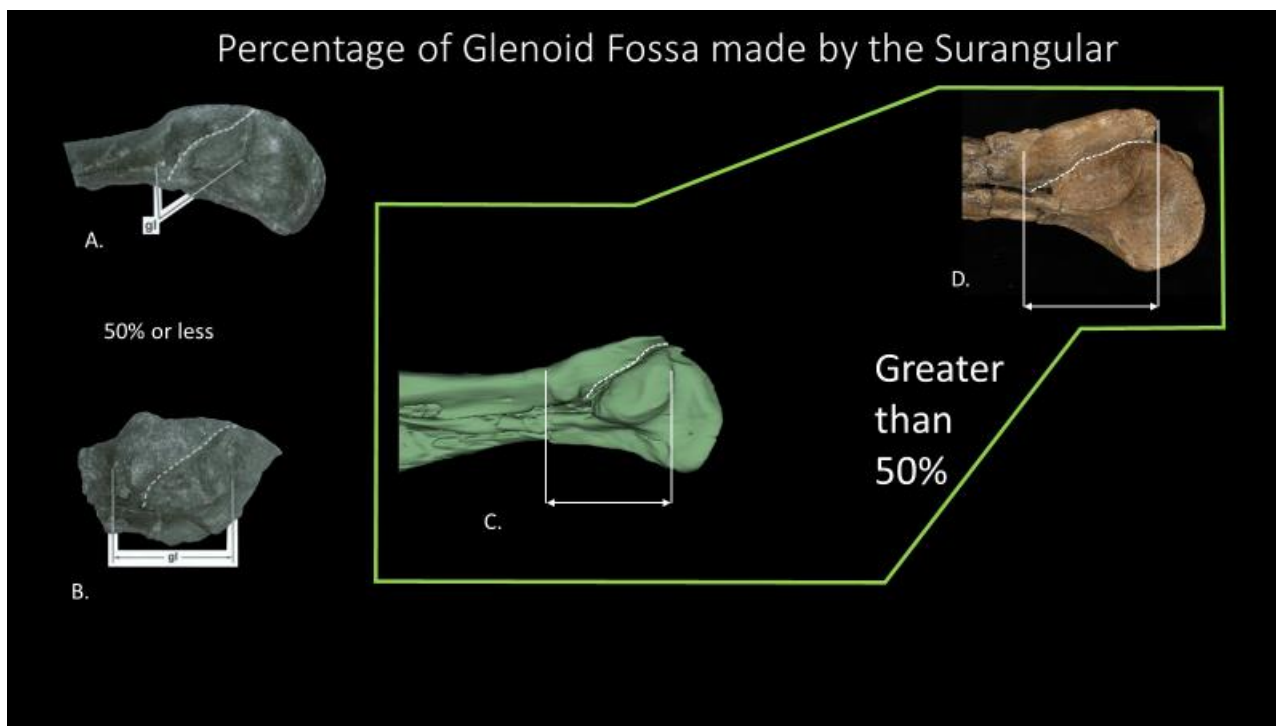


Figure A17. Percentage of the glenoid fossa that is made by the surangular in A. *Latoplatecarpus willistoni* (modified from Konishi and Caldwell, 2011), B. *Plioplatecarpus nichollsae* (modified from Konishi and Caldwell, 2011), C. MOR 10855, D. *Plioplatecarpus peckensis*. The surangular makes up 50% or less of the glenoid fossa in A and B and makes 50% or more of the glenoid fossa in C and D. These elements are not to scale.

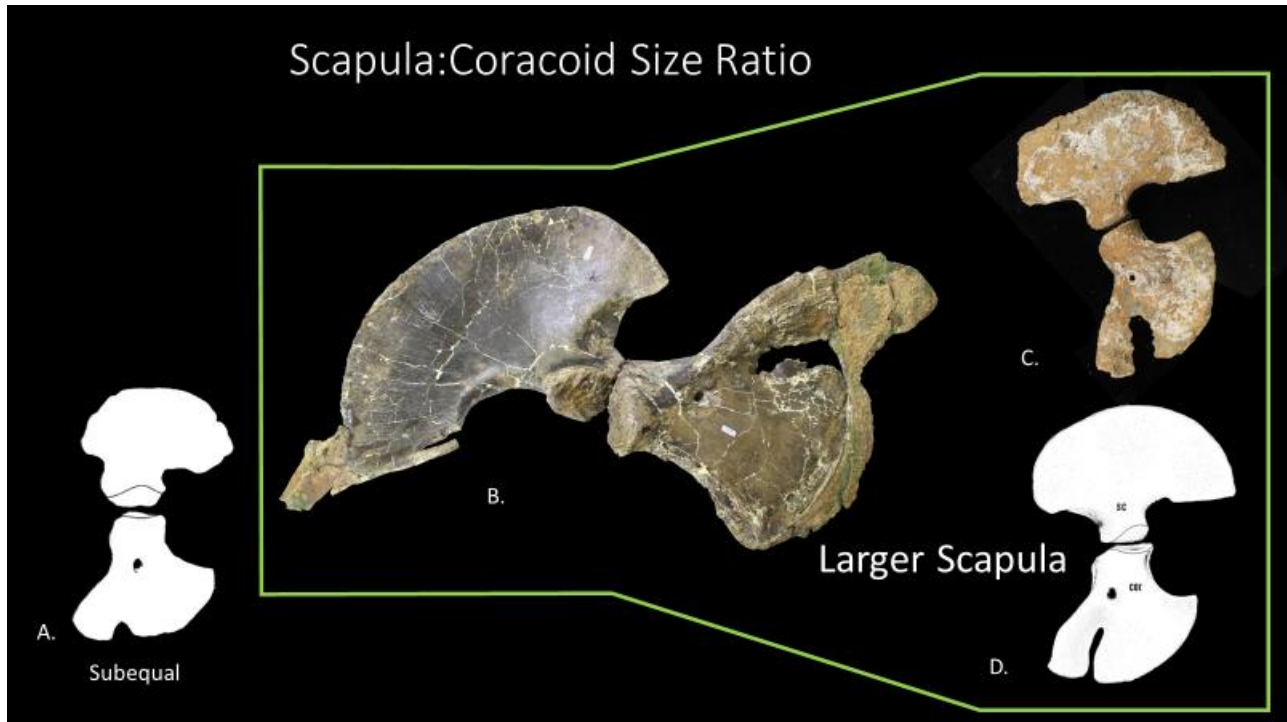


Figure A18. Size ratio of the scapula to the coracoid in A. *Plioplatecarpus nichollsae* (modified from Konishi and Caldwell, 2011), B. MOR 10855, C. *Plioplatecarpus peckensis*, D. *Plioplatecarpus primaevus* (modified from Holmes, 1996). The scapula and coracoid are subequal in size in A but in B-D the scapula is larger than the coracoid. These elements are not to scale.

**Fort Hays State University
FHSU Scholars Repository
Non-Exclusive License Author Agreement**

I hereby grant Fort Hays State University an irrevocable, non-exclusive, perpetual license to include my thesis ("the Thesis") in *FHSU Scholars Repository*, FHSU's institutional repository ("the Repository").

I hold the copyright to this document and agree to permit this document to be posted in the Repository, and made available to the public in any format in perpetuity.

I warrant that the posting of the Thesis does not infringe any copyright, nor violate any proprietary rights, nor contains any libelous matter, nor invade the privacy of any person or third party, nor otherwise violate FHSU Scholars Repository policies.

I agree that Fort Hays State University may translate the Thesis to any medium or format for the purpose of preservation and access. In addition, I agree that Fort Hays State University may keep more than one copy of the Thesis for purposes of security, back-up, and preservation.

I agree that authorized readers of the Thesis have the right to use the Thesis for non-commercial, academic purposes, as defined by the "fair use" doctrine of U.S. copyright law, so long as all attributions and copyright statements are retained.

To the fullest extent permitted by law, both during and after the term of this Agreement, I agree to indemnify, defend, and hold harmless Fort Hays State University and its directors, officers, faculty, employees, affiliates, and agents, past or present, against all losses, claims, demands, actions, causes of action, suits, liabilities, damages, expenses, fees and costs (including but not limited to reasonable attorney's fees) arising out of or relating to any actual or alleged misrepresentation or breach of any warranty contained in this Agreement, or any infringement of the Thesis on any third party's patent, trademark, copyright or trade secret.

I understand that once deposited in the Repository, the Thesis may not be removed.

Thesis: The Anatomy and Phylogeny of a New Large Plioplatecarpine Mosasaur From the Campanian Bearpaw Shale of Montana (USA)

Author: Richard A. Carr

Signature: Richard Carr

Date: 2 May 2023